

# Interaction of electrons with vibrating molecules: molecular electronics applications

Ivan A. Pshenichnyuk

A Thesis presented for the degree of  
Doctor of Philosophy



Institute of Theoretical Physics  
Faculty of Mathematics and Physics  
Charles University in Prague

October 2010

**Ph.D. thesis supervisor:** doc. RNDr. Martin Čížek, Ph.D.

**Author's address:** Institute of theoretical physics  
Faculty of Mathematics and Physics  
Charles University in Prague  
V Holešovičkách 2  
18000 Prague 8  
Czech Republic

**E-mail:** [ivan.pshenichnyuk@gmail.com](mailto:ivan.pshenichnyuk@gmail.com)

*Dedicated to*

my parents

# Interaction of electrons with vibrating molecules: molecular electronics applications

Ivan A. Pshenichnyuk

Submitted for the degree of Doctor of Philosophy  
October 2010

## Abstract

Interaction of the electric current, flowing through the molecular junction, with the internal vibrations of the bridging molecule is investigated. Two different theoretical approaches which allow us to calculate the current and other characteristics of the junction are compared. The first method is based on the scattering theory and Landauer formula, and the second on the Wangsness-Bloch-Redfield master equation technique. A set of original models of the molecular bridge with anharmonic vibrational mode and asymmetric coupling to the leads is formulated. Influence of anharmonic vibrations and different types of symmetry in the junction on the current-voltage dependencies of the bridge are discussed. As an example of the phenomenon, which can only be found beyond the harmonic approximation, we demonstrate the existence of the so called "motor effect", i. e. the strong dependence of the average angular momentum of the molecule on the voltage, applied across the junction. The key parameters, responsible for the effect appearance, such as the rotational barrier height and the symmetry in the junction are discussed.

# Interakce elektronu s vibrujícími molekulami: aplikace v molekulární elektronice

Ivan A. Pshenichnyuk

Doktorská disertační práce

Říjen 2010

## Abstrakt

V této práci studujeme interakci elektrického proudu procházejícího molekulárním můstkem s vibračními stupni volnosti tohoto můstku. Porovnááme dva různé teoretické přístupy, které umožňují počítat procházející proud a další charakteristiky můstku. První z metod je založena na teorii rozptylu a Landauerově formuli a druhá na Wangsnessove-Blochově-Redfieldově přístupu mistrovských rovnic. Navrhujeme rovněž sadu původních modelů pro anharmonický vibrační mód a asymetrické připojení k vodičům. Diskutujeme vliv anharmonicity a různých druhů asymetrie můstku na vodivostní charakteristiku. Jako příklad jevu, který může být pozorován jen nad rámeček harmonické aproximace, ukazujeme přítomnost tzv. "motorového efektu", t.j. silné závislosti momentu hybnosti molekuly na připojeném napětí. Diskutujeme hlavní proměnné ovlivňující možnost pozorování tohoto efektu, jako jsou výška potenciálové bariéry a symetrie můstku.

# Declaration

The work in this thesis is based on research carried out at the Institute of Theoretical Physics, Faculty of Mathematics and Physics, Charles University in Prague. No part of this thesis has been submitted elsewhere for any other degree or qualification and it is all my own work unless referenced to the contrary in the text.

Ivan A. Pshenichnyuk

# Acknowledgements

It is a pleasure to thank those who made this thesis possible. I am heartily thankful to my supervisor, Martin Čížek, for his patience and time, spent in discussions. His encouragement, guidance and support throughout the project enabled me to develop an understanding of the subject. I owe my deepest gratitude to the head of the Institute of Theoretical Physics, Jiří Horáček, for the possibility to work in his group. Without his huge support this thesis would never have been written. I would like to thank my colleagues from the Charles University and other universities. I am thankful to Michael Thoss and members of his group, especially Rainer Härtle, for the fruitful discussions and inspiration. Lastly, I offer my regards and blessings to all of those who supported me in any respect during the completion of the project.

# Contents

<b>Abstract</b>	<b>iv</b>
<b>Declaration</b>	<b>vi</b>
<b>Acknowledgements</b>	<b>vii</b>
<b>1 Introduction</b>	<b>1</b>
<b>2 Theoretical overview</b>	<b>7</b>
2.1 General model of a molecular junction . . . . .	8
2.1.1 One dimensional tight-binding chain . . . . .	8
2.1.2 Model of an isolated lead . . . . .	13
2.1.3 Junction Hamiltonian partitioning . . . . .	15
2.2 Scattering approach . . . . .	17
2.2.1 Landauer formula . . . . .	17
2.2.2 Transmission probability . . . . .	19
2.2.3 Green's function of the bridge . . . . .	20
2.3 Master equation approach . . . . .	22
2.3.1 Derivation of the WBR ME . . . . .	23
2.3.2 Current and other observables . . . . .	27
<b>3 Models of the molecular junction</b>	<b>29</b>
3.1 Elastic bridge (model 1) . . . . .	30
3.2 Bridge with one harmonic vibrational mode (model 2) . . . . .	33
3.3 Rotating bridge (models 3 and 4) . . . . .	38

---

<b>4</b>	<b>Computations</b>	<b>45</b>
4.1	Scattering approach . . . . .	45
4.1.1	Self-energy . . . . .	45
4.1.2	Elastic transport . . . . .	48
4.1.3	Inelastic transport . . . . .	49
4.2	Master equation approach . . . . .	51
4.2.1	Tensor form of the ME . . . . .	51
4.2.2	Observables . . . . .	57
4.2.3	Details of numerical implementation . . . . .	61
4.2.4	Analytical solution for the elastic model . . . . .	64
<b>5</b>	<b>Results and Discussion</b>	<b>67</b>
5.1	Comparison of scattering and ME approaches . . . . .	68
5.1.1	Weak coupling limit . . . . .	68
5.1.2	Importance of vibrational populations . . . . .	70
5.1.3	Balance equation . . . . .	74
5.1.4	Fluxes analysis . . . . .	76
5.2	Molecular motor models . . . . .	78
5.2.1	Current and excitation function . . . . .	78
5.2.2	Angular momentum and motor effect . . . . .	85
5.2.3	Towards realistic models . . . . .	89
<b>6</b>	<b>Conclusion</b>	<b>94</b>
	<b>Bibliography</b>	<b>97</b>

# Chapter 1

## Introduction

It's hard to overestimate the importance of microelectronics nowadays. The process of improvement and miniaturization of microelectronic devices have reached great results. However, there is an obstacle on this way. While the size of different elements in the electronic chip is getting smaller<sup>1</sup> and becomes comparable with a size of a molecule, laws of quantum mechanics start to play an important role in the chip and standard workhorses of the microelectronics, such as the Ohm's law, for example, lose their validity. In this sense, traditional microelectronics approaches its natural limit and getting ready to enter the quantum world, where all basic principles should be revised to create a new type of electronics [40].

The idea of the molecular electronics (or moletronics, as it is also called sometimes [26]) is to use molecules as a building blocks of an electronic circuits, while electrons keep their role of data carriers. It shouldn't be mixed with the solid state nanoelectronics, which stands somewhere in between the microelectronics and moletronics at the size scale. Manufacturing devices at this level promises both great possibilities and challenges, and differs very much from the approaches which are used in ordinary electronics. Following this way, the whole philosophy of device production can be changed. Instead of going "top down" direction, like carving elements out of bulk materials, chemical lab can be used to synthesize necessary elements in a "bottom up" way. This allows to produce elements in enormous amounts with

---

<sup>1</sup>A transistor size in modern chips is already less than 50 nm

a great reproducibility of each element. Being complicated objects, molecules have their own internal structure and degrees of freedom. Electrons, that pass through a molecular device, can change its geometry and properties. Moreover, since there is an interaction between electronic and nuclear degrees of freedom in molecules, energy exchange between them should be taken into account. It was demonstrated that atomic vibrational degrees of freedom have strong influence on the charge transport properties of molecules [34].

At a moment hundreds of theoretical and experimental works are published where different aspects of molecular electronics are discussed and many single-molecule devices are proposed. Without going deep into the history, which can be tracked down at least until the year 1940 ([21]), we would rather mention few important early works on the subject. In the year 1974 Aviram and Ratner published the paper [2], where they suggested and motivated theoretically the idea of single molecule diode. In 1997 Reed et al. [41] performed conductance measurement of the single molecule. One year later inelastic electron tunneling spectroscopy with the scanning tunneling microscope (IETS-STM) method was used for the first time to study conductance of the isolated acetylene molecule [45].

During decades of development few mainstream experimental methods were established to investigate molecular conductance. Scanning probe technique ([19], [14]) is among them. Another sort of experiments were performed manufacturing so called molecular junctions. These contacts are produced from the single molecule or a chain of molecules which are called molecular bridges, connected between two (or more) solid electrodes. It was shown that they can act as both passive and active elements in electronic circuits and, thus, may play a key role in new electronics. Despite the obvious success in the field, these experiments are still capricious and suffer from the lack of reproducibility. There are other issues, like room temperature functionality and long-term stability. According to the way of production molecular junctions can be mainly divided to mechanically controllable break junctions ([32], [44]) and break junctions formed by electromigration ([35], [36]). For the review see [43].

Before now numerous theoretical simulations were performed to show, that single

molecules can act as a vast variety of different devices: molecular switches ([37], [25]), memory bits, molecular rectifiers or diodes, transistors ([4], [8]) and pumps. Some of them were demonstrated experimentally, like, for example, the single-molecule transistor in the work [36]. Current driven molecular motors, which constitute the subject of this work, can be classified using the modern terminology as nanoelectromechanical systems (NEMS), i.e. devices integrating electrical and mechanical functionality on the nanoscale. Another example of NEMS, which stimulates research interest during the last decade, is a quantum shuttle ([33], [7], [16]).

As it was already mentioned, internal molecular mechanical degrees of freedom play an important role in the charge transport phenomena. It is especially so in the low coupling regime, when electrons spent significant time at the molecular bridge and high energy exchange between electronic and vibrational degrees of freedom should be expected. There are experimental and theoretical works which demonstrate, that electron-phonon interactions are responsible for many specific phenomena (for the review see [12]). For example, this interaction may become a reason of heating of the bridge and even its dissociation [42]. So, the question about the role of internal degrees of freedom is connected with the stability question. Vibrational excitations often reveal itself as steps ([17]) at current voltage characteristics (CVC) of the bridge, which correspond to certain quantized vibrational energy transitions in the molecule. And vice versa: vibrational steps at CVC provide certain information about the internal structure of the molecule. In this sense charge transport experiments can be used as some kind of spectroscopy to determine the details of molecular structure [45]. One can also think about manipulating molecular vibrations (for example with an external field) to influence the current through the junction. It was shown ([37]), for example, that an electrostatical field can be used to influence a central benzene ring torsional dynamics in the "phenylene ethynylene oligomer" molecule and thus control the conductance switching.

The electron-phonon interaction phenomenon lies in the basis of the electromechanical molecular motor idea, which is discussed in details in this work. Along with current driven motors there are other possible mechanisms, like, for example, motors driven by light or stochastic fluctuations due to interaction with thermal

bath (Brownian motion). At this point the subject of molecular electronics seems to have certain overlap with the molecular biology, since molecular motor mechanisms play important roles in functional biology of the living cell. There is a whole class of so called "motor proteins" that are able to move along the surface of a suitable substrate. They are powered by the hydrolysis of ATP molecules (which are the common energy currency of the body powering everything including muscle movement) and convert chemical energy into mechanical work. The kinesin protein, for example, is a nanoscale molecular motor that carries a molecular cargo through the cell. Another example is the prestin, which is responsible for the signal transduction in the human ear [40]. Returning to the artificially built molecular motors it's worth mentioning here, that externally driven torsional motion of small parts of molecules has been already demonstrated for molecules both in gas [29] and mounted on surfaces [20]. In this work molecular motor is introduced as a molecular junction with a bridging molecule possessing certain groups which can perform rotational motion in response to bias voltage across the junction. Such elements have already been anticipated in [52]. In this form the motor can be considered as a molecular electronics element, which can be connected to some other molecular devices.

There are few theoretical methods developed to calculate CVC and other properties of molecular junctions, taking into account vibrational effects in the junction [12]. In the approach based on the generalized Landauer formula [48, 50] current can be expressed through the transmission function of the bridge and the scattering theory is used to calculate the transmission. Electron correlations are not taken into account in this method. Another possible way is to use various rate equations theories [47]. By solving the Wangsness-Bloch-Redfield master equation (ME), which is second order in molecule-lead coupling, the reduced density matrix (RDM) of a molecular bridge can be determined. RDM contains detailed information about the bridge while leads in this method are treated as large particle reservoirs in the equilibrium. The RDM can be used to calculate any observable of interest, including a current [17] and the angular momentum of the bridge which is important for the motor effect studies. These two approaches are discussed and compared in this work. There are also approaches based on many body physics methodologies, in particular

the nonequilibrium Green function technique [18] [39], which are not covered here.

One important point that makes molecular motor models challenging from computational point of view is the impossibility to use the harmonic approximation, which suits well in other cases like, for example, in quantum shuttle studies. Molecular bridges with torsional degrees of freedom, which may potentially act as rotors, should allow for the moving part to perform 360 degrees free rotation. It's not possible if the potential energy is parabolic. Investigation of molecules torsional motion demonstrates, that their potentials usually resemble the sine/cosine functions of the angle or their superposition [49]. Even though molecular dynamics beyond the harmonic approximation was already applied in molecular junctions modeling ([51]) it is much less well studied than harmonic approximation regime and some new effects can be expected to appear there.

In this work few models of molecular junctions are discussed. To make the discussion continuous we start from well studied models which are used to introduce all the main concepts and theories (models 1 and 2). Simple theoretical models allows us to understand better the details of the processes. They are used to test the FORTRAN code, link our studies with previous works and prepare the ground to switch to the anharmonic regime. They are also used to discuss different theoretical approaches and compare them. As the next step more complicated motor models are introduced (models 3 and 4). To analyze and understand the effect of anharmonicity in more-less well controlled conditions we first define the model 3 which doesn't correspond to any real molecular system and should be considered as purely theoretical. We then switch to the more realistic model 4 of molecular vibrations motivated by real molecular rotors used in the previous experiment with light driven artificial molecular motors [20]. This thesis has the following structure: first all necessary theoretical formalisms will be introduced in the chapter 2. In the chapter 3 models of the molecular junctions will be formulated and motivated. Later, in the chapter 4, computation process will be discussed and all necessary analytical equations will be derived. Some attention will also be payed to numerics. Results of calculations are presented in the chapter 5, which can be logically divided to two parts. First theoretical methods are compared and discussed using basic

models 1 and 2. Some possible improvements for the scattering theory approach are proposed. In the second part the motor effect and conditions of its existence are discussed. Charge transport properties of molecular junctions with anharmonic vibrational degrees of freedom are also studied there. Thesis will be finished by the conclusion in chapter 6.

# Chapter 2

## Theoretical overview

In this chapter all main theoretical tools and concepts, which are used in the thesis, are brought together. It's started from the description of the general model of a molecular junction, which consists of two solid electrodes and a molecular bridge, connected between them. The nearest neighbor tight-binding chain concept, taken from the solid state physics, is used to model metallic properties of electrodes, while the detailed discussion of different types of molecular bridges is postponed until the chapter 3. Thus, theoretical approaches described here are quite general and can be applied to all molecular junctions discussed in this work. The rest of the chapter is devoted to the general description of two different approaches, which allow to calculate CVC and other characteristics of molecular junctions. "Scattering theory approach" which is based on the Landauer formula for current and quantum scattering theory concepts is discussed in the section 2.2. The approach, which is referred throughout the work as just the "master equation approach" for simplicity, is described in the section 2.3. It is demonstrated there, how the second order Wangsness-Bloch-Redfield master equation can be derived from the von Neumann equation using the projection superoperators technique. It is also showed there how the solution of the master equation - the reduced density matrix of a molecular bridge, can be used to calculate the current and other observables.

## 2.1 General model of a molecular junction

### 2.1.1 One dimensional tight-binding chain

In this section we are going to derive few important formulas for the nearest neighbor tight binding model (NNTBM) and introduce terminology which is used throughout the work. It's also important for better understanding of the physical meaning of quantities which we parametrize in the chapter 3. Additional details about NNTBM can be found, for example, in [1].

Let's take one dimensional chain of atoms. Their positions are defined by the one dimensional vector  $R = na$ , where  $n$  is integer and  $a$  is the distance between atoms (lattice constant). All possible values of  $R$  then constitute the Bravais lattice. Schroedinger equation for such a chain reads

$$(H_{at} + \Delta U)\psi = \varepsilon\psi. \quad (2.1)$$

The tight binding Hamiltonian is periodical (with the same periodicity as the lattice) and consist of two terms.  $H_{at}$  is the potential which coincide with the Hamiltonian of a separate atom at each atom's side. In the vicinity of each atom equation  $H_{at}\psi_n = E_n\psi_n$  can be solved exactly, providing localized atomic orbitals  $\psi_n$ . Each orbital is infinitely many times degenerate, since it may belong to any atom in the chain.  $\Delta U$  should be considered as a small perturbation, which makes it possible for electrons to jump to other atoms.

We search the eigenfunctions of the full Hamiltonian in the form

$$\psi(r) = \sum_R e^{ikR} \phi(r - R), \quad (2.2)$$

where summation goes through all the Bravais lattice vectors  $R$ . Quantum number  $k$  distinguishes different solutions. Sometimes it's called quasimomentum, as a generalization of similar quantum number of free electrons (where it has a meaning of momentum) for Bloch's electrons, when the translational symmetry of the space is lower than in the continuous space case. Its possible values will be discussed in details later. Function  $\phi(r)$  (which they call sometimes Wannier function) for each atom side is in general a linear combination of atomic orbitals (LCAO)

$\phi(r) = \sum_n b_n \psi_n$ . In this decomposition we limit ourselves by just one term, which correspond to the s-orbital  $\psi_s$  of the atomic Hamiltonian  $H_{at}$ . It is easy to show, that the function  $\psi(r)$  taken in the form (2.2) satisfies the Bloch's theorem

$$\psi(r + R) = e^{ikR}\psi(r). \quad (2.3)$$

Let's multiply the Schrodinger equation from the left hand side by the function  $\psi_s$  (with energy  $E_s$ ) and integrate it through all  $r$

$$(\varepsilon - E_s) \int \psi_s^* \psi dr = \int \psi_s^* \Delta U \psi dr. \quad (2.4)$$

Now we substitute  $\phi = \psi_s$  to the equation and split the sum over  $R$  to the term with  $R = 0$  and  $R \neq 0$

$$\begin{aligned} (\varepsilon - E_s) + (\varepsilon - E_s) \sum_{R \neq 0} e^{ikR} \int \psi_s^* \psi_s(r - R) dr = \\ \int \psi_s^* \Delta U \psi_s dr + \sum_{R \neq 0} e^{ikR} \int \psi_s^* \Delta U \psi_s(r - R) dr. \end{aligned} \quad (2.5)$$

Introducing new notations

$$\begin{aligned} \int \psi_s^* \Delta U \psi_s dr &= \Delta E, \\ \int \psi_s^* \Delta U \psi_s(r - R) dr &= \beta(R), \\ \int \psi_s^* \psi_s(r - R) dr &= \alpha(R), \end{aligned} \quad (2.6)$$

and expressing the energy  $\varepsilon$  from the equation we get the formula

$$\varepsilon = E_s + \frac{\Delta E + \sum_{R \neq 0} e^{ikR} \beta(R)}{1 + \sum_{R \neq 0} e^{ikR} \alpha(R)}. \quad (2.7)$$

Overlap integrals  $\alpha(R)$  are assumed to be equal to zero, since atomic functions  $\psi_s$  are well localized. We assume also, that integrals  $\beta(R)$ , representing the coupling between various atomic sites, differ from zero only for interaction with nearest neighbors, like  $\beta(\pm a) = \beta$ . For the full energy of the electron, localized at the certain atom site, we use the notation  $\mu \equiv E_s + \Delta E$ . Finally, all necessary assumptions about the chain are made. Resulting model schematic representation is depicted at the fig. 2.1. We also get the final formula for the energy

$$\varepsilon = \mu + 2\beta \cos ka. \quad (2.8)$$

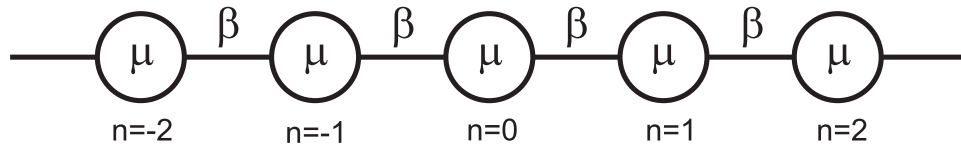


Figure 2.1: Schematic representation of the infinite one dimensional nearest neighbor tight-binding chain. It is defined by two parameters: atomic sites energy  $\mu$  and the nearest neighbors coupling strength  $\beta$

This is the dispersion relation for our chain. All possible Bloch wave's energies should belong to the interval  $[\mu - 2\beta; \mu + 2\beta]$  which is called the conduction band. Such a behavior, being quite typical for metals, is qualitatively different from the "free electrons" case, where dispersion relation is parabolic. Such differences are connected with the lower translational symmetry of the lattice discrete coordinate space as compared with continuous space in the "free electrons" model.

We deal with two types of electronic states in the chain:  $|n\rangle$  when electron sits on the atom  $n$  and  $|k\rangle$ , when electron has quasimomentum  $k$ . In the coordinate space this two types of states are represented by wavefunctions  $\psi_s(r - na)$  and  $\psi(r)$  respectively. From now on we don't use the coordinate representation any more and integrals  $\mu$  and  $\beta$  are assumed to be model parameters. On the contrary, both  $n$ - and  $k$ -representations will be used throughout the work.

We can draw the Hamiltonian  $H$  in the  $n$ -representation, where it's a tridiagonal infinite dimensional matrix

$$H = \begin{pmatrix} \dots & \beta & & 0 \\ \beta & \mu & \beta & \\ & \beta & \mu & \beta \\ & & \beta & \mu & \beta \\ 0 & & & \beta & \dots \end{pmatrix}. \quad (2.9)$$

Diagonalizing the matrix one can find its eigenvalues  $\varepsilon$  (which is of course just (2.8) again) and its eigenvectors

$$C_n^k = e^{ikna} \quad (2.10)$$

which are plane waves. We are familiar with them as with decomposition coefficients from (2.2). Now we can look at them from a bit different point of view, and use

them as the overlap matrix  $\langle n|k\rangle$  to switch between two representations

$$|k\rangle = \sum_n C_n^k |n\rangle. \quad (2.11)$$

It is clear from (2.11), that in the tight binding approximation  $k$ -states are running waves. Mean velocity of the electron with wavenumber  $k$  is given by the formula

$$v(k) = \frac{\partial \varepsilon}{\partial k} = -2a\beta \sin ka. \quad (2.12)$$

So, decreasing the coupling  $\beta$  between neighbor atoms will not prevent free movement of electrons through the chain. It will just decrease its velocity.

To make  $k$ -states (2.11) normalized we have to normalize vectors  $C_n^k$  (states  $|n\rangle$  are normalized by definition). To do it we assume, that the number of atoms in the chain is  $N$  and its length is  $L = aN$  ( $N$  is supposed to be very large and at all final results we assume  $N \rightarrow \infty$ ). And norm

$$\left( \sum_{n=1}^N |C_n^k|^2 \right)^{-\frac{1}{2}} = \frac{1}{\sqrt{N}}. \quad (2.13)$$

If we adopt this norm and assume that  $N$  is infinitely large, states are still correctly normalized and orthogonalized since

$$\lim_{N \rightarrow \infty} \frac{1}{N} \sum_{n=1}^N C_n^k (C_n^{k'})^* = \delta_{kk'}. \quad (2.14)$$

Thus, properly normalized Bloch's wave for the infinite TBC reads

$$|k\rangle = \frac{1}{\sqrt{N}} \sum_{n=1}^N e^{ikna} |n\rangle. \quad (2.15)$$

One more thing to do in this section is to apply the so-called Born von Karman boundary conditions  $\psi(x + L) = \psi(x)$ . This type of description is a computational trick, since those "non-reflecting" boundary conditions applied at the ends of the very long chain of atoms can't change its inner properties, but allows us to use integration instead of summation over  $k$ , if necessary. This conditions together with Bloch's theorem (2.3) lead to the following allowed values of the vectors  $k$

$$k = \frac{m}{N} \frac{2\pi}{a}, \quad (2.16)$$

where  $m$  is integer. In the first Brillouin zone  $[-\frac{\pi}{a}; \frac{\pi}{a}]$  we have  $N$  physically different  $k$ -vectors. From this moment we work only inside this zone.

If  $N \rightarrow \infty$ , minimum possible volume in  $k$ -space  $\Delta k = \frac{2\pi}{Na}$  goes to zero and  $k$  vector in the first Brillouin zone becomes continuous. Summation over all possible values of  $k$  of some arbitrary function  $F(k)$ , which we will face later, can be transformed to integration. We illustrate it here in few steps

$$\sum_k F(k) = 2 \sum_{k=-\pi/a}^{+\pi/a} F(k) \quad (2.17)$$

(each state can contain two electrons with different spins, for this reason we double the sum, see also [1]). Now we add  $\Delta k$  under the sum

$$\sum_k F(k) = \frac{Na}{\pi} \sum_{k=-\pi/a}^{+\pi/a} F(k) \Delta k. \quad (2.18)$$

Taking the limit  $N \rightarrow \infty$ ,  $\Delta k \rightarrow 0$  we can write

$$\lim_{N \rightarrow \infty} \frac{1}{N} \sum_k F(k) = \frac{a}{\pi} \int_{-\pi/a}^{+\pi/a} F(k) dk \quad (2.19)$$

We also use the fact, that all functions we deal with usually depend not on  $k$  but on  $\kappa = ka$ . So, we can rewrite the integral as

$$\lim_{N \rightarrow \infty} \frac{1}{N} \sum_k F(k) = \frac{1}{\pi} \int_{-\pi}^{+\pi} F(\kappa) d\kappa. \quad (2.20)$$

From now on we call the vector  $\kappa$  just  $k$  and assume that it always belong to the interval  $[-\pi; +\pi]$  (thus, we modify the first Brillouin zone definition). At this point we get rid of the lattice constant  $a$  completely.

In many cases  $F(k)$  depends on  $k$  through the energy  $\varepsilon$ . Using dispersion relation (2.8) we can change variables in the integral and write

$$\frac{1}{\pi} \int_{-\pi}^{+\pi} F(\varepsilon(k)) dk = \int_{-\infty}^{+\infty} D(\varepsilon) F(\varepsilon) d\varepsilon, \quad (2.21)$$

where we use the quantity  $D(\varepsilon)$ , which is called the density of states. It's defined as

$$D(\varepsilon) = \frac{1}{\pi} \frac{\partial k}{\partial \varepsilon} = \begin{cases} \frac{1}{\pi} [4\beta^2 - (\varepsilon - \mu)^2]^{-\frac{1}{2}}, & \varepsilon \in [\mu - 2\beta, \mu + 2\beta] \\ 0, & \varepsilon \notin [\mu - 2\beta, \mu + 2\beta] \end{cases}. \quad (2.22)$$

To find more details about it see [1].

### 2.1.2 Model of an isolated lead

As a model of the lead we adopt the half infinite tight binding chain (HITBC). The Hamiltonian of the HITBC in  $n$ -representation we get by "cutting it out" of the TBC Hamiltonian matrix (2.9). It's the half infinite tridiagonal matrix, which reads

$$H_l = \begin{pmatrix} \mu & \beta & & 0 \\ \beta & \mu & \beta & \\ & \beta & \mu & \beta \\ 0 & & \beta & \dots \end{pmatrix}. \quad (2.23)$$

Cutting the chain in this way is mathematically equivalent to the additional "fully reflecting" boundary condition which is applied at one end of the chain. Diagonalization task can be written as two equations containing energies  $\varepsilon$  and eigenvector components  $C_n^k$

$$\begin{aligned} (\varepsilon - \mu)C_1^k - \beta C_2^k &= 0 \\ (\varepsilon - \mu)C_n^k - \beta(C_{n-1}^k + C_{n+1}^k) &= 0, \quad (n = 2, 3, \dots) \end{aligned} \quad (2.24)$$

First of them is the new boundary condition. It's easy to check, that the solution which satisfy both equations is

$$C_n^k = \sin(kn). \quad (2.25)$$

And the dispersion relation  $\varepsilon(k)$  is again (2.8). Normalization of vectors  $C_n^k$  should be changed since

$$\lim_{N \rightarrow \infty} \frac{1}{N} \sum_{n=1}^N \sin(kn) \cdot \sin(k'n) = \frac{1}{2} \delta_{k',k} - \frac{1}{2} \delta_{k',-k}. \quad (2.26)$$

Properly normalized Bloch's wave for half infinite chain reads

$$|k\rangle = \sqrt{\frac{2}{N}} \sum_{n=1}^N \sin(kn) |n\rangle. \quad (2.27)$$

One more consequence of the new boundary condition, which is reflected in the limit (2.26), is that states which are characterized by vectors  $k$  and  $-k$  becomes linearly dependent. It makes usage of the first Brillouin zone for  $k$  the bad choice. Instead of it we have to adopt another elementary cell in  $k$ -space, like, for example, the interval  $[0; 2\pi]$ .

The Hamiltonian (2.23) can be written in the  $\{|n\rangle\}$  basis as

$$H_l = \sum_{n=1}^N |n\rangle\mu\langle n| + \sum_{n=1}^N |n\rangle\beta\langle n+1| + \sum_{n=2}^N |n\rangle\beta\langle n-1|. \quad (2.28)$$

But it's easier to work with  $H_l$  in  $k$ -representation, since it's diagonal there

$$H_l = \sum_k |k\rangle\varepsilon_k\langle k| \quad (2.29)$$

( $\varepsilon_k$  is given by the formula (2.8)). To transform the  $H_l$  we may multiply it from both sides by the closure relation  $I = \sum_k |k\rangle\langle k|$  and use the explicit expression for matrices  $\langle n|k\rangle$ .

Another way to write  $H_l$  is to use the second quantization representation. Passing through the standard transformation procedure (which we omit here) we get

$$H_l = \sum_k \varepsilon_k c_k^\dagger c_k, \quad (2.30)$$

where operators  $c_k$  and  $c_k^\dagger$  annihilate and create electrons with quasimomentum  $k$  in the lead. There is a conceptual difference between (2.29) and (2.30), since (2.29) defines the behavior of one electron, while (2.30) acts in the Fock space and appears to be the many-electron Hamiltonian.

Fermionic creation/annihilation operators satisfy anticommutational relations

$$[c_k, c_{k'}^\dagger]_+ = c_k c_{k'}^\dagger + c_{k'}^\dagger c_k = \delta_{kk'}. \quad (2.31)$$

Later we will also need the time evolution of this operators in Heisenberg picture. One can write, by definition

$$c_k(t) = e^{+iH_l t} c_k e^{-iH_l t} \quad (2.32)$$

(where  $c_k = c_k(0)$ ). To calculate it explicitly first we need the time derivative

$$\frac{\partial}{\partial t} c_k(t) = -i e^{+iH_l t} [c_k, H_l] e^{-iH_l t} \quad (2.33)$$

and commutator

$$[c_k, H_l] = \varepsilon_k c_k. \quad (2.34)$$

Next they can be combined to write the differential equation for  $c_k(t)$

$$\frac{\partial}{\partial t} c_k(t) = -i \varepsilon_k c_k(t). \quad (2.35)$$

Solving it we get the desired formulas

$$c_k(t) = c_k e^{-i\varepsilon_k t}, \quad c_k^\dagger(t) = c_k^\dagger e^{+i\varepsilon_k t} \quad (2.36)$$

(the formula for the creation operator  $c_k^\dagger$  is obtained using the hermitian conjugation).

### 2.1.3 Junction Hamiltonian partitioning

Molecular junction consist of two metallic electrodes and a molecular bridge connected between them. Thus, the whole Hamiltonian can be divided to the bridge, leads and coupling parts

$$H = H_s + H_l + H_{sl}. \quad (2.37)$$

Index "s" is used in this work to denote the molecular bridge. It comes from more general "system"+"reservoir" notations. To address a certain lead, when it's necessary, we divide leads part  $H_l$  to the left and right lead Hamiltonians

$$H_l = H_{ll} + H_{rl}. \quad (2.38)$$

And the same with coupling

$$H_{sl} = H_{s,ll} + H_{s,rl}. \quad (2.39)$$

Only lead parts are completely specified at a moment. We don't need to know much about other parts now, since formalism, described in the present chapter is quite general. Moreover, it's useful to have in mind, that we deal only with one-level bridges in this work. Or, in other words, there is only one electron level on the bridge, which can be used by electrons to tunnel through it. Thus, we can introduce fermionic operators  $d^\dagger$  and  $d$  which create and annihilate electron on the bridge and write the general expression for coupling part  $H_{sl}$  as

$$H_{sl} = \sum_k V_{dk} (d^\dagger c_k + c_k^\dagger d), \quad (2.40)$$

assuming that the coupling coefficients  $V_{dk}$  are real (which is always the case in this work). Expression (2.40) is used at the end of the chapter to derive the general formula for the current. In addition to this, bridge Hamiltonian  $H_s$  contains internal

vibrational and rotational degrees of freedom, so do the coupling  $H_{sl}$  (through the coupling coefficients  $V_{dk}$ ). The next chapter is fully dedicated to the discussion of different bridge models and forms of coupling.

As it was already mentioned in the previous section the structure of the state space is different in one electron formulation and in the second quantization representation, where the Fock space is implied. We use the one electron formulation in the scattering approach (see the section 2.2). In this case electronic spaces  $\kappa_s$ ,  $\kappa_{ll}$  and  $\kappa_{rl}$  which correspond to the bridge, left lead and right lead respectively can be considered separately. Direct sum of this spaces gives the molecular junction electronic space  $\kappa_{el} = \kappa_{ll} \oplus \kappa_s \oplus \kappa_{rl}$ . To take into account intramolecular vibrations electronic space  $\kappa_{el}$  should be multiplied with the space  $\kappa_{vib}$  which incorporates vibrational degrees of freedom to the system, i.e.  $\kappa = \kappa_{el} \otimes \kappa_{vib}$ . The basis in  $\kappa_{el}$  is  $\{|n\rangle\}$ . Its basis vectors can be sorted into three groups, corresponding to the left lead, bridge and the right lead. According to this partitioning concept all operators in  $n$ -representation can be divided to nine blocks. For example, the "free" Hamiltonian

$$H_0 = H_{ll} + H_s + H_{rl} = \begin{pmatrix} H_{ll} & 0 & 0 \\ 0 & H_s & 0 \\ 0 & 0 & H_{rl} \end{pmatrix} \quad (2.41)$$

represents three isolated systems. And the  $H_{sl}$  which couples parts together reads

$$H_{sl} = \begin{pmatrix} 0 & V_l & 0 \\ V_l^\dagger & 0 & V_r^\dagger \\ 0 & V_r & 0 \end{pmatrix}. \quad (2.42)$$

(we have denoted blocks of  $H_{sl}$  by  $V$  matrices). Assuming, that leads can't interact directly, but only through the bridge, (2.42) is the most general form of coupling. We are going to apply similar partitioning to other operators, like, for example the  $T$ -operator or Green's operator to derive scattering theory approach formulas in the section 2.2.

In the master equation approach (see the section 2.3) the many-electron formulation is used. In this case we denote the Fock space of the junction by  $\mathcal{F}$ . Assuming that many-electron spaces of leads and bridge are  $\mathcal{F}_l$  and  $\mathcal{F}_s$  and the vibrational

space is denoted as  $\mathcal{F}_{vib}$ , the full space  $\mathcal{F} = \mathcal{F}_s \otimes \mathcal{F}_l \otimes \mathcal{F}_{vib}$ . This structure of the space obviously differs from  $\kappa$  since it allows an arbitrary amount of electrons which can occupy states at the bridge and in leads at the same time.

Dividing of the whole system to the "continuum" with well known structure (leads) and "resonance", which is in our case represented by the molecular bridge we come to the concept of the Feshbach-Fano partitioning which is widely used in scattering theory (see [6]). Without direct introduction of projection operators we implicitly use the approach in the section 2.2 applying the principle described here. Projection superoperators technique, which is again the similar idea, is used explicitly to derive the master equation in the section 2.3.

## 2.2 Scattering approach

### 2.2.1 Landauer formula

The Landauer formula expresses a current through a transmission function  $\omega(E)$  of the molecular bridge. It's a function of energy<sup>1</sup> which gives the probability for an electron to pass through the bridge. In the elastic case the Landauer formula reads

$$I = \frac{1}{2\pi} \int \omega(E)[f_l(E) - f_r(E)]dE. \quad (2.43)$$

Atomic units are assumed here and everywhere in this thesis. In the formula (2.43) two electron fluxes, which pass through the bridge in two opposite directions, are summed. When energy is fixed, electron flux, which passes the bridge from the left lead to the right

$$i(E) = \frac{1}{2\pi} \omega(E)f_l(E) \quad (2.44)$$

is proportional to the probability to find an electron with this energy in the left lead, which is defined by the Fermi-Dirac distribution

$$f(\varepsilon) = \frac{1}{1 + e^{\frac{\varepsilon - \mu}{kT}}}. \quad (2.45)$$

---

<sup>1</sup> $E$  is a full energy of the system. In the elastic transport case it coincide with the energy of tunneling electron. In both elastic and nonelastic tunneling events  $E$  is conserved.

Thus, leads are assumed to be in the thermal equilibrium all the time. Formula (2.43) also demonstrates, that if the energy  $E$  is fixed, transmission probabilities for both tunneling directions are equal, which is true in the elastic transport regime. Formula (2.43) is well tested and works in a case of coherent transport, but it can fail in non coherent case, where it should be modified [5].

Using the scattering theory formalism, transmission probability  $\omega(E)$  can be easily expressed in terms of the  $T$ -matrix of the bridge [48]

$$\omega(E) = 4\pi^2 \sum_{l,r} |t(r \leftarrow l)|^2 \delta(\varepsilon_l - E) \delta(\varepsilon_r - E). \quad (2.46)$$

According to [46], probability of a scattering event is equal to the corresponding  $S$ -matrix element squared. Interrelation of  $S$ - and  $T$ - matrices leads to the formula (2.46). The sum runs through all in- and out-states which belong to different (left or right) leads. Delta functions under the sum express the energy conservation law: energy  $E$  should coincide with the output electron energy  $\varepsilon_r$  and the input energy  $\varepsilon_l$  which belong to the conduction bands in the right and left lead respectively.

Situation is a bit more complicated when the transport is inelastic. In this case  $T$ -matrix  $t(r, m' \leftarrow l, m)$  depends also on initial and final vibrational states  $m$  and  $m'$  of the bridge and transmission from the left lead to the right reads

$$\omega_{mm'}^{r \leftarrow l}(E) = 4\pi^2 \sum_{lr} |t(r, m' \leftarrow l, m)|^2 \delta(\varepsilon_l + E_m - E) \delta(\varepsilon_r + E_{m'} - E), \quad (2.47)$$

where  $E_m$  and  $E_{m'}$  are initial and final vibrational states energies. They participate in the inelastic energy conservation law which reads  $E = \varepsilon_l + E_m = \varepsilon_r + E_{m'}$ . Transmission function for electrons tunneling from the right lead to the left is not equal to (2.47), but, according to the principle of microscopic reversibility  $\omega_{mm'}^{r \leftarrow l} = \omega_{m'm}^{l \leftarrow r}$ .

In inelastic transport regime we use the modified Landauer formula ([48])

$$I = \frac{1}{2\pi} \int dE \sum_{mm'} P_m \left\{ \omega_{mm'}^{r \leftarrow l}(E) f_l(E - E_m) [1 - f_r(E - E_{m'})] - \omega_{mm'}^{l \leftarrow r}(E) f_r(E - E_m) [1 - f_l(E - E_{m'})] \right\}, \quad (2.48)$$

where, to compare with (2.43), the sum over all possible nuclear transitions is added. Additional Fermi-Dirac factors are there to take into account the fact, that the final

electron state shouldn't be occupied to make a tunneling event possible. Molecular bridge is assumed to be in equilibrium and its vibrational states are populated according to the Boltzmann distribution

$$P_m = \frac{e^{-E_m/kT}}{\sum_m e^{-E_m/kT}}. \quad (2.49)$$

This assumption doesn't allow to take into account indirect electron interactions (when electrons exchange their energy through the bridge excitations). We thus assume that the average time between two subsequent electron scattering events is longer than the relaxation time for the vibrations due to interactions with some external bath (not included explicitly in the Hamiltonian) It is a reasonable approximation if the molecule is strongly coupled to the heat bath. Otherwise, more detailed description should be considered to get more realistic vibrational populations. One possible enhancement of the scattering theory approach is discussed in the chapter 5.

### 2.2.2 Transmission probability

Transmission probability in the formulas (2.46) and (2.47) is expressed through the  $T$ -matrix elements. According to the partitioning principle, which was described in the section 2.1.3,  $T$ -operator<sup>2</sup> can be written as

$$T = \begin{pmatrix} T_{11} & T_{12} & T_{13} \\ T_{21} & T_{22} & T_{23} \\ T_{31} & T_{32} & T_{33} \end{pmatrix}. \quad (2.50)$$

To calculate a certain element of the  $T$ -matrix we need to specify initial and final scattering states. Moreover, we are interested only in those scattering processes, which start in one lead and finish in the other one, since only this processes contribute to the current. In other words we can say that initial and final states belong to the different spaces. For left to right tunneling, for example, we can write those

---

<sup>2</sup>Following the scattering theory tradition the  $T$ -matrix and the  $T$ -operator are denoted with small and capital letters respectively.

states as

$$|\text{in}\rangle = \begin{pmatrix} |l\rangle \\ 0 \\ 0 \end{pmatrix}, \quad \langle \text{out}| = \left( 0 \quad 0 \quad \langle r| \right), \quad (2.51)$$

where vector  $|l\rangle$  belongs to the space  $\kappa_{ll} \otimes \kappa_{vib}$  and vector  $\langle r|$  to the space  $\kappa_{rl} \otimes \kappa_{vib}$ . Performing the block multiplication, for the relevant  $T$ -matrix elements we get

$$t(r \leftarrow l) = \langle \text{out}|T|\text{in}\rangle = \langle r|T_{31}|l\rangle. \quad (2.52)$$

Thus, we need not the whole  $T$ -operator, but only the block  $T_{31}$ .

Practically it's more convenient to work not with the  $T$ -operator of the junction, but with it's Green's operator  $G$ . This two operators contain the same information about the system ([46]). They are connected by definition through the coupling operator

$$T = H_{sl} + H_{sl}GH_{sl}. \quad (2.53)$$

Substituting this definition to the previous equation and using the coupling partitioning (2.42) to perform the block multiplication we get

$$t(r \leftarrow l) = \langle r|V_r G_{22} V_l^\dagger |l\rangle. \quad (2.54)$$

And again we are interested not in the whole Green's operator, but only in it's part. Being written as a matrix in  $n$ -representation,  $G_{22}$  becomes a square finite dimensional matrix. It happens because  $G_{22}$  belongs to the molecular bridge space  $\kappa_s \otimes \kappa_{vib}$  which has a finite number of electronic states<sup>3</sup> or, in other words, it is spatially limited. It's a great computational advantage to compare with  $T_{31}$  which is presented by the half infinite matrix.

### 2.2.3 Green's function of the bridge

Green's operator of the molecular junction is defined as

$$G^R(E) = [(E + i\eta)I - H]^{-1}, \quad (2.55)$$

---

<sup>3</sup>In this work we always consider just one electronic state at the bridge

where  $H$  is the full Hamiltonian of the junction. The usual infinitesimal imaginary term  $i\eta$  where  $\eta \rightarrow +0$  is used to distinguish the retarded Green's operator. Another possible choice  $\eta \rightarrow -0$  would lead to the advanced Green's operator, which is the Hermitian conjugate of (2.55):  $G^A = [G^R]^\dagger$ . We are going to use only the retarded Green's operator and omit the index  $R$  in what follows. By definition operator  $G$  satisfies the equation  $[(E + i\eta)I - H]G = I$ , where  $I$  is the unit operator.

According to the formulas (2.41) and (2.42) the Hamiltonian  $H = H_0 + H_{sl}$  of the junction reads

$$H = \begin{pmatrix} H_{ll} & V_l & 0 \\ V_l^\dagger & H_s & V_r^\dagger \\ 0 & V_r & H_{rl} \end{pmatrix}. \quad (2.56)$$

Using this partitioning, the equation for the Green's operator can be written as

$$\begin{pmatrix} (E + i\eta)I - H_{ll} & -V_l & 0 \\ -V_l^\dagger & EI - H_s & -V_r^\dagger \\ 0 & -V_r & (E + i\eta)I - H_{rl} \end{pmatrix} \cdot \begin{pmatrix} G_{11} & G_{12} & G_{13} \\ G_{21} & G_{22} & G_{23} \\ G_{31} & G_{32} & G_{33} \end{pmatrix} = I. \quad (2.57)$$

We don't add any complex terms in the central block of the first matrix in purpose. It will be obvious later that it doesn't make any changes there. From all the equations we choose those 3, which contain the relevant part  $G_{22}$

$$\begin{aligned} [(E + i\eta)I - H_{ll}]G_{12} - V_l G_{22} &= 0, \\ -V_l^\dagger G_{12} + [EI - H_s]G_{22} - V_r^\dagger G_{32} &= I, \\ -V_r G_{22} + [(E + i\eta)I - H_{rl}]G_{32} &= 0. \end{aligned} \quad (2.58)$$

We express the blocks  $G_{12}$  and  $G_{32}$  from the 1st and 3rd equations and substitute them to the second equation for  $G_{22}$ . At the same time we notice, that the quantities

$$\begin{aligned} g_l &\equiv [(E + i\eta)I - H_{ll}]^{-1}, \\ g_r &\equiv [(E + i\eta)I - H_{rl}]^{-1} \end{aligned} \quad (2.59)$$

are, by definition, Green's operators for isolated left and right leads. The equation for  $G_{22}$  reads

$$-V_l^\dagger g_l V_l G_{22} + [EI - H_s]G_{22} - V_r^\dagger g_r V_r G_{22} = I. \quad (2.60)$$

Introducing new notations

$$\begin{aligned} \Sigma_l &\equiv V_l^\dagger g_l V_l, \\ \Sigma_r &\equiv V_r^\dagger g_r V_r, \end{aligned} \quad (2.61)$$

$G_{22}$  can be expressed from (2.60) in the form

$$G_{22} = [(EI - H_s) - \Sigma_l - \Sigma_r]^{-1}. \quad (2.62)$$

Technically, expression (2.62) is appropriate for the numerical treatment, since it assumes an inversion of the finite-dimensional matrix.

The  $G_{22}$  block is the part of the whole Green's operator of the junction, which correspond to the molecular bridge. To compare with the Green's operator of the isolated bridge

$$G_{22}^0 = [EI - H_s]^{-1}, \quad (2.63)$$

operator (2.62) contains the quantities  $\Sigma_l$  and  $\Sigma_r$  which are called self energies. They represent the influence of the leads. Self-energy of the lead possess information about isolated lead itself through it's Green's operator  $g_\alpha$  and, also, about the way, how it is connected to the bridge, through the coupling matrices  $V_\alpha$  ( $\alpha = l, r$ ). Influence of the leads is additive: we can remove one of them or add one, it will appear as additional term in (2.62).

At the end we get a scheme which includes the calculation of self-energies of the leads using formula (2.61) and the bridge's Green's operator (2.62) to compute the  $T$ -matrix (2.54). Subsequently formulas (2.46) and (2.43) can be used to calculate the current in the case of elastic transport regime and formulas (2.47) and (2.48) in inelastic case. The details of application of this scheme to the particular models are discussed in the chapter 4.

## 2.3 Master equation approach

The master equation (ME) theory is quite a general approach to describe an open quantum systems in nonequilibrium, when a whole system can be divided to a reservoir and a small system under interest. Such small system, in our case, is the molecular bridge. It's connected to two solid leads with infinite number of electronic degrees of freedom and can exchange electrons with them. Each lead is assumed to be in equilibrium with its own chemical potential. It provides a voltage across the junction and, thus, absence of equilibrium at the molecular bridge. Such a partitioning of the junction is expressed in the Hamiltonian structure (2.37).

In this formalism a reduced density matrix (RDM) concept, introduced by Paul Dirac in 1930, is used to describe a quantum state of an open system ([3]). If we denote the full density matrix (DM) of the system by  $R$ , RDM is defined by the equation

$$\rho \equiv \text{Tr}_l[R], \quad (2.64)$$

where partial trace should be taken through the degrees of freedom of the leads.

Time evolution of the DM is governed by the von Neumann equation

$$\frac{\partial}{\partial t} R(t) = -i[H, R(t)]. \quad (2.65)$$

Similar equation for RDM is called ME. Since we are interested mainly in the state of the bridge, which is given by RDM, the full density matrix  $R$  practically contains unnecessary information about the leads state. Moreover, there are no chances to solve the von Neumann equation for systems considered here, since the unknown  $R(t)$  is an infinite dimensional matrix. On the other hand, ME can be effectively treated numerically and for some simple models analytically. Standard ME approach ([27, 31, 17]) is a quite common method to treat the charge transport phenomena in the weak coupling regime<sup>4</sup>.

### 2.3.1 Derivation of the WBR ME

Here we present one of the ways to derive the second order ME which is called Wangsness-Bloch-Redfield (WBR) ME. There are few other types listed in the work [47]. Superoperators will be used throughout the derivation, i.e. mapping which acts on operators and produce another operators. Only linear superoperators are used in this work. Being written in a basis they are presented by the 4th rank tensors. Superoperators act in the Fock space of the junction  $\mathcal{F}$ .

Let's define two superprojectors

$$PR(t) \equiv \rho_l \otimes \text{Tr}_l[R(t)] = \rho_l \otimes \rho(t), \quad (2.66)$$

and

$$Q = I - P. \quad (2.67)$$

---

<sup>4</sup>Coupling in this approach is treated perturbatively and it should be small

Here, as usual,  $I$  is a notation for the unit superoperator which maps every operator to itself and  $\rho_l$  is RDM of isolated leads. We assume it to be in equilibrium all the time, because weak interaction with a small system does not change its state. These superprojectors possess usual projector's properties  $P^2 = P$ ,  $Q^2 = Q$ ,  $PQ = 0$ .

Superoperator  $L$ , which is defined as

$$LR(t) \equiv [H, R(t)], \quad (2.68)$$

is also in use here. It allows to rewrite the von Neumann equation in the form

$$\frac{\partial}{\partial t} R(t) = -iLR(t), \quad (2.69)$$

with symbolical solution

$$R(t) = e^{-iL(t-t_0)} R(t_0). \quad (2.70)$$

We also assume the initial condition  $R(t_0) = \rho_l \otimes \rho_0$ . It means that  $PR(t_0) = R(t_0)$  and  $QR(t_0) = 0$ . Of course in some arbitrary moment of time  $R(t) \neq \rho_l \otimes \rho(t)$  and  $QR(t) \neq 0$ . It would be so, if system and reservoir parts would be independent.

Superprojectors can be used to rewrite eq. (2.69) as

$$\begin{aligned} P\dot{R} &= -iPLPR - iPLQR, \\ Q\dot{R} &= -iQLPR - iQLQR. \end{aligned} \quad (2.71)$$

To express  $QR(t) = u(t)$  from the second equation we solve the linear initial value problem

$$\begin{aligned} \dot{u}(t) + qu(t) &= \phi(t), \\ u(t) &= e^{-q(t-t_0)} u(t_0) + \int_{t_0}^t e^{-q(t-\xi)} \phi(\xi) d\xi, \end{aligned} \quad (2.72)$$

i.e.

$$QR(t) = e^{-iQLQ(t-t_0)} QR(t_0) - i \int_{t_0}^t e^{-iQLQ(t-\tau)} QLPR(\tau) d\tau. \quad (2.73)$$

To get the equation for  $PR$  we substitute this "solution" to the first equation in (2.71)

$$P\dot{R} = -iPLPR - iPLQe^{-iQLQ(t-t_0)} QR(t_0) - \int_{t_0}^t PLQe^{-iQLQ(t-\tau)} QLPR(\tau) d\tau. \quad (2.74)$$

Similar result is obtained in [47] using the Laplace transformation. Before this moment there were no approximations introduced and the equation is exact.

Having in mind logical partitioning of the whole system into the small bridge-system, leads and coupling (2.37), superoperator  $L$  can be partitioned (and it's easy to show) in a similar way  $L = L_s + L_l + L_{sl}$ . We will use properties

$$\begin{aligned} PL_s &= L_s P, \\ PL_l &= L_l P = 0, \\ PL_{sl} P &= 0, \end{aligned} \quad (2.75)$$

which can either be proved by reader or taken from the work [47]. With these properties equation can be slightly changed

$$\begin{aligned} \frac{\partial}{\partial t} PR &= -iPL_s PR - iPL_{sl} e^{-iQ(L_s+L_l+L_{sl})Q(t-t_0)} QR(t_0) \\ &\quad - \int_{t_0}^t PL_{sl} e^{-iQ(L_s+L_l+L_{sl})Q(t-\tau)} L_{sl} PR(\tau) d\tau. \end{aligned} \quad (2.76)$$

Second term at the right hand side disappears if we assume the initial condition  $t_0 = 0$ ,  $QR(t_0) = 0$ . Another step on the way of simplification is to expand the equation to the second order in  $L_{sl}$ . It brings in one of the main limitations of the ME approach, which obliges the coupling to be small. To leave only second order terms we have to remove  $L_{sl}$  from decomposition of exponent in the 3-rd term. After it we use the fact, that  $Q$  commute with  $L_s$  and  $L_l$  (it follows from the properties (2.75)) and remove  $Q$  from the exponent

$$\frac{\partial}{\partial t} PR = -iPL_s PR - \int_0^t PL_{sl} e^{-i(L_s+L_l)(t-\tau)} L_{sl} PR(\tau) d\tau. \quad (2.77)$$

Changing variables in the integral  $\tau \rightarrow t - \tau'$  and then switching back the notation  $\tau' \rightarrow \tau$  we get

$$\frac{\partial}{\partial t} PR = -iPL_s PR - \int_0^t PL_{sl} e^{-i(L_s+L_l)\tau} L_{sl} PR(t - \tau) d\tau. \quad (2.78)$$

Formula (2.70) is used to write

$$PR(t - \tau) = e^{iL\tau} PR(t) = e^{i(L_s+L_l+L_{sl})\tau} PR(t). \quad (2.79)$$

When we substitute it to the equation, second order requirement removes  $L_{sl}$  from this exponent. Part  $PR(t)$  can be moved out of the integral

$$\frac{\partial}{\partial t} PR = -iPL_s PR - \int_0^t PL_{sl} e^{-i(L_s+L_l)\tau} L_{sl} P e^{i(L_s+L_l)\tau} d\tau PR(t). \quad (2.80)$$

Next approximation comes to make the integral time-independent. We assume  $t \rightarrow \infty$  and write

$$\frac{\partial}{\partial t} PR = -iPL_s PR - \int_0^\infty PL_{sl} e^{-i(L_s+L_l)\tau} L_{sl} P e^{+i(L_s+L_l)\tau} d\tau PR(t). \quad (2.81)$$

This is called the Markov's approximation. It's useful to point here, that the Q-projection of DM at our level of approximation is

$$QR(t) = -i \int_0^\infty e^{-i(L_s+L_l)\tau} L_{sl} P e^{+i(L_s+L_l)\tau} d\tau PR(t). \quad (2.82)$$

It is used in the next section to derive the general formula for the current.

Using the property  $e^{-iL\tau} A = e^{-iH\tau} A e^{+iH\tau}$  and definitions of super operators  $L_{sl}$  and  $P$  we can rewrite the next fragment through the commutators as

$$e^{-i(L_s+L_l)\tau} L_{sl} P e^{+i(L_s+L_l)\tau} PR(t) = [e^{-i(H_s+H_l)\tau} H_{sl} e^{+i(H_s+H_l)\tau}, \rho(t) \otimes \rho_l]. \quad (2.83)$$

Using this, the last two equations can be modified

$$QR(t) = -i \int_0^\infty d\tau [e^{-i(H_s+H_l)\tau} H_{sl} e^{+i(H_s+H_l)\tau}, \rho(t) \otimes \rho_l], \quad (2.84)$$

$$\frac{\partial}{\partial t} \rho(t) \otimes \rho_l = -i[H_s, \rho(t) \otimes \rho_l] - P \int_0^\infty d\tau [H_{sl}, [e^{-i(H_s+H_l)\tau} H_{sl} e^{+i(H_s+H_l)\tau}, \rho(t) \otimes \rho_l]]. \quad (2.85)$$

The last thing to do here is to substitute the definition of the superprojector P. "Dividing" the equation to  $\rho_l$  we finally get the Wangsness-Bloch-Redfield master equation

$$\frac{\partial}{\partial t} \rho(t) = -i[H_s, \rho(t)] - \text{Tr}_l \int_0^\infty d\tau [H_{sl}, [e^{-i(H_s+H_l)\tau} H_{sl} e^{+i(H_s+H_l)\tau}, \rho(t) \otimes \rho_l]], \quad (2.86)$$

like it's defined in [47]

Analogically to the von Neumann equation (2.69) for full DM, we can write ME for RDM in the form

$$\frac{\partial}{\partial t}\rho(t) = \mathcal{L}\rho(t), \quad (2.87)$$

where the right hand side of the equation is denoted by the superoperator  $\mathcal{L}$ . It acts to operators in the bridge variables space. As we can see from (2.86) it consists of two terms which we denote  $\mathcal{L} = \mathcal{L}_0 + \mathcal{L}_1$ . If the molecule is disconnected from the leads  $\mathcal{L}_1 = 0$  and the system's time evolution is governed by  $\mathcal{L}_0$ , or, in other words, by the Hamiltonian  $H_s$ . In this case equation (2.86) coincide with the von Neumann equation for the isolated molecular bridge. It's straightforward to deduce, that the term  $\mathcal{L}_1$  incorporates the influence of the leads.

If we have few reservoirs in the ME, their impact to the equation is additive. It means, that we can add  $\alpha$  reservoirs and each of them appears as an additional term  $\mathcal{L}_{1,\alpha}$  in the equation. Since we have two leads, which are, actually, independent reservoirs (they can't interact directly), we can split the leads part  $\mathcal{L}_1$  to the left and right lead terms

$$\mathcal{L}_1 = \mathcal{L}_{1,l} + \mathcal{L}_{1,r}. \quad (2.88)$$

Each of them is of the same form as in the equation (2.86). But instead of operators  $H_l$  and  $H_{sl}$ , which describe the total energy of leads and both couplings, we should take analogical operators for one specific (left or right) lead.

The solution of the equation (2.86) gives the time evolution of the RDM  $\rho(t)$ . We are more interested in a state of the system after some large amount of time, when it reaches its stationary value and doesn't change anymore. For this reason, in practice, we solve not the equation (2.86), but the equation

$$\mathcal{L}\rho(\infty) = 0 \quad (2.89)$$

to determine the stationary RDM.

### 2.3.2 Current and other observables

DM of the whole system  $R$  completely describes it's state. Mean value of any observable  $O$  can be calculated using the formula

$$\langle O \rangle = \text{Tr} [RO]. \quad (2.90)$$

If  $O$  exclusively belongs to the bridge variables space the similar formula can be used but with RDM instead of DM. It is the case for all observables of interest in this work (like, for example, the angular momentum, which is important for motor models), except of the current, since its operator contains leads variables as well.

Particle's current is the number of particles, which passes through one of the leads per unit of time. To be specific we chose the left lead<sup>5</sup> Thus, the mean value of the current reads

$$I = \left\langle \frac{dN_{ll}}{dt} \right\rangle, \quad (2.91)$$

where

$$N_{ll} = \sum_k c_k^\dagger c_k \quad (2.92)$$

is the number of particles operator for the left lead. Using the equation (2.65) and calculating commutator we write

$$I = -i \langle [H, N_{ll}] \rangle = -i \left\langle \sum_k V_{dk} (d^\dagger c_k - c_k^\dagger d) \right\rangle. \quad (2.93)$$

Now we use the formula (2.90) to write

$$I = -i \text{Tr} \left\{ R \sum_k V_{dk} (d^\dagger c_k - c_k^\dagger d) \right\}. \quad (2.94)$$

It's time to remember about superprojectors and write DM as  $R = PR + QR$ .  $PR = \rho \otimes \rho_l$  doesn't contribute to the current, since after substitution terms  $\text{Tr}_l(\rho_l c_k) = \text{Tr}_l(\rho_l c_k^\dagger) = 0$ . Using expression (2.84) for  $QR$  we get

$$I = - \int_0^\infty d\tau \text{Tr} \{ [e^{-i(H_s + H_l)\tau} H_{sl} e^{+i(H_s + H_l)\tau}, \rho(t) \otimes \rho_l] \sum_k V_{dk} (d^\dagger c_k - c_k^\dagger d) \}, \quad (2.95)$$

which is the general formula for the current in the ME approach. It is general enough to cover all one level model bridges in this work. In a case of necessity the generalization to many level bridges is straightforward (reader can find it, for example, in [17]).

---

<sup>5</sup>All operators without lead specification index further in this section are assumed to belong to the left lead.

# Chapter 3

## Models of the molecular junction

In this chapter we describe in details 4 different models of molecular junctions for the future discussion. Model 1 represents a junction with the purely elastic electron transport mechanism, i.e. without energy exchange between electronic and nuclear degrees of freedom of the molecule. It's an important limiting case for more complicated models, where electron-phonon interaction is taken into account. Moreover, charge transport equations for the model 1 can be solved analytically and, thus, it's interesting from theoretical point of view. For example it allows to formulate mathematically the limit, when the scattering and master equation approach calculations coincide. In the model 2 the harmonic approximation is used to include a vibrational degree of freedom of the molecule, which participate in the electron-phonon interaction. Formulae for current in the model 2 are used to outline principle differences between ME and scattering approaches in the chapter 5. It helps to formulate one possible improvement, which makes scattering approach more accurate in the inelastic regime. All together models 1 and 2 provide a good basis for comparison of two approaches. They also provide a good ground to make a step beyond the harmonic approximation. Models 3 and 4 are formulated to study the motor effect. In the model 3 we want to capture the basic features of usual models for study of a molecular conduction junction coupled to vibrations (like, for example, the model 2), but to allow for large amplitude anharmonic motion. The model 4 is motivated by more realistic parameters expected for real molecular systems. Both models are divided to few "submodels" to investigate the influence of different types of coupling

symmetry to the conductive and rotational properties of junctions.

### 3.1 Elastic bridge (model 1)

To construct the simplest possible model of the molecular junction we remove the atom with  $n = 0$  from the tight binding chain (TBC) in the fig. 2.1 and put another atom of different type (impurity) on it's place, like it's depicted in the fig. 3.1<sup>1</sup>. The corresponding Hamiltonian matrix in the  $n$ -representation reads

$$H = \begin{pmatrix} \cdots & \beta_1 & & & & \\ \beta_1 & \mu_l & \beta_2 & & & \\ & \beta_2 & \varepsilon_0 & \beta_2 & & \\ & & \beta_2 & \mu_r & \beta_1 & \\ & & & \beta_1 & \cdots & \end{pmatrix}. \quad (3.1)$$

Despite its simplicity, the model is very important from theoretical point of view. It's analytically solvable in both scattering and ME approaches and provides a basis for discussion and comparison. The atom of impurity plays a role of the molecular bridge, which contains one electronic level with energy  $\varepsilon_0$ , available for tunneling, and no internal degrees of freedom. Changing the notation of the basis vector  $|n = 0\rangle$  to  $|d\rangle$ , bridge's Hamiltonian reads

$$H_s = |d\rangle\varepsilon_0\langle d|. \quad (3.2)$$

Leads, as always in this work, are presented by two half-infinite tight binding chains (HITBC). Their Hamiltonian in  $k$ -representation reads

$$H_l = \sum_{k\alpha} |k\alpha\rangle\varepsilon_{k\alpha}\langle k\alpha|, \quad (3.3)$$

where  $\alpha = l, r$  is used to distinguish left and right lead. Chemical potential  $\mu_\alpha$  is in general different for different leads. When we speak about a voltage  $U$ , applied to the junction, we assume  $\mu_l = +\frac{V}{2}$  and  $\mu_r = -\frac{V}{2}$ .

---

<sup>1</sup>We also assume that chemical potentials can be different from both sides of the impurity

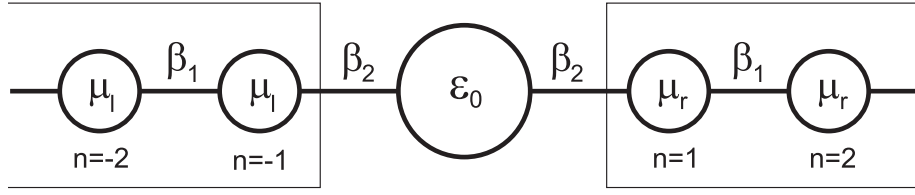


Figure 3.1: Infinite one dimensional tight-binding chain with impurity may be considered as a simplest example of the molecular junction

The bridge state  $|d\rangle$  is connected to the leads through its nearest neighbors, i.e. lead states  $|n\rangle$  where  $n = \pm 1$ , with coupling strength  $\beta_2$

$$H_{sl} = |d\rangle\beta_2\langle 1| + |1\rangle\beta_2\langle d| + |d\rangle\beta_2\langle -1| + |-1\rangle\beta_2\langle d|. \quad (3.4)$$

Or, equivalently, switching from  $n$ - to  $k$ -representation

$$H_{sl} = \sum_{k\alpha} |d\rangle V_{dk}\langle k\alpha| + |k\alpha\rangle V_{dk}\langle d|, \quad (3.5)$$

where we have introduced coupling coefficients

$$V_{dk} = \beta_2\langle 1|k\alpha\rangle = \sqrt{\frac{2}{N}}\beta_2 \sin(k). \quad (3.6)$$

Using the leads creation/annihilation operators  $c_{k\alpha}^\dagger$  and  $c_{k\alpha}$  which were introduced in the previous chapter and similar operators for the bridge  $d^\dagger$  and  $d$ , which were also mentioned there, we can write the whole junction Hamiltonian  $H = H_s + H_l + H_{sl}$  for the model 1 in the second quantization representation

$$\begin{aligned} H_s &= \varepsilon_0 d^\dagger d, \\ H_l &= \sum_{k\alpha} \varepsilon_{k\alpha} c_{k\alpha}^\dagger c_{k\alpha}, \\ H_{sl} &= \sum_{k\alpha} V_{dk} \left( d^\dagger c_{k\alpha} + c_{k\alpha}^\dagger d \right). \end{aligned} \quad (3.7)$$

Operators  $d$  and  $d^\dagger$  are fermionic operators and, thus, satisfy commutation relations

$$[d, d^\dagger]_+ = dd^\dagger + d^\dagger d = 1. \quad (3.8)$$

It's useful to mention here, that their products, i.e. operators  $d^\dagger d$  and  $dd^\dagger$ , form a complete set of orthogonal projectors. We denote  $Q = d^\dagger d$ ,  $P = dd^\dagger$  and notice that  $P + Q = 1$ ,  $P^2 = P$ ,  $Q^2 = Q$ ,  $PQ = QP = 0$ . It means that they have also some other useful properties of projectors, which will be used later. For example if  $A$  and  $B$  are some operators and  $[A, P] = [B, P] = [A, Q] = [B, Q] = 0$ , then

$$e^{AP} = e^A P + Q, \quad (3.9)$$

$$e^{AP+BQ} = e^A P + e^B Q, \quad (3.10)$$

as it can easily be proved decomposing the exponent to the Taylor series.

In the case of just one electronic state on the bridge (which is always the case in this thesis) the structure of its Fock space is quite simple. The space is spanned on two basis vectors  $|0\rangle$  and  $|1\rangle$ , which correspond to unoccupied and occupied bridge. In this basis creation and annihilation operators can be written as

$$\begin{aligned} d^\dagger &= |1\rangle\langle 0|, & d &= |0\rangle\langle 1|, \\ d^\dagger d &= |1\rangle\langle 1|, & dd^\dagger &= |0\rangle\langle 0|. \end{aligned} \quad (3.11)$$

Any operator  $A$ , which acts inside the bridge space can be decomposed to four blocks

$$A = |0\rangle\langle 0|A|0\rangle\langle 0| + |0\rangle\langle 0|A|1\rangle\langle 1| + |1\rangle\langle 1|A|0\rangle\langle 0| + |1\rangle\langle 1|A|1\rangle\langle 1| \quad (3.12)$$

(it can be shown, multiplying  $A$  from both sides by the completeness relation  $I = |1\rangle\langle 1| + |0\rangle\langle 0|$ ). Or, which is equivalent

$$A = A_{00}dd^\dagger + A_{11}d^\dagger d + A_{01}d + A_{10}d^\dagger, \quad (3.13)$$

where  $A_{ij} \equiv \langle i|A|j\rangle$ . The RDM, for example, which is also an operator in the bridge space, can be presented as

$$\rho = \rho_{00}dd^\dagger + \rho_{11}d^\dagger d + \rho_{01}d + \rho_{10}d^\dagger. \quad (3.14)$$

This decomposition is widely used later in this work.

Presenting the calculations results for the model 1 in the chapter 5 we assume, if it's not stated differently, the following parametrization:  $\varepsilon_0 = 0.5$  eV,  $\beta_1 = 1.0$  eV,  $\beta_2 = 0.2$  eV,  $T = 10$  K.

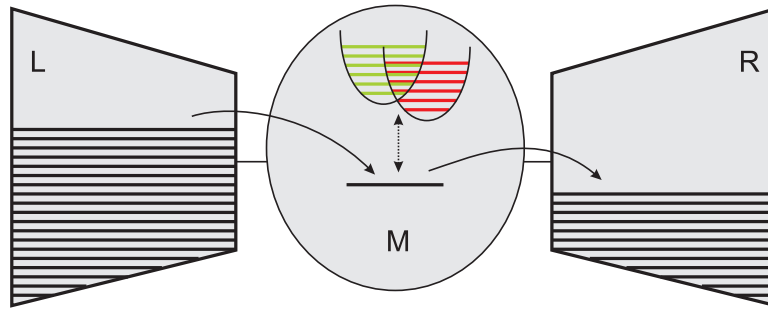


Figure 3.2: Schematic representation of the molecular junction in the model 2

## 3.2 Bridge with one harmonic vibrational mode (model 2)

To get a model of the molecular bridge with one vibrational mode we connect electronic state  $|d\rangle$  from the model 1 to the harmonic oscillator. It doesn't change the full junction Hamiltonian parts  $H_l$  and  $H_{sl}$ , which have the same form in models 1 and 2. The molecular part  $H_s$  is represented here with the so called independent boson model (see [30]). It reads

$$H_s = \varepsilon_0 d^\dagger d + \Omega a^\dagger a + \lambda(a + a^\dagger)d^\dagger d. \quad (3.15)$$

Harmonic oscillator with the frequency  $\Omega$  is governed by the bosonic operators  $a^\dagger$  and  $a$ , which create and annihilate a vibrational quantum (phonon) at the bridge. Parameter  $\lambda$  controls the strength of the electron-phonon interaction. Such models are often used (see, for example, [50]) to model the molecular bridges with harmonic vibrational mode. One of the advantages of this description is that the molecular Hamiltonian part  $H_s$  can be diagonalized analytically. Schematic representation of the junction in the model 2 is showed in the fig. 3.2. Vibrational mode is represented there by two parabolic potential energy curves, which correspond to the unoccupied and occupied molecular bridge (see the rest of this section for an explanation). Corresponding quantized vibrational energies are plotted with red and green lines.

Using commutation relation  $d^\dagger d + d d^\dagger = 1$  we can rewrite the molecular Hamiltonian part as

$$H_s = h_0 d d^\dagger + h_1 d^\dagger d, \quad (3.16)$$

where

$$h_0 = \Omega a^\dagger a, \quad h_1 = \Omega a^\dagger a + \lambda(a + a^\dagger) + \varepsilon_0. \quad (3.17)$$

Written in this way, it reflects the important fact: when an electron jumps from the lead to the molecular bridge, bridge changes its geometry. We can interpret  $h_0$  and  $h_1$  physically as full energies of unoccupied and occupied molecule respectively. All bridge Hamiltonians  $H_s$  in this work can be written in the form (3.16) (in the model 1, for example,  $h_0 = 0$  and  $h_1 = \varepsilon_0$ ). Assuming  $H_s$  to be in this form we may use definition

$$d(t) = e^{+iH_s t} d e^{-iH_s t} \quad (3.18)$$

to derive the general formula for the time evolution of  $d$ , which will be used later. Using property (3.10) we get

$$d(t) = e^{+ih_0 t} d e^{-ih_1 t}, \quad d^\dagger(t) = e^{+ih_1 t} d^\dagger e^{-ih_0 t}. \quad (3.19)$$

Since we explicitly know the expressions for creation/annihilation operators of the harmonic oscillator

$$\begin{aligned} a &= \sqrt{\frac{M\Omega}{2}} \left( x + \frac{i}{M\Omega} p \right), \\ a^\dagger &= \sqrt{\frac{M\Omega}{2}} \left( x - \frac{i}{M\Omega} p \right), \end{aligned} \quad (3.20)$$

Hamiltonians  $h_0$  and  $h_1$  can be rewritten in first quantization as

$$h_0 = \frac{p^2}{2M} + \frac{M\Omega^2}{2} x^2, \quad h_1 = \frac{p^2}{2M} + \frac{M\Omega^2}{2} x^2 + x\lambda\sqrt{2M\Omega} + \varepsilon_0. \quad (3.21)$$

Thus, we deal here with two potential energy curves which correspond to occupied and unoccupied molecules, and both of them have parabolic form. When the electron-phonon interaction is switched off, i.e.  $\lambda = 0$ , the shapes of the two potentials are identical, and the only difference between them is that the occupied bridge potential is shifted up by the energy  $\varepsilon_0$ . This logic works in the opposite direction: if the only difference between potentials of unoccupied and occupied bridges is vertical shift, molecular vibrations are decoupled from the electronic degree of freedom.

The Hamiltonian (3.15) can be diagonalized using the so called polaron transformation (see [30])

$$\bar{H} = e^S H e^{-S}, \quad (3.22)$$

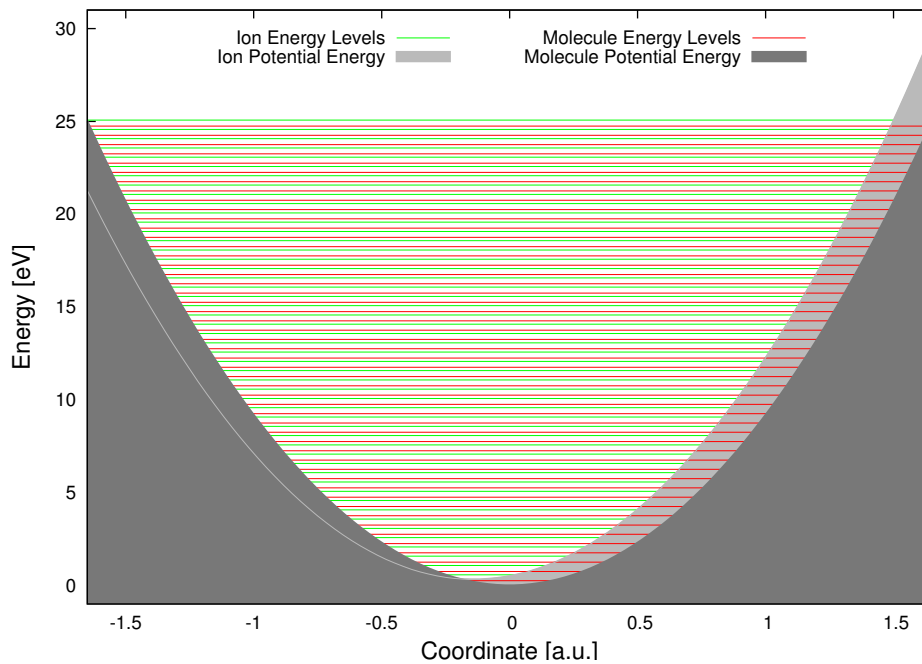


Figure 3.3: Potential energies of unoccupied and occupied bridge in model 2.

where

$$S \equiv d^\dagger d \frac{\lambda}{\Omega} (a^\dagger - a). \quad (3.23)$$

For future convenience we introduce also the operator

$$X = e^{-\frac{\lambda}{\Omega}(a^\dagger - a)}, \quad (3.24)$$

which is unitary, i.e.  $X^\dagger = X^{-1} \neq X$ . Transformed Hamiltonian reads

$$\bar{H} = (\Omega a^\dagger a) d d^\dagger + (\Omega a^\dagger a + \varepsilon_0 - \frac{\lambda^2}{\Omega}) d^\dagger d = h_0 d d^\dagger + (X^\dagger h_1 X) d^\dagger d. \quad (3.25)$$

To get the eigenstates of  $h_0$  and  $h_1$  the Schroedinger equations

$$\begin{aligned} h_0 |m\rangle &= E_m |m\rangle, \\ h_1 |v\rangle &= E_v |v\rangle \end{aligned} \quad (3.26)$$

must be solved. Notations for eigenfunctions and energies of  $h_0$  and  $h_1$ , which follows from (3.26), will be widely used in the thesis. We thus always reserve  $m$  for levels of the neutral molecule and  $m'$ ,  $m''$  are used if more than one different levels appear in the same formula. The same convention is used for the charged molecule states  $|v\rangle$ .

Hamiltonian  $h_0$  corresponds to the harmonic oscillator with frequency  $\Omega$  and mass  $M$ . Its wavefunctions  $\psi_m(x)$  and eigenenergies are well known

$$E_m = \Omega(m + 1/2),$$

$$\psi_m(x) = \sqrt{\frac{1}{2^m m!}} \left(\frac{M\Omega}{\pi}\right)^{1/4} \exp\left[-\frac{M\Omega x^2}{2}\right] H_m[x\sqrt{M\Omega}]. \quad (3.27)$$

To solve the second equation we transform it using the operator  $X$ :  $\bar{h}_1 = X^\dagger h_1 X$ . The solution of Schroedinger equation with Hamiltonian  $\bar{h}_1$  is easy to write (see (3.25)), and we transform it back using the same operator  $X$ . To perform the transformation we notice, that  $X$  acts as a shift operator  $\mathcal{T}$  in the coordinate space. Compare

$$\mathcal{T}(a) \equiv e^{-a\frac{\partial}{\partial x}}, \quad \mathcal{T}(a)\psi(x) = \psi(x - a) \quad (3.28)$$

and

$$X = e^{-\frac{\lambda}{\Omega}(a^\dagger - a)} = e^{\sqrt{\frac{2\lambda^2}{M\Omega^3}}\frac{\partial}{\partial x}}. \quad (3.29)$$

For an occupied molecule states we have expressions

$$E_v = \Omega(v + 1/2) + \varepsilon_0 - \frac{\lambda^2}{\Omega},$$

$$\psi_v(x) = X\psi_m(x) = \psi_m\left(x + \sqrt{\frac{2\lambda^2}{M\Omega^3}}\right), \quad (3.30)$$

where  $m = v$ . Thus, Hamiltonian  $h_1$ , to compare with  $h_0$ , describes the "shifted" oscillator. It's energies are shifted up by the value  $\varepsilon_0 - \frac{\lambda^2}{\Omega}$  and eigenfunctions are shifted to the left by  $\sqrt{\frac{2\lambda^2}{M\Omega^3}}$ . Potential energies for unoccupied and occupied molecular bridges together with quantized energy states are showed in the fig. 3.3. To parametrize the model 2 we use the following values:  $\lambda = 0.3$  eV,  $\Omega = 0.5$  eV,  $M = 2000$  a.u. Other parameters are the same as in the model 1.

Now, when the molecular bridge  $H_s$  is completely specified we may write the full Hamiltonian  $H$  of the junction

$$H = h_0 d d^\dagger + h_1 d^\dagger d + \sum_{k\alpha} \varepsilon_{k\alpha} c_{k\alpha}^\dagger c_{k\alpha} + \sum_{k\alpha} V_{dk\alpha} \left( d^\dagger c_{k\alpha} + c_{k\alpha}^\dagger d \right). \quad (3.31)$$

To apply the scattering theory approach to the model 2 we have to write the same Hamiltonian in the single electron formulation, i. e. in the  $\{|k\rangle, |d\rangle\}$  basis. As it can be verified by the direct projection of (3.31) on basis vectors  $|d\rangle \equiv d^\dagger|0\rangle$  and

$|k\rangle \equiv c_k^\dagger|0\rangle^2$ , single electron Hamiltonian reads

$$H = |d\rangle h_1 \langle d| + \sum_{k\alpha} |d\rangle V_{dk} \langle k\alpha| + |k\alpha\rangle V_{dk} \langle d| + \sum_{k\alpha} |k\alpha\rangle (\varepsilon_{k\alpha} + h_0) \langle k\alpha|. \quad (3.32)$$

Thus, we see that  $h_0$  is moved from  $H_s$  to  $H_l$  part. When electron belongs to the left or right lead, it automatically means, that it doesn't belong to the bridge. In this case bridge is unoccupied and governed by the  $h_0$  operator.

Overall Hamiltonian matrix in  $n$ -representation reads

$$H = \begin{pmatrix} \cdots & \beta_1 & & & & & \\ \beta_1 & \mu_l + h_0 & \beta_2 & & & & \\ & \beta_2 & h_1 & \beta_2 & & & \\ & & \beta_2 & \mu_r + h_0 & \beta_1 & & \\ & & & \beta_1 & \cdots & & \end{pmatrix} \quad (3.33)$$

To compare with the matrix (3.1) from the model 1, each element here is itself an operator in the vibrational space  $\kappa_{vib}$ .

### Overlap matrix

Overlaps  $\langle m|v\rangle$  between states of occupied and unoccupied bridge play an important role in charge transport theories. Motivated by molecular physics they are often referred to as Franck-Condon factors [53]. In the independent boson model framework this matrix can be calculated analytically.

Eigenstates of occupied bridge  $|v\rangle$  can be produced from corresponding eigenstates of unoccupied bridge, which we denote as  $|m'\rangle$ , using the  $X$ -transformation<sup>3</sup>

$$\langle m|v = m'\rangle = \langle m|X|m'\rangle = \langle m|e^{-\frac{\lambda}{\Omega}(a^\dagger - a)}|m'\rangle. \quad (3.34)$$

There is a theorem (see [30]) which says, that if commutator  $[A, B] = C$  commutes with both  $A$  and  $B$ , then

$$e^{A+B} = e^A e^B e^{-\frac{1}{2}[A,B]} \quad (3.35)$$

<sup>2</sup>Fock space vacuum state is denoted as  $|0\rangle$  here.

<sup>3</sup> $v$  and  $m'$  are equal numbers, but according to our convention we have to use different letters to distinguish between eigenstates of  $h_0$  and  $h_1$  operators.

We use this theorem to split the  $X$  operator. Since comutator

$$\left[-\frac{\lambda}{\Omega}a^\dagger, +\frac{\lambda}{\Omega}a\right] = \frac{\lambda^2}{\Omega^2} \quad (3.36)$$

itself commute with both terms under the exponent, we may write

$$X = e^{-\frac{\lambda}{\Omega}(a^\dagger - a)} = e^{-\frac{\lambda}{\Omega}a^\dagger} e^{+\frac{\lambda}{\Omega}a} e^{-\frac{\lambda^2}{2\Omega^2}}. \quad (3.37)$$

The overlap matrix reads

$$\langle m|v\rangle = e^{-\frac{\lambda^2}{2\Omega^2}} \langle m|e^{-\frac{\lambda}{\Omega}a^\dagger} e^{+\frac{\lambda}{\Omega}a}|m'\rangle \quad (3.38)$$

Decomposing the exponent

$$e^{+\frac{\lambda}{\Omega}a}|m'\rangle = \sum_{i=0}^{\infty} \left(\frac{\lambda}{\Omega}\right)^i \frac{1}{i!} a^i |m'\rangle \quad (3.39)$$

and applying the annihilation operator  $i$  times

$$a^i |m'\rangle = \begin{cases} \sqrt{\frac{m'!}{(m'-i)!}} |m'-i\rangle & \text{if } i \leq m' \\ 0 & \text{if } i > m' \end{cases}, \quad (3.40)$$

the following formula can be derived

$$e^{+\frac{\lambda}{\Omega}a}|m'\rangle = \sum_{i=0}^{m'} \left(\frac{\lambda}{\Omega}\right)^i \frac{1}{i!} \sqrt{\frac{m'!}{(m'-i)!}} |m'-i\rangle. \quad (3.41)$$

In a similar way we derive the formula for  $\langle m|e^{-\frac{\lambda}{\Omega}a^\dagger}$  and substitute them both to (3.38). At this point we also remember that  $m' = v$ . Final expression for the overlap matrix reads

$$\langle m|v\rangle = e^{-\frac{\lambda^2}{2\Omega^2}} \sum_{i=0}^v \sum_{j=0}^m \delta_{m-j, v-i} (-1)^j \left(\frac{\lambda}{\Omega}\right)^{i+j} \frac{1}{i!j!} \sqrt{\frac{m!v!}{(m-j)!(v-i)!}}. \quad (3.42)$$

### 3.3 Rotating bridge (models 3 and 4)

To build a bridge model with more interesting and realistic vibrational properties one have to go beyond the harmonic approximation. Developing the models 3 and 4 in this section we have in mind a molecular bridge schematically depicted in the fig. 3.4. Let's consider a molecule consisting of the chain of three aromatic rings. While two

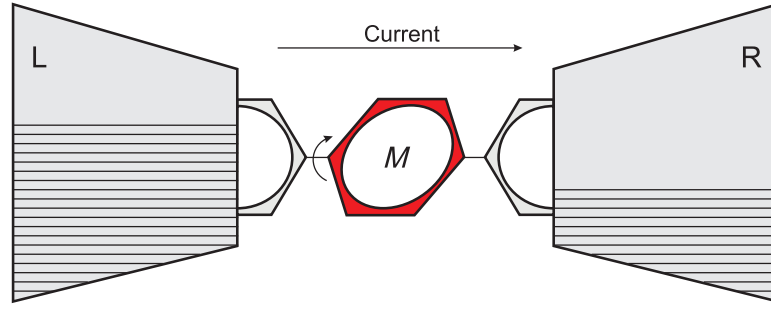


Figure 3.4: Schematic representation of a molecular junction with the bridge, which can perform rotational movement

side rings are connected to the electrodes, central ring can perform a rotational movement. There exist a number of works ([49], [11]), where torsional degrees of freedom of biphenyl-like molecules are investigated. Summarizing their experience we take a simple analytic yet rather general shape of potentials. Assuming the molecular bridge energy operator  $H_s$  in the form (3.16), unoccupied and occupied bridge Hamiltonians reads

$$\begin{aligned} h_0 &= -\frac{1}{2I} \frac{\partial^2}{\partial \varphi^2} + \varepsilon_0 + A_0 \cos(n_0 \varphi), \\ h_1 &= -\frac{1}{2I} \frac{\partial^2}{\partial \varphi^2} + \varepsilon_1 + A_1 \cos(\varphi + \varphi_1), \end{aligned} \quad (3.43)$$

where  $I$  is the moment of inertia of the rotor and  $\varphi$  is the angle of rotation (thus it belongs to the interval  $[0; 2\pi]$ ). Other coefficients define positions and amplitudes of the potentials.

Eigenstates and energies equations (3.26) can't be solved analytically for the models 3 and 4 (with cosinusoidal potentials mathematicians call them the Mathieu equations). Thus, numerics should be involved at early stages of calculation. Using the free rotor basis  $\{|n\rangle\}$  (see the table 3.1), eigenstates  $|m\rangle$  and  $|v\rangle$  can be computed numerically and presented in the form of decomposition

$$\begin{aligned} |m\rangle &= \sum_n \langle n|m\rangle |n\rangle, \\ |v\rangle &= \sum_n \langle n|v\rangle |n\rangle. \end{aligned} \quad (3.44)$$

Those states constitute a convenient basis  $\{|m\rangle, |v\rangle\}$  in the space of molecular motion, which will be used later to present the RDM of the bridge. Energies  $E_m$  and  $E_v$  ( $m, v = 0, 1, \dots$ ) of unoccupied and occupied molecule respectively are shown in the fig. 3.5 for the model 3 (parameters of the model are listed in the table 3.2).

$n$	$\langle \varphi   n \rangle$	$n$	$\langle \varphi   n \rangle$
0	$1/2\pi$	3	$1/\pi \sin(2\varphi)$
1	$1/\pi \sin(\varphi)$	4	$1/\pi \cos(2\varphi)$
2	$1/\pi \cos(\varphi)$	...	...

Table 3.1: Free rotor basis, which was used for the numerical calculations in the models 3 and 4

From the point of view of classical mechanics, cosinusoidal form of the potentials, similar to those depicted in the fig. 3.5, provides a rotational barrier at the energy  $\epsilon_0 + A_0$  ( $\epsilon_1 + A_1$  for occupied bridge), which divides two types of the motion: vibrational (when the energy of the system is below the barrier) and rotational. In quantum mechanical description wavefunctions of the states which are located well below the barrier are localized in space (according to the angle  $\varphi$ ) and in this sense can be called vibrational. On the contrary, states well above the barrier are delocalized through the whole interval  $[0; 2\pi]$ . Those states are two times degenerate<sup>4</sup>, which is connected with the fact that above the barrier two possible directions of rotation are possible and they are energetically equivalent. We call them rotational states. Well above the classical barrier, when system has a lot of energy and doesn't feel potential anymore, states are close to the free rotor states. Unlike in classical mechanics, in quantum mechanics the division to vibrational and rotational states is not strictly determined, since between localized and delocalized states there is a "transition region" where states smoothly change their "degree of localization".

System-lead coupling  $H_{sl}$  is taken in the same general form as for models 1 and 2

$$H_{sl} = \sum_{\alpha=l,r} \sum_k V_{dk\alpha}(\varphi) (d^\dagger c_{k\alpha} + c_{k\alpha}^\dagger d), \quad (3.45)$$

but coupling coefficients  $V_{dk\alpha}(\varphi)$  in the model 3 are, in general, different for left and right lead and depend on the rotational angle. We set up 3 models with different coefficients.

<sup>4</sup>Or, to be more precise, near degenerate

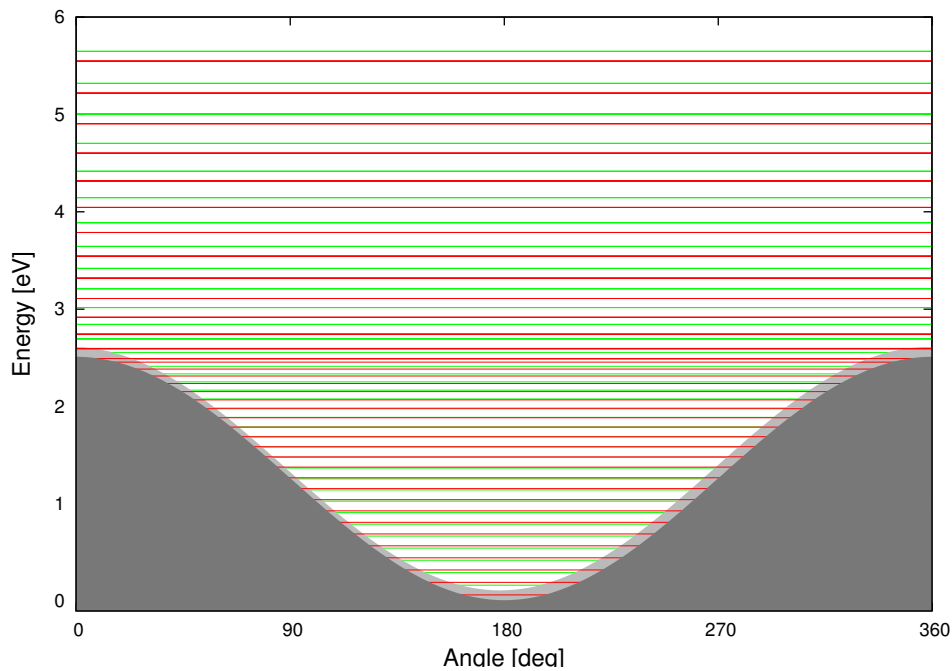


Figure 3.5: Energy levels of unoccupied (red lines) and occupied (green lines) molecular bridge in model 3. Respective potentials are plotted with dark gray and light gray.

- Model 3a.  $V_{dk\alpha} = \beta_2 \sin(k)$ . The angle-independent coupling is less natural for the motor models discussed here, than the better motivated coupling proposed in the next two items (3b and 3c), but it simplifies the treatment of the dynamics significantly. Furthermore this is the case most often considered by other studies [50] and it's identical to one we use in models 1 and 2. For this reasons it's an interesting case for comparison and discussion.
- Model 3b.  $V_{dk\alpha} = \beta_2 \sin(k) \cos(\varphi - \varphi_\alpha)$  and  $\varphi_l = \varphi_r$ . To motivate the symmetrical angle dependent coupling, let's look again to the fig. 3.4. The position of the central ring is determined by the angle  $\varphi$ . When the central ring moves, overlap between the  $\pi$ -orbitals of neighbor rings changes. It affect the conductivity which appears to be  $\varphi$ -dependent. When all benzene rings lie in the same plane, i.e.  $\varphi = \varphi_l = \varphi_r$  the overlap is maximal as well as coupling. When  $\varphi$  is perpendicular to  $\varphi_l$  and  $\varphi_r$  the coupling is equal to zero. Such behavior is well modeled by the factor  $\cos(\varphi - \varphi_\alpha)$  in  $V_{dk\alpha}$ . It can be also motivated with Hückel model (see [51]).

- Model 3c.  $V_{dk\alpha} = \beta_2 \sin(k) \cos(\varphi - \varphi_\alpha)$  and  $\varphi_l \neq \varphi_r$ . The same form like in model 3b, but different for left and right lead. Braking of the symmetry provides the circumstances for observation of the "motor effect", i.e. preferential rotation of the rotor in one or other direction depending on the direction of the current through the junction. In reality asymmetrically coupled bridges may exist for different reasons. If we speak, for example, about phenyl chains, like at the fig. 3.4, we can expect that the first and the last benzene rings of the chain are attached to the leads in different ways.

In the next chapter we will use the notation

$$V_{dk\alpha} = V_k V_{d\alpha}(\varphi) \quad (3.46)$$

to separate the part  $V_k = \sqrt{\frac{2}{N}} \beta_2 \sin(k)$ , which contains leads variable  $k$  (i. e. energy dependence), and all the rest. Thus the only difference between models 3a, 3b and 3c is the dimensionless coefficient  $V_{d\alpha}(\varphi)$ , which defines the angle-dependent coupling strength. Coupling coefficients  $V_{dk\alpha}$  and its parts shouldn't be mixed up with coupling matrices  $V_\alpha$  and  $V_\alpha^\dagger$  used in the previous chapter.

Model 3, being just an anharmonic generalization of the independent boson model, should be considered as a purely theoretical model. For this reason we don't pay much attention to its parametrization, choosing parameters to reproduce regimes we consider to be interesting. On the contrary, in the model 4, we make an attempt to choose parameters in the reasonable range of values and, thus, make a step in the direction of more realistic models. All parameters from the models 3 and 4 are summarized in the table 3.2.

Potential energies for the model 4 are showed in the fig. 3.6. Unoccupied bridge potential, taken in this way, resembles the energy of the central benzene ring tilt motion in the phenylene ethynylene oligomer (PEO) molecule, which was described in the work [37]. From the same paper we know, that amplitudes of such potentials can be changed under the influence of an external electrostatic field. So, we have certain freedom to change amplitudes and stay inside the reasonable range of values. The vibrational potential for the charged molecule is characterized by larger amplitude and smaller number of oscillations than the potential for the neutral molecule [51].

Model	$I$ , a.u.	$\varepsilon_0$ , eV	$\varepsilon_1$ , eV	$A_0$ , eV	$A_1$ , eV	$n_0$	$\varphi_1, ^\circ$	$\varphi_l, ^\circ$	$\varphi_r, ^\circ$
3a	2000	1.25	1.35	1.25	1.25	1	1.72	-	-
3b	2000	1.25	1.35	1.25	1.25	1	1.72	180	180
3c	2000	1.25	1.35	1.25	1.25	1	1.72	180	270
4a	226852	-0.05	0.10	0.05	0.20	2	181.72	0	57
4b	226852	-0.05	0.10	0.05	0.20	2	181.72	0	115

Table 3.2: Parameters summary for the models 3 and 4

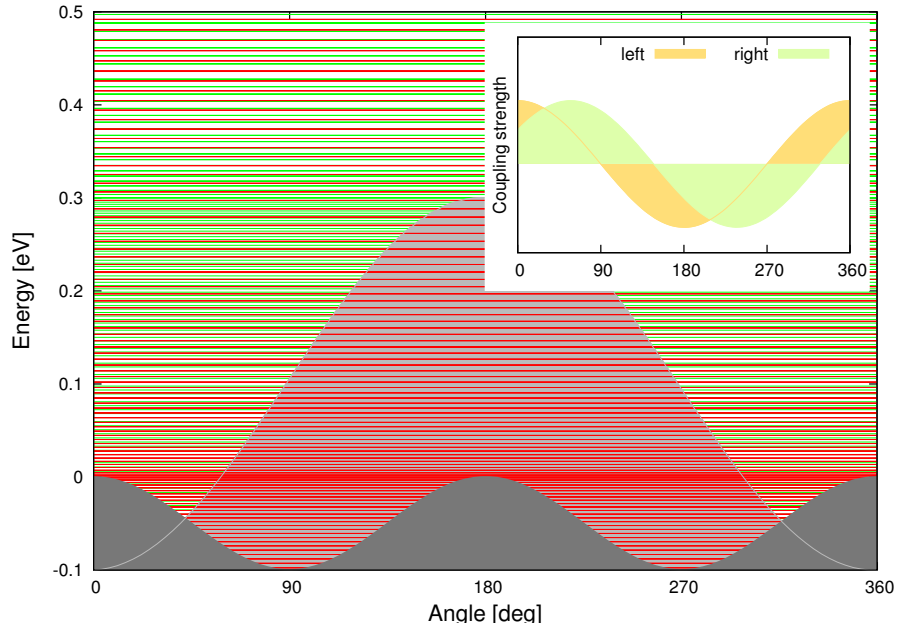


Figure 3.6: Potential energies of unoccupied (dark gray) and occupied (light gray) bridge for the model 4. Quantized energy levels are showed by vertical red and green lines respectively. The angular dependence of molecule-lead couplings  $V_{d\alpha}(\varphi)$ , which correspond to the model 4a, is shown in the inset.

The moment of inertia  $I$ , according to the model of PEO molecule, is the moment of the benzene ring, i.e.  $I = \frac{1}{2}Md^2$ , where  $M$  is the mass of the carbon atom and  $d$  is the diameter of the benzene ring. It is approximately 100 times larger than the value from the model 3. Large moment of inertia leads to the small distance between energy levels, which is clear from the the fig. 3.6 to compare with the fig. 3.5. It's the source of additional numerical challenges, since we need more energy levels (i.e. larger basis) for calculation. Coupling parameters  $\varphi_l$  and  $\varphi_r$  were used, together with potentials shifts  $\varphi_0$  and  $\varphi_1$ , to set up a certain symmetry in the  $\varphi$ -space and investigate its influence to the rotations. The existence of certain asymmetry in the junction is one of the necessary conditions to observe the motor effect. It will be discussed in the chapter 5.

# Chapter 4

## Computations

In this chapter we demonstrate how to apply theoretical tools which are reviewed in the chapter 2 to our particular models from the chapter 3. It's divided to two parts where we discuss scattering and master equation approaches separately. In both parts the charge transport problem for model 1 is solved analytically. For other models analytical part of computation, discussed here, includes the derivation of the equations and formulas which are appropriate for further numerical treatment.

### 4.1 Scattering approach

To apply the scattering approach we simply use the scheme which was described at the end of section 2.2.3. First we calculate self-energies of the leads using the formula (2.61). Next we show how to calculate the  $T$ -matrix and transmission probability for elastic and inelastic cases, which can be substituted to the Landauer formula to get current. Since the scattering approach is used for discussion and comparison in this work, but not for the molecular motor studies, anharmonic potentials are not discussed in this section. However, the generalization is straightforward [51].

#### 4.1.1 Self-energy

To calculate self-energies using the formula

$$\Sigma_\alpha = V_\alpha^\dagger g_\alpha V_\alpha \quad (\alpha = l, r), \quad (4.1)$$

we notice first, that the coupling matrices  $V_\alpha$  (see (2.42)) contain only one nonzero element each. This is valid for all models, since we consider the nearest neighbor interactions only and the whole Hamiltonian matrix (2.56) is tridiagonal. We are going to confine ourselves only to models 1 and 2 in this section, coupling matrices are therefore assumed to be angle independent, i.e. according to the notation (3.46)  $V_{d\alpha}(\varphi) = 1$ . Since the calculation procedure is similar for different leads, indexes  $\alpha$  are omitted in this section. Performing matrix multiplication in (4.1) (in  $n$ -representation) we find

$$\Sigma = \beta_2^2 g_{11}. \quad (4.2)$$

It means, that from the whole Green's operator of isolated lead  $g$  we need only one matrix element  $g_{11} = \langle n_1 | g | n_1 \rangle^1$ . Using the closure relation  $\sum_k |k\rangle \langle k| = I$  we may write

$$\Sigma = \beta_2^2 \sum_{kk'} \langle n_1 | k \rangle \langle k | [(E + i\eta)I - H_l]^{-1} | k' \rangle \langle k' | n_1 \rangle. \quad (4.3)$$

Using the orthogonality of states with different  $k$  and the fact that  $f(H_l)|k\rangle = f(\varepsilon_k)|k\rangle$  (where  $\varepsilon_k$  is defined by the dispersion relation (2.8)) we obtain for the model 1

$$\Sigma = \beta_2^2 \sum_k \frac{|\langle n_1 | k \rangle|^2}{E + i\eta - \varepsilon_k}. \quad (4.4)$$

For the model 2 lead Hamiltonian  $H_l$  contains also  $h_0$  (see (3.32)), and instead of  $E$  in denominator we have  $E' = E - h_0$ . We should have this difference in mind to distinguish models at the end, however, this will not change the derivation procedure. After substitution of  $\langle n_1 | k \rangle = C_1^k$  for half infinite chain (see the section 2.1.2)

$$\Sigma = \frac{2\beta_2^2}{N} \sum_k \frac{\sin^2 k}{E + i\eta - \varepsilon_k}. \quad (4.5)$$

Now we use dispersion relation (2.8) to rewrite the nominator

$$\Sigma = \frac{\beta_2^2}{2\beta_1^2} \frac{1}{N} \sum_k \frac{(2\beta_1)^2 - (\varepsilon_k - \mu)^2}{E + i\eta - \varepsilon_k}, \quad (4.6)$$

---

<sup>1</sup>It is called the surface Green's function

and transform summation to integration using formulas (2.20) and (2.21) with the density of states (2.22)

$$\Sigma = \frac{\beta_2^2}{2\pi\beta_1^2} \int_{\mu-2\beta_1}^{\mu+2\beta_1} d\varepsilon \frac{\sqrt{(2\beta_1)^2 - (\varepsilon - \mu)^2}}{E + i\eta - \varepsilon}. \quad (4.7)$$

This integral can be transformed to contour integration in the complex plane and evaluated using the residuum theorem . The result is

$$\Sigma = \frac{\beta_2^2}{2\beta_1^2} \begin{cases} (E - \mu) + \sqrt{(E - \mu)^2 - (2\beta_1)^2} & \text{if } E < (\mu - 2\beta_1), \\ (E - \mu) - i\sqrt{(2\beta_1)^2 - (E - \mu)^2} & \text{if } (\mu - 2\beta_1) < E < (\mu + 2\beta_1), \\ (E - \mu) - \sqrt{(E - \mu)^2 - (2\beta_1)^2} & \text{if } E > (\mu + 2\beta_1). \end{cases} \quad (4.8)$$

More details about the integral (4.7) reader can find, for example, in [38]. Formula (4.8) specifies the self-energy function  $\Sigma = \Sigma(E)$  of the leads for the model 1. For the vibrating bridge we should use the same formula but with a different argument:  $\Sigma = \Sigma(E - h_0)$ . As a result self-energy in a case of model 2 turns into an operator in the space of molecular vibrations  $\kappa_{vib}$ .

It is common to divide the self-energy to real and imaginary parts as  $\Sigma = \Delta - \frac{1}{2}i\Gamma$ . The real part  $\Delta$  is usually neglected in charge transport theories. It provides a small energy shift (as, for example, in the formula (4.20)) and doesn't influence the observables much. The imaginary part  $\Gamma$  follows directly from (4.7) if we separate the imaginary part of the integrand and use the well known property of the Cauchy-Lorentz distribution

$$\frac{1}{E - \varepsilon + i\eta} = \frac{1}{E - \varepsilon} - i \lim_{\eta \rightarrow +0} \frac{\eta}{\eta^2 + (E - \varepsilon)^2} = \frac{1}{E - \varepsilon} - i\pi\delta(E - \varepsilon). \quad (4.9)$$

The integration over the delta function is straightforward and in accordance with (4.8) we get the formula

$$\Gamma = \begin{cases} \frac{\beta_2^2}{\beta_1^2} \sqrt{(2\beta_1)^2 - (E - \mu)^2} & \text{if } E \in [\mu - 2\beta_1; \mu + 2\beta_1], \\ 0 & \text{if } E \notin [\mu - 2\beta_1; \mu + 2\beta_1]. \end{cases} \quad (4.10)$$

After this transformation singularity remain only in the real part of the integral, which must be understood in a sens of Cauchy principal value. It's also interesting

to notice, that the real part of the self energy  $\Delta$  can be expressed as the Hilbert transformation of its imaginary part

$$\Delta = \frac{1}{2\pi} \int_{\mu-2\beta_1}^{\mu+2\beta_1} d\varepsilon \frac{\Gamma}{E - \varepsilon}. \quad (4.11)$$

### 4.1.2 Elastic transport

To get the  $T$ -matrix we start from the formula (2.54), derived in the chapter 2

$$t(r \leftarrow l) = \langle r | V_r G_{22} V_l^\dagger | l \rangle. \quad (4.12)$$

Scattering states in the case of model 1 are  $|l\rangle = |k; l\rangle$  and  $\langle r| = \langle k; r|$ . Coupling matrices can be written as

$$\begin{aligned} V_r &= \sum_k |k; r\rangle V_{dkr} \langle d|, \\ V_l^\dagger &= \sum_k |d\rangle V_{dkl} \langle k; l|. \end{aligned} \quad (4.13)$$

Substituting it to the (4.12) and using the orthogonality of states with different  $k$  we get

$$t(r \leftarrow l) = V_{dkr} G_s V_{dkl}, \quad (4.14)$$

where we introduce notation  $G_s \equiv \langle d | G_{22} | d \rangle$ . Now we substitute it to the formula (2.46) to get the transmission probability in the elastic case

$$\omega(E) = 4\pi^2 \sum_{l,r} V_{dkr}^2 |G_s|^2 V_{dkl}^2 \delta(\varepsilon_l - E) \delta(\varepsilon_r - E), \quad (4.15)$$

or, equivalently

$$\omega(E) = 4\pi^2 \left[ \sum_r V_{dkr}^2 \delta(\varepsilon_r - E) \right] |G_s|^2 \left[ \sum_l V_{dkl}^2 \delta(\varepsilon_l - E) \right]. \quad (4.16)$$

Sums in square brackets can be calculated, transforming them into integrals using formulas (2.20) and (2.21). Delta functions removes those integrals and, for example, for the first sum we get the formula

$$\sum_{k \in r} V_{dkr}^2 \delta(\varepsilon_r - E) = \frac{1}{2\pi} \frac{\beta_2^2}{\beta_1^2} \sqrt{4\beta_1^2 - (E - \mu_r)^2}, \quad (4.17)$$

if energy  $E$  belongs to the band in the right lead, and zero if not. Comparing it with the formula (4.10) we notice, that the sum is proportional to the  $\Gamma_r$  of the

right lead. Second sum can be treated in a same way. As a result we can rewrite the transmission probability in the form

$$\omega(E) = \Gamma_r(E)|G_s|^2\Gamma_l(E). \quad (4.18)$$

Since we already know self-energies for the leads in model 1, we can easily calculate the Green's function of the bridge

$$G_s = \frac{1}{1 - \varepsilon_0 - \Sigma_l(E) - \Sigma_r(E)}. \quad (4.19)$$

We substitute it to the formula for the transmission probability, and, doing elementary algebraic transformation, we get

$$\omega(E) = \frac{\Gamma_l(E)\Gamma_r(E)}{[E - \varepsilon_0 - \Delta_l(E) - \Delta_r(E)]^2 + \frac{1}{4}[\Gamma_l(E) + \Gamma_r(E)]^2}. \quad (4.20)$$

To calculate the current one should substitute it to the Landauer formula (2.43), where (4.20) is integrated over energy  $E$

$$I = \frac{1}{2\pi} \int dE \frac{\Gamma_l(E)\Gamma_r(E)}{[E - \varepsilon_0 - \Delta_l(E) - \Delta_r(E)]^2 + \frac{1}{4}[\Gamma_l(E) + \Gamma_r(E)]^2} [f_l(E) - f_r(E)]. \quad (4.21)$$

This formula is discussed and compared with the similar formula derived using the ME approach in the next chapter.

### 4.1.3 Inelastic transport

We start from the same general formula (4.12) for a  $T$ -matrix. But this time we should take into account also the molecular bridge vibrational state change from  $m_i$  to  $m_f$ , which accompanies electron tunneling events

$$t(r, m_f \leftarrow l, m_i) = \langle m_f | \langle k; r | V_r G_{22} V_l^\dagger | k; l \rangle | m_i \rangle. \quad (4.22)$$

After substitution of coupling matrices the formula reads

$$t(r, m_f \leftarrow l, m_i) = V_{dkr} \langle m_f | G_s | m_i \rangle V_{dkl}. \quad (4.23)$$

Using the expression (2.47) for the transmission probability and the similar procedure as in the elastic case we can write

$$\omega_{m_i m_f}^{r \leftarrow l}(E) = \Gamma_r(E - E_{m_f}) |\langle m_f | G_s | m_i \rangle|^2 \Gamma_l(E - E_{m_i}). \quad (4.24)$$

This function gives the probability for electron to tunnel from the left lead to the right and excite the bridge from the vibrational state  $m_i$  to  $m_f$ .

Vibrational state of the bridge can be changed not only by electrons, which pass through it, but also by electrons, which are reflected from the contact back to the same lead from where they come. The same procedure used to derive (4.24) can be applied to write

$$\begin{aligned}\omega_{m_i m_f}^{l \leftarrow l}(E) &= \Gamma_l(E - E_{m_f}) |\langle m_f | G_s | m_i \rangle|^2 \Gamma_l(E - E_{m_i}), \\ \omega_{m_i m_f}^{r \leftarrow r}(E) &= \Gamma_r(E - E_{m_f}) |\langle m_f | G_s | m_i \rangle|^2 \Gamma_r(E - E_{m_i}).\end{aligned}\quad (4.25)$$

Such "reflection probabilities" don't contribute to the current, but they participate in the overall molecular junction's dynamics. They are used, for example, in the chapter 5 to write the balance equation for probability fluxes in the junction.

The transmission probability 4.24 can be substituted to the Landauer formula (2.48). But before it Green's function  $G_s$  of the bridge should be calculated. In the model 2  $G_s$  is an operator which acts in the vibrational space of the bridge. To calculate it, according to the definition (2.62), one should invert the operator

$$F = E - h_1 - \Sigma_l(E - h_0) - \Sigma_r(E - h_0). \quad (4.26)$$

Matrix elements of this operator read

$$\langle m_f | F | m_i \rangle = \delta_{m_i m_f} [E - \Sigma_l(E - E_{m_i}) - \Sigma_r(E - E_{m_i})] - \langle m_f | h_1 | m_i \rangle. \quad (4.27)$$

Or, using the spectral decomposition of the operator  $h_1$ ,

$$\langle m_f | F | m_i \rangle = \delta_{m_i m_f} [E - \Sigma_l(E - E_{m_i}) - \Sigma_r(E - E_{m_i})] - \sum_v E_v \langle m_f | v \rangle \langle v | m_i \rangle. \quad (4.28)$$

The matrix with elements (4.28) can be inverted numerically to calculate the Green's function. To express the current through the Green's function we substitute transmission probabilities to (2.48)

$$\begin{aligned}I &= \frac{1}{2\pi} \sum_{m_i m_f} P_{m_i} \int dE |\langle m_f | G_s | m_i \rangle|^2 \times \\ &\quad \left\{ \Gamma_l(E - E_{m_i}) f_l(E - E_{m_i}) \Gamma_r(E - E_{m_f}) [1 - f_r(E - E_{m_f})] \right. \\ &\quad \left. - \Gamma_r(E - E_{m_i}) f_r(E - E_{m_i}) \Gamma_l(E - E_{m_f}) [1 - f_l(E - E_{m_f})] \right\}.\end{aligned}\quad (4.29)$$

We leave the analysis and discussion of this formula for the chapter 5.

## 4.2 Master equation approach

In this section it's demonstrated how to write the WBR ME in the tensor form, which can be treated numerically. Since the ME approach is chosen as a main tool to study the motor effect in this thesis, the proposed form is general enough to cover all models from the previous chapter, including models 3 and 4 with their anharmonic potentials and angle dependent coupling. Formulas for different observables of interest, including angular momentum, and the way of efficient numerical solution of ME are also discussed here. At the end of the section it's showed how the equation can be solved analytically for the model 1.

### 4.2.1 Tensor form of the ME

As it's stressed in the chapter 2, Liouvillian operator  $\mathcal{L}$  in WBR ME of the molecular junction

$$\frac{\partial}{\partial t}\rho(t) = \mathcal{L}\rho(t) \quad (4.30)$$

consists of three parts  $\mathcal{L} = \mathcal{L}_0 + \mathcal{L}_{1l} + \mathcal{L}_{1r}$  which read

$$\mathcal{L}_0\rho(t) = -i[H_s, \rho(t)], \quad (4.31)$$

$$\mathcal{L}_{1l}\rho(t) = -\text{Tr}_{ll} \int_0^\infty d\tau [H_{sll}, [e^{-i(H_s+H_{ll})\tau} H_{sll} e^{+i(H_s+H_{ll})\tau}, \rho(t) \otimes \rho_{ll}^0]], \quad (4.32)$$

$$\mathcal{L}_{1r}\rho(t) = -\text{Tr}_{rl} \int_0^\infty d\tau [H_{srl}, [e^{-i(H_s+H_{rl})\tau} H_{srl} e^{+i(H_s+H_{rl})\tau}, \rho(t) \otimes \rho_{rl}^0]]. \quad (4.33)$$

Let's consider them separately.

#### Action of $\mathcal{L}_0$

This part of the Liouvillian describes the dynamics of the isolated bridge. Let's denote the result of an action of the  $\mathcal{L}_0$  superoperator to RDM as  $\rho'$ , i.e.

$$\mathcal{L}_0\rho = \rho'. \quad (4.34)$$

Using the decomposition (3.14) both sides of this equation can be modified:

$$\mathcal{L}_0\rho = -i\{dd^\dagger[h_0, \rho_{00}] + d^\dagger d[h_1, \rho_{11}] + d(h_0\rho_{01} - \rho_{01}h_1) + d^\dagger(h_1\rho_{10} - \rho_{10}h_0)\}, \quad (4.35)$$

$$\rho' = \rho'_{00} d d^\dagger + \rho'_{11} d^\dagger d + \rho'_{01} d + \rho'_{10} d^\dagger. \quad (4.36)$$

Thus, we have four expressions to calculate four block of resulting RDM independently

$$\begin{aligned} \rho'_{00} &= -i(h_0 \rho_{00} - \rho_{00} h_0), \\ \rho'_{11} &= -i(h_1 \rho_{11} - \rho_{11} h_1), \\ \rho'_{01} &= -i(h_0 \rho_{01} - \rho_{01} h_1), \\ \rho'_{10} &= -i(h_1 \rho_{10} - \rho_{10} h_0). \end{aligned} \quad (4.37)$$

Practically we are interested only in two diagonal blocks  $\rho_{00}$  and  $\rho_{11}$  of RDM, since we need only them to calculate observables of interest (it's shown later in this chapter).

Using spectral decomposition of operators  $h_0$  and  $h_1$

$$\begin{aligned} h_0 &= \sum_m E_m |m\rangle \langle m|, \\ h_1 &= \sum_v E_v |v\rangle \langle v|, \end{aligned} \quad (4.38)$$

we may rewrite the result of an action of  $\mathcal{L}_0$  on two important diagonal blocks as

$$\begin{aligned} \rho'_{00}(m_1, m_2) &= i(E_{m_2} - E_{m_1}) \rho_{00}(m_1, m_2), \\ \rho'_{11}(v_1, v_2) &= i(E_{v_2} - E_{v_1}) \rho_{11}(v_1, v_2), \end{aligned} \quad (4.39)$$

where we use notations  $\langle m_1 | \rho_{00} | m_2 \rangle \equiv \rho_{00}(m_1, m_2)$  and  $\langle v_1 | \rho_{11} | v_2 \rangle \equiv \rho_{11}(v_1, v_2)$ .

Rewriting the same formulas in a tensor form we get

$$\begin{aligned} \rho'_{00}(m_1, m_2) &= \sum_{M_1 M_2} \mathcal{L}_0^{00}(m_1, m_2, M_1, M_2) \rho_{00}(M_1, M_2), \\ \rho'_{11}(v_1, v_2) &= \sum_{V_1 V_2} \mathcal{L}_0^{11}(v_1, v_2, V_1, V_2) \rho_{11}(V_1, V_2) \end{aligned} \quad (4.40)$$

where

$$\begin{aligned} \mathcal{L}_0^{00}(m_1, m_2, M_1, M_2) &= i(E_{M_2} - E_{M_1}) \delta_{m_2 M_2} \delta_{m_1 M_1}, \\ \mathcal{L}_0^{11}(v_1, v_2, V_1, V_2) &= i(E_{V_2} - E_{V_1}) \delta_{v_2 V_2} \delta_{v_1 V_1}. \end{aligned} \quad (4.41)$$

are elements of the 4th rank tensor  $\mathcal{L}_0$ .

### Action of $\mathcal{L}_1$

Tensor  $\mathcal{L}_1$  is called the Redfield tensor by some authors ([9]). It represents the perturbation to the dynamics of the molecular bridge as a result of weak interaction with the leads. It's enough to discuss  $\mathcal{L}_1$  for one of the leads here, since the derivation

procedure is identical for both of them. For the purpose of convenience we omit all lead specifying indexes. Adopting short notation for the time dependence of operators in Dirac representation

$$e^{-i(H_s+H_l)\tau} A e^{+i(H_s+H_l)\tau} \equiv A(-\tau), \quad (4.42)$$

we expand commutators in  $\mathcal{L}_1$  as

$$\begin{aligned} \mathcal{L}_1 \rho = & - \int_0^\infty d\tau Tr_l \{ H_{sl} H_{sl}(-\tau) [\rho_l^0 \otimes \rho] - H_{sl} [\rho_l^0 \otimes \rho] H_{sl}(-\tau) \\ & + [\rho_l^0 \otimes \rho] H_{sl}(-\tau) H_{sl} - H_{sl}(-\tau) [\rho_l^0 \otimes \rho] H_{sl} \} \end{aligned} \quad (4.43)$$

and substitute the coupling operators

$$\begin{aligned} H_{sl} &= \sum_k V_{dk} [d^\dagger c_k + c_k^\dagger d], \\ H_{sl}(-\tau) &= \sum_{k'} V_{dk'}(-\tau) [d^\dagger(-\tau) c_{k'}(-\tau) + c_{k'}^\dagger(-\tau) d(-\tau)]. \end{aligned} \quad (4.44)$$

there. In the resulting 16-terms expression (which is not presented here) we calculate leads correlation functions  $Tr_l [c_k c_{k'}^\dagger(-\tau) \rho_l^0]$  and  $Tr_l [c_k^\dagger c_{k'}(-\tau) \rho_l^0]$ . It's easily done expanding the  $c$ -operators time evolution (see formulas (2.36)) and using the fact, that the RDM of the lead  $\rho_l^0$  is populated according to the Fermi-Dirac distribution (2.45)

$$\begin{aligned} \langle c_k c_{k'}^\dagger(-\tau) \rangle_l &\equiv Tr_l [c_k c_{k'}^\dagger e^{-i\varepsilon_{k'}\tau} \rho_l^0] = e^{-i\varepsilon_{k'}\tau} (1 - f_k) \delta_{kk'}, \\ \langle c_k^\dagger c_{k'}(-\tau) \rangle_l &\equiv Tr_l [c_k^\dagger c_{k'} e^{+i\varepsilon_{k'}\tau} \rho_l^0] = e^{+i\varepsilon_{k'}\tau} (f_k) \delta_{kk'}. \end{aligned} \quad (4.45)$$

All other correlation functions (which contain only creation or only annihilation operators) are equal to zero. It destroys half of the terms in the equation.  $\mathcal{L}_1$  now reads

$$\begin{aligned} \mathcal{L}_1 \rho = & - \int_0^\infty d\tau \sum_k \{ \\ & + e^{-i\varepsilon_k\tau} (1 - f_k) V_{dk} d^\dagger V_{dk}(-\tau) d(-\tau) \rho + e^{+i\varepsilon_k\tau} (f_k) V_{dk} d V_{dk}(-\tau) d^\dagger(-\tau) \rho \\ & - e^{-i\varepsilon_k\tau} (f_k) V_{dk} d^\dagger \rho V_{dk}(-\tau) d(-\tau) - e^{+i\varepsilon_k\tau} (1 - f_k) V_{dk} d \rho V_{dk}(-\tau) d^\dagger(-\tau) \\ & + e^{+i\varepsilon_k\tau} (1 - f_k) \rho V_{dk}(-\tau) d^\dagger(-\tau) V_{dk} d + e^{-i\varepsilon_k\tau} (f_k) \rho V_{dk}(-\tau) d(-\tau) V_{dk} d^\dagger \\ & - e^{+i\varepsilon_k\tau} (f_k) V_{dk}(-\tau) d^\dagger(-\tau) \rho V_{dk} d - e^{-i\varepsilon_k\tau} (1 - f_k) V_{dk}(-\tau) d(-\tau) \rho V_{dk} d^\dagger \} \end{aligned} \quad (4.46)$$

Now we use formulas (3.19) for time evolution of  $d$ -operators and similarly derived formulas for  $V_{dk}$

$$V_{dk}(-\tau) = d d^\dagger [e^{-ih_0\tau} V_{dk} e^{+ih_0\tau}] + d^\dagger d [e^{-ih_1\tau} V_{dk} e^{+ih_1\tau}] \quad (4.47)$$

to substitute explicitly to the equation. Instead of operators  $h_0$  and  $h_1$  we use again its spectral representation (4.38). Coupling coefficients  $V_{dk}$  are partitioned according to the formula (3.46), to separate part  $V_k$  which commute with  $\varphi$ -dependent vectors and operators. For later convenience we multiply the equation to  $1 = (-i)i$  and introduce the notation  $E_v - E_m \equiv \omega_{mv}$ . The resulting equation reads

$$\begin{aligned} \mathcal{L}_1 \rho = & -i \sum_{mv} \{ \\ & + \xi_2^*(m, v) V_d |m\rangle \langle m| V_d |v\rangle \langle v| (d^\dagger d \rho) + \xi_1^*(m, v) V_d |v\rangle \langle v| V_d |m\rangle \langle m| (d d^\dagger \rho) \\ & + \xi_1(m, v) V_d (d^\dagger \rho d) |m\rangle \langle m| V_d |v\rangle \langle v| + \xi_2(m, v) V_d (d \rho d^\dagger) |v\rangle \langle v| V_d |m\rangle \langle m| \\ & - \xi_2(m, v) (\rho d^\dagger d) |v\rangle \langle v| V_d |m\rangle \langle m| V_d - \xi_1(m, v) (\rho d d^\dagger) |m\rangle \langle m| V_d |v\rangle \langle v| V_d \\ & - \xi_1^*(m, v) |v\rangle \langle v| V_d |m\rangle \langle m| (d^\dagger \rho d) V_d - \xi_2^*(m, v) |m\rangle \langle m| V_d |v\rangle \langle v| (d \rho d^\dagger) V_d \}. \end{aligned} \quad (4.48)$$

where

$$\begin{aligned} \xi_1(m, v) & \equiv i \int_0^\infty d\tau \sum_k e^{-i(\varepsilon_k - \omega_{mv})\tau} (f_k) V_k^2 \\ \xi_2(m, v) & \equiv i \int_0^\infty d\tau \sum_k e^{+i(\varepsilon_k - \omega_{mv})\tau} (1 - f_k) V_k^2 \end{aligned} \quad (4.49)$$

(we calculate these functions in the next section). Let's denote the result of the action of  $\mathcal{L}_1$  on  $\rho$  as  $\rho''$  and use the decomposition (3.14) to divide the equation to blocks, in a similar way as we did for  $\mathcal{L}_0$

$$\begin{aligned} \rho''_{00} & = -i \sum_{mv} \{ \xi_1^* V_d |v\rangle \langle v| V_d |m\rangle \langle m| \rho_{00} + \xi_2 V_d \rho_{11} |v\rangle \langle v| V_d |m\rangle \langle m| \\ & \quad - \xi_1 \rho_{00} |m\rangle \langle m| V_d |v\rangle \langle v| V_d - \xi_2^* |m\rangle \langle m| V_d |v\rangle \langle v| \rho_{11} V_d \}, \\ \rho''_{11} & = -i \sum_{mv} \{ \xi_2^* V_d |m\rangle \langle m| V_d |v\rangle \langle v| \rho_{11} + \xi_1 V_d \rho_{00} |m\rangle \langle m| V_d |v\rangle \langle v| \\ & \quad - \xi_2 \rho_{11} |v\rangle \langle v| V_d |m\rangle \langle m| V_d - \xi_1^* |v\rangle \langle v| V_d |m\rangle \langle m| \rho_{00} V_d \}, \\ \rho''_{10} & = -i \sum_{mv} \{ \xi_2^* V_d |m\rangle \langle m| V_d |v\rangle \langle v| \rho_{10} - \xi_1 \rho_{10} |m\rangle \langle m| V_d |v\rangle \langle v| V_d \}, \\ \rho''_{01} & = -i \sum_{mv} \{ \xi_1^* V_d |v\rangle \langle v| V_d |m\rangle \langle m| \rho_{01} - \xi_2 \rho_{01} |v\rangle \langle v| V_d |m\rangle \langle m| V_d \}. \end{aligned} \quad (4.50)$$

First and second pair of equations are independent. Since only first pair contains diagonal blocks  $\rho_{00}$  and  $\rho_{11}$  which are important for us, we don't consider the second pair. As in the previous subsection we adopt basis  $\{|m\rangle\}$  in unoccupied bridge space to represent  $\rho_{00}$  and  $\{|v\rangle\}$  basis for  $\rho_{11}$ . After renaming indexes and adding

Kronecker deltas expression can be presented in a tensor form

$$\begin{aligned}
\rho''_{00}(m_1, m_2) &= \sum_{M_1 M_2} \mathcal{L}_1^{00}(m_1, m_2, M_1, M_2) \rho_{00}(M_1, M_2) \\
&\quad + \sum_{V_1 V_2} \mathcal{L}_1^{01}(m_1, m_2, V_1, V_2) \rho_{11}(V_1, V_2), \\
\rho''_{11}(v_1, v_2) &= \sum_{M_1 M_2} \mathcal{L}_1^{10}(v_1, v_2, M_1, M_2) \rho_{00}(M_1, M_2) \\
&\quad + \sum_{V_1 V_2} \mathcal{L}_1^{11}(v_1, v_2, V_1, V_2) \rho_{11}(V_1, V_2),
\end{aligned} \tag{4.51}$$

with tensor elements

$$\begin{aligned}
\mathcal{L}_1^{00}(m_1, m_2, M_1, M_2) &= i\delta_{M_1 m_1} \sum_v \xi_1(M_2, v) V_d(M_2, v) V_d(v, m_2) \\
&\quad - i\delta_{M_2 m_2} \sum_v \xi_1^*(M_1, v) V_d(m_1, v) V_d(v, M_1), \\
\mathcal{L}_1^{01}(m_1, m_2, V_1, V_2) &= i\xi_2^*(m_1, V_1) V_d(m_1, V_1) V_d(V_2, m_2) \\
&\quad - i\xi_2(m_2, V_2) V_d(m_1, V_1) V_d(V_2, m_2), \\
\mathcal{L}_1^{11}(v_1, v_2, V_1, V_2) &= i\delta_{V_1 v_1} \sum_m \xi_2(m, V_2) V_d(V_2, m) V_d(m, v_2) \\
&\quad - i\delta_{V_2 v_2} \sum_m \xi_2^*(m, V_1) V_d(v_1, m) V_d(m, V_1), \\
\mathcal{L}_1^{10}(v_1, v_2, M_1, M_2) &= i\xi_1^*(M_1, v_1) V_d(v_1, M_1) V_d(M_2, v_2) \\
&\quad - i\xi_1(M_2, v_2) V_d(v_1, M_1) V_d(M_2, v_2).
\end{aligned} \tag{4.52}$$

### Functions $\xi_1$ and $\xi_2$

In this section we calculate functions

$$\begin{aligned}
\xi_1(E) &= i \int_0^\infty d\tau \sum_k e^{-i(\varepsilon_k - E)\tau} (f_k) V_k^2, \\
\xi_2(E) &= i \int_0^\infty d\tau \sum_k e^{+i(\varepsilon_k - E)\tau} (1 - f_k) V_k^2.
\end{aligned} \tag{4.53}$$

The integral over  $\tau$  is well known

$$\int_0^\infty d\tau e^{\pm i\alpha\tau} = \pi\delta(\alpha) \pm i\alpha^{-1}. \tag{4.54}$$

Expressions (4.53) reads

$$\begin{aligned}
\xi_1(E) &= \sum_k (f_k) V_k^2 [(\varepsilon_k - E)^{-1} + i\pi\delta(\varepsilon_k - E)], \\
\xi_2(E) &= \sum_k (1 - f_k) V_k^2 [-(\varepsilon_k - E)^{-1} + i\pi\delta(\varepsilon_k - E)].
\end{aligned} \tag{4.55}$$

Using the scheme, described in chapter 2 (see formulas (2.20) and (2.21)), sum over  $k$  may be transformed to integral. To do it we need also density of states (2.22). Coefficient  $V_k$  should be modified using dispersion relation (2.8)

$$V_k = \sqrt{\frac{2}{N}} \beta_2 \sin(k) = \frac{1}{\sqrt{2N}} \frac{\beta_2}{\beta_1} \sqrt{4\beta_1^2 - (\varepsilon - \mu)^2}. \quad (4.56)$$

As a result we have

$$\begin{aligned} \xi_1(E) &= \frac{1}{\pi} \frac{\beta_2^2}{2\beta_1^2} \int_{\mu-2\beta_1}^{\mu+2\beta_1} d\varepsilon [f(\varepsilon)] \sqrt{4\beta_1^2 - (\varepsilon - \mu)^2} [(\varepsilon - E)^{-1} + i\pi\delta(\varepsilon - E)], \\ \xi_2(E) &= \frac{1}{\pi} \frac{\beta_2^2}{2\beta_1^2} \int_{\mu-2\beta_1}^{\mu+2\beta_1} d\varepsilon [1 - f(\varepsilon)] \sqrt{4\beta_1^2 - (\varepsilon - \mu)^2} [-(\varepsilon - E)^{-1} + i\pi\delta(\varepsilon - E)]. \end{aligned} \quad (4.57)$$

It's easy to calculate imaginary parts, since delta function removes the integral

$$\begin{aligned} \text{Im}[\xi_1(E)] &= \frac{\beta_2^2}{2\beta_1^2} [f(E)] \sqrt{4\beta_1^2 - (E - \mu)^2}, \\ \text{Im}[\xi_2(E)] &= \frac{\beta_2^2}{2\beta_1^2} [1 - f(E)] \sqrt{4\beta_1^2 - (E - \mu)^2}. \end{aligned} \quad (4.58)$$

According to the properties of delta function imaginary parts are equal to zero outside the band (i.e. when  $E \notin [\mu - 2\beta_1, \mu + 2\beta_1]$ ). Or, using definitions (4.10)

$$\begin{aligned} \text{Im}[\xi_1(E)] &= \frac{1}{2} [f(E)] \Gamma(E), \\ \text{Im}[\xi_2(E)] &= \frac{1}{2} [1 - f(E)] \Gamma(E). \end{aligned} \quad (4.59)$$

Real parts are presented by the integrals

$$\begin{aligned} \text{Re}[\xi_1(E)] &= \frac{1}{\pi} \frac{\beta_2^2}{2\beta_1^2} \int_{\mu-2\beta_1}^{\mu+2\beta_1} d\varepsilon \frac{\sqrt{4\beta_1^2 - (\varepsilon - \mu)^2}}{\varepsilon - E} f(\varepsilon), \\ \text{Re}[\xi_2(E)] &= -\frac{1}{\pi} \frac{\beta_2^2}{2\beta_1^2} \int_{\mu-2\beta_1}^{\mu+2\beta_1} d\varepsilon \frac{\sqrt{4\beta_1^2 - (\varepsilon - \mu)^2}}{\varepsilon - E} [1 - f(\varepsilon)]. \end{aligned} \quad (4.60)$$

Those integrals are similar to self-energies real parts  $\Delta$ . The difference is, that Fermi-Dirac distributions stands under the integral. For this reason we can't calculate them analytically. But they can be calculated numerically. In a case, when  $E \in [\mu - 2\beta_1, \mu + 2\beta_1]$ , integral contain singularity. For numerical treatment one may use the following trick to remove singularity from the integral

$$\begin{aligned} \int_a^b \frac{f(t)}{t-t_0} dt &= \int_a^b \frac{f(t)-f(t_0)}{t-t_0} dt + f(t_0) \int_a^b \frac{dt}{t-t_0} = \\ &= \int_a^b \frac{f(t)-f(t_0)}{t-t_0} dt + f(t_0) \ln \left( \frac{t_0-b}{a-t_0} \right) \end{aligned} \quad (4.61)$$

**Matrices**  $V_d(m, v)$ 

Matrices  $V_d(m, v)$  for model 2 coincide with the overlap matrices which were discussed in the section 3.2. When coupling between the molecular bridge and leads contains angle dependence, like in models 3 and 4, matrices  $V_d(m, v)$  can be considered as some kind of generalization of Franck-Condon factors

$$V_d(m, v) \equiv \langle m | \cos(\varphi - \varphi_\alpha) | v \rangle. \quad (4.62)$$

Numerically we express the states  $|m\rangle$  and  $|v\rangle$  as a decomposition in the free rotor basis (3.44). Expanding the cosine of sum and applying this decomposition we get

$$V_d(m, v) = \sum_{n'n''} \langle m | n' \rangle \langle n'' | v \rangle [\cos \varphi_\alpha \langle n' | \cos \varphi | n'' \rangle + \sin \varphi_\alpha \langle n' | \sin \varphi | n'' \rangle]. \quad (4.63)$$

Operators  $\cos \varphi$  and  $\sin \varphi$  can be easily expressed in the free rotor basis.

**Structure of full  $\mathcal{L}$** 

Now, when we know how to write superoperators  $\mathcal{L}_0$  and  $\mathcal{L}_1$  in the tensor form and how exactly they act on  $\rho$ , we can organize two relevant diagonal blocks of RDM  $\rho_{00}$  and  $\rho_{11}$  as "vector" and write the action of whole  $\mathcal{L}$  operator in the form

$$\mathcal{L} \begin{pmatrix} \rho_{00} \\ \rho_{11} \end{pmatrix} = \left[ \begin{pmatrix} \mathcal{L}_0^{00} & 0 \\ 0 & \mathcal{L}_0^{11} \end{pmatrix} + \begin{pmatrix} \mathcal{L}_{1l}^{00} & \mathcal{L}_{1l}^{01} \\ \mathcal{L}_{1l}^{10} & \mathcal{L}_{1l}^{11} \end{pmatrix} + \begin{pmatrix} \mathcal{L}_{1r}^{00} & \mathcal{L}_{1r}^{01} \\ \mathcal{L}_{1r}^{10} & \mathcal{L}_{1r}^{11} \end{pmatrix} \right] \begin{pmatrix} \rho_{00} \\ \rho_{11} \end{pmatrix}, \quad (4.64)$$

where tensor elements  $\mathcal{L}_0^{00}$  and  $\mathcal{L}_0^{11}$  are given by formulas (4.41) and elements  $\mathcal{L}_{1\alpha}^{00}$ ,  $\mathcal{L}_{1\alpha}^{01}$ ,  $\mathcal{L}_{1\alpha}^{10}$ ,  $\mathcal{L}_{1\alpha}^{11}$  by formulas (4.52)

**4.2.2 Observables**

Working formula for current can be derived from the general formula (2.95). The derivation procedure includes the similar stages we passed deriving the formula (4.52). First we substitute the coupling (4.44) to (2.95) and expand commutator. We also calculate explicitly a part of the trace which correspond to the leads degrees of freedom using expressions for correlation functions (4.45). We omit again lead number index  $\alpha$ , but, to compare with the previous section all operators here belong

to one specific (left) lead. After all this transformations the formula for current reads

$$\begin{aligned}
I = - \int d\tau \text{Tr}_s \sum_k \{ & \\
& -e^{+i\varepsilon_k\tau} f_k V_{dk}(-\tau) d^\dagger(-\tau) \rho V_{dk} d + e^{-i\varepsilon_k\tau} (1 - f_k) V_{dk}(-\tau) d(-\tau) \rho V_{dk} d^\dagger \\
& + e^{+i\varepsilon_k\tau} (1 - f_k) \rho V_{dk}(-\tau) d^\dagger(-\tau) V_{dk} d - e^{-i\varepsilon_k\tau} f_k \rho V_{dk}(-\tau) d(-\tau) V_{dk} d^\dagger \}.
\end{aligned} \quad (4.65)$$

Now we substitute time evolutions (3.19) and (4.47), split  $V_{dk}$  to  $V_d$  and  $V_k$  and use the spectral representations (4.38) of operators  $h_0$  and  $h_1$ . Finally we use definitions (4.49) to introduce  $\xi$ -functions. Current reads

$$\begin{aligned}
I = -i \text{Tr}_s \sum_{mv} \{ & \\
& -\xi_1^*(\omega_{mv}) |v\rangle \langle v| V_d |m\rangle \langle m| (d^\dagger \rho d) V_d + \xi_2^*(\omega_{mv}) |m\rangle \langle m| V_d |v\rangle \langle v| (d \rho d^\dagger) V_d \\
& -\xi_2(\omega_{mv}) (\rho d^\dagger d) |v\rangle \langle v| V_d |m\rangle \langle m| V_d + \xi_1(\omega_{mv}) (\rho d d^\dagger) |m\rangle \langle m| V_d |v\rangle \langle v| V_d \}.
\end{aligned} \quad (4.66)$$

The decomposition (3.14) should be substituted into the equation at this moment. After certain manipulations with  $d$ -operators (using the commutation relation (3.8)) the whole right hand side of the equation may be presented as a superposition of four terms, projected to  $dd^\dagger$ ,  $d^\dagger d$ ,  $d$  and  $d^\dagger$

$$\begin{aligned}
I = -i \text{Tr}_s \sum_{mv} \{ & \\
& -d^\dagger d [\xi_1^*(m, v) |v\rangle \langle v| V_d |m\rangle \langle m| \rho_{00} V_d + \xi_2(m, v) \rho_{11} |v\rangle \langle v| V_d |m\rangle \langle m| V_d] \\
& + dd^\dagger [\xi_2^*(m, v) |m\rangle \langle m| V_d |v\rangle \langle v| \rho_{11} V_d + \xi_1(m, v) \rho_{00} |m\rangle \langle m| V_d |v\rangle \langle v| V_d] \\
& -d [\xi_2(m, v) \rho_{01} |v\rangle \langle v| V_d |m\rangle \langle m| V_d] + d^\dagger [\xi_1(m, v) \rho_{10} |m\rangle \langle m| V_d |v\rangle \langle v| V_d] \}.
\end{aligned} \quad (4.67)$$

The notation  $\xi_i(\omega_{mv}) \equiv \xi_i(m, v)$  ( $i = 1, 2$ ) is used here.

Each term correspond to a certain block of some matrix in the molecular bridges space. Since we have to take the trace over bridge's degrees of freedom, we ignore  $d$  and  $d^\dagger$  terms which correspond to off diagonal blocks. Other two blocks we trace in a usual way. Result reads

$$\begin{aligned}
I = -i \sum_{mv} \{ & \\
& -\xi_1^*(m, v) \sum_{m'} V_d(m, v) \rho_{00}(m, m') V_d(m', v) \\
& -\xi_2(m, v) \sum_{v'} \rho_{11}(v', v) V_d(m, v) V_d(m, v') + \xi_2^*(m, v) \sum_{v'} V_d(m, v) \rho_{11}(v, v') V_d(m, v') \\
& + \xi_1(m, v) \sum_{m'} \rho_{00}(m', m) V_d(m, v) V_d(m', v) \}.
\end{aligned} \quad (4.68)$$

Since first two terms in brackets are complex conjugation of last two terms (matrices  $V_d$  are real and RDM blocks  $\rho_{00}$  and  $\rho_{11}$  are hermitian) overall equation can be rewritten to get the final formula for current in the form

$$I = 2 \operatorname{Im} \left\{ \sum_{mv} \xi_1(m, v) V_d(m, v) \sum_{m'} \rho_{00}(m', m) V_d(m', v) + \sum_{mv} \xi_2^*(m, v) V_d(m, v) \sum_{v'} \rho_{11}(v, v') V_d(m, v') \right\}. \quad (4.69)$$

Vibrational excitation energy<sup>2</sup>

$$\langle H_s \rangle = \operatorname{Tr}_s [H_s \rho] \quad (4.70)$$

is another observable of interest, which we calculate in this work as a function of voltage. It gives a mean amount of energy, accumulated at the bridge. Using the definition  $H_s = h_0 d d^\dagger + h_1 d^\dagger d$  and decomposition (3.14) the formula can be modified

$$\langle H_s \rangle = \operatorname{Tr}_m [h_0 \rho_{00}] + \operatorname{Tr}_v [h_1 \rho_{11}]. \quad (4.71)$$

Traces here must be taken through the unoccupied and occupied bridge spaces. The same formula in the  $\{|m\rangle, |v\rangle\}$  basis reads

$$\langle H_s \rangle = \sum_{mm'} \langle m | h_0 | m' \rangle \langle m' | \rho_{00} | m \rangle + \sum_{vv'} \langle v | h_1 | v' \rangle \langle v' | \rho_{11} | v \rangle. \quad (4.72)$$

Since operators  $h_0$  and  $h_1$  are diagonal in  $m$ - and  $v$ -representations, it is

$$\langle H_s \rangle = \sum_m E_m \rho_{00}(m, m) + \sum_v E_v \rho_{11}(v, v). \quad (4.73)$$

Thus, to calculate the mean excitation energy of the molecule it is enough to know only populations of the RDM.

Another important observable which is used to study the motor effect in models 3 and 4 is the mean value of angular momentum  $\langle L_z \rangle$ . Since there is only one rotational axis, which we call  $z$ , the operator  $L_z$  reads

$$L_z = -i \frac{\partial}{\partial \varphi} = -i \frac{\partial}{\partial \varphi} d d^\dagger - i \frac{\partial}{\partial \varphi} d^\dagger d. \quad (4.74)$$

Similarly to (4.72), mean value can be written as

$$\langle L_z \rangle = \sum_{mm'} \langle m | L_z | m' \rangle \langle m' | \rho_{00} | m \rangle + \sum_{vv'} \langle v | L_z | v' \rangle \langle v' | \rho_{11} | v \rangle. \quad (4.75)$$

---

<sup>2</sup>In principle it contains also a charging energy of the bridge

Using the formula (3.44) angular momentum operator in  $m$ -representation can be expressed through the angular momentum in the free rotor basis

$$\langle m|L_z|m'\rangle = \sum_{n_1 n_2} \langle m|n_1\rangle \langle n_1|L_z|n_2\rangle \langle n_2|m'\rangle, \quad (4.76)$$

where it can be calculated analytically. As a result we get<sup>3</sup>

$$\langle m|L_z|m'\rangle = \sum_{n=2,4,\dots} \frac{in}{2} [\langle m|n-1\rangle \langle n|m'\rangle - \langle m|n\rangle \langle n-1|m'\rangle]. \quad (4.77)$$

Similar formula can be derived for  $L_z$  matrix elements in  $v$ -representation. Substituting it back to (4.75) and using the fact that  $\rho_{00}$  and  $\rho_{11}$  are hermitian we get

$$\begin{aligned} \langle L_z \rangle &= \sum_{m'>m} \text{Im}\{\rho_{00}(m', m)\} \sum_{n=2,4,\dots} n [\langle m|n\rangle \langle n-1|m'\rangle - \langle m|n-1\rangle \langle n|m'\rangle] \\ &+ \sum_{v'>v} \text{Im}\{\rho_{11}(v', v)\} \sum_{n=2,4,\dots} n [\langle v|n\rangle \langle n-1|v'\rangle - \langle v|n-1\rangle \langle n|v'\rangle]. \end{aligned} \quad (4.78)$$

It may be also convenient in some situations to express  $\langle L_z \rangle$  through the RDM, written in the basis, where momentum is diagonal, i.e. in the basis assembled from the states  $|l\rangle$ , defined by the equation

$$L_z|l\rangle = l|l\rangle \quad (4.79)$$

( $l = 0, \pm 1, \pm 2, \dots$ ). Substituting the closure relation  $\sum_l |l\rangle \langle l| = 1$  to (4.75) it's easy to show, that

$$\langle L_z \rangle = \sum_l l \rho_{00}(l, l) + \sum_l l \rho_{11}(l, l), \quad (4.80)$$

where we defined populations  $\rho_{00}(l, l)$  and  $\rho_{11}(l, l)$  of rotational eigenstates for unoccupied and occupied states of the molecule respectively, i. e.

$$\rho_{00}(l, l) = \sum_{mm'} \langle l|m'\rangle \langle m'|\rho_{00}|m\rangle \langle m|l\rangle, \quad (4.81)$$

$$\rho_{11}(l, l) = \sum_{vv'} \langle l|v'\rangle \langle v'|\rho_{11}|v\rangle \langle v|l\rangle. \quad (4.82)$$

It is apparent from (4.78) that  $\langle L_z \rangle$  doesn't depend on the diagonal elements of RDM (the populations). If the RDM is presented in the basis  $\{|m\rangle, |v\rangle\}$ , where

---

<sup>3</sup> $|n\rangle$  here are the free rotor states, see the table 3.1

energy is diagonal, only imaginary parts of coherences enter the formula for the mean value of angular momentum. On the other hand, the mean values of the current and bridge energy  $H_s$  are defined<sup>4</sup> by diagonal terms of RDM, despite the fact that coherences, in principle, enter the formula (4.69) for current. It's also important to stress here, that all final formulas for the observables contain only two diagonal blocks  $\rho_{00}$  and  $\rho_{11}$  of the RDM, while two other blocks  $\rho_{01}$  and  $\rho_{10}$  are not important for calculations.

### 4.2.3 Details of numerical implementation

To determine a stationary RDM of the bridge the equation (2.89) must be solved. Equivalently, it can be written in a tensor form

$$\sum_{j_1 j_2} \mathcal{L}_{i_1 i_2 j_1 j_2} \rho_{j_1 j_2} = 0. \quad (4.83)$$

To get a properly normalized  $\rho$  we should add one more equation to the system, which reads

$$\text{Tr}\rho = \sum_m \rho_{00}(m, m) + \sum_v \rho_{11}(v, v) = 1. \quad (4.84)$$

For the numerical convenience we reshape the tensors  $\mathcal{L}$  of the fourth rank into matrix  $\mathcal{L}^r$ . It can be done associating a unique number  $i$  with each pair of indexes  $(i_1, i_2)$  and  $j$  with each  $(j_1, j_2)$ . In the same way the RDM becomes a vector. Reshaped ME and normalization condition can be written as

$$\mathcal{L}^r \vec{\rho} = 0 \quad (4.85)$$

and

$$\mathcal{N} \vec{\rho} = \begin{pmatrix} 1 \\ 0 \\ \dots \\ 0 \end{pmatrix} \quad (4.86)$$

respectively. First row of the matrix  $\mathcal{N}$  is composed from elements "0" and "1" and, been multiplied to the vector  $\vec{\rho}$ , should reproduce the normalization condition

---

<sup>4</sup>According to our calculations.

(4.84). All other elements of  $\mathcal{N}$  are zeros. Combining last two equations we may express  $\vec{\rho}$  out of them

$$\vec{\rho} = (\mathcal{L}^r + \mathcal{N})^{-1} \begin{pmatrix} 1 \\ 0 \\ \dots \\ 0 \end{pmatrix}. \quad (4.87)$$

For numerical inversion of the matrix  $(\mathcal{L}^r + \mathcal{N})$  the LAPACK package is used. When the "density vector"  $\vec{\rho}$  is determined, it can be reshaped back to become a matrix again.

Along with the proposed approach, we tested few other numerical methods in attempt to get the stationary solution of the ME. Standard time propagation method was used to calculate the RDM of the system far enough in time to reach the stationary state. Arnoldi iterative method with and without preconditioner ([10],[15]) were also tested. For different reasons (poor convergence and fast numerical errors accumulation) this approaches didn't work for our motor models as efficient as the direct one described above.

To accelerate numerical computations, which can be quite long for models 3 and 4 (see the table 4.1), some simplifications were used. It was demonstrated in this chapter that blocks  $\rho_{01}$  and  $\rho_{10}$  of the RDM are independent from two other blocks. They also do not enter the formulae for the observables. It allows us to exclude from the consideration half of RDM elements. It is also often argued that the nondiagonal elements ( $\rho_{00}(m, m')$  and  $\rho_{11}(v, v')$  for  $m \neq m'$ ,  $v \neq v'$ ) in RDM decay fast in time and they can be neglected in search of the stationary state. In our case the nondiagonal elements lead to the nonzero angular momentum of the rotor (see the formula (4.78)) and we can't neglect them completely. To increase the numerical efficiency we assume that RDM has a band structure and ignore elements outside the band. Validity and stability of this treatment was approved in multiple numerical tests. Final results are presented for RDM, which includes 14 sub diagonals, while its overall dimensions are  $202 \times 202$  for the model 3 and  $402 \times 402$  for the model 4 (see the table 4.1).

Another possible way to increase the numerical efficiency is connected with func-

	Model 3	Model 4
Liouvillian tensor size	130 Mb	534 Mb
Number of basis functions	202	402
Lines of RDM taken into account	15	15
Rotor's moment of inertia	2000 a.u.	226852 a.u.
Maximum voltage	1.5 V	0.5 V
Time per graph (150 points)	3.5 hours	19 hours

Table 4.1: Computational parameters comparison for the models 3 and 4

tions  $\xi_1$  and  $\xi_2$ , which can be considered as "generalized self energies" in the ME approach. Their real parts, similarly as in the scattering case, lead to the renormalization of the energy levels and they can be neglected in calculations, which is a usual practice in the ME approach [17] (see also discussion in [28] where it is argued that the real parts are canceled in higher orders).

The most complicated from the computational point of view is the model 4. To calculate a current at a fixed voltage one should invert the matrix which is half of a gigabyte in size. It takes about 19 hours at ordinary PC to calculate the CVC inside the selected voltage window (150 points). Basis size is a parameter which is highly responsible for speed. One should take enough  $|m\rangle$  and  $|v\rangle$  basis states to get the converged results (in general more states are needed for higher voltages). Large moment of inertia in the model 4, to compare with model 3, is responsible for higher density of  $|m\rangle$  and  $|v\rangle$  states. It forces us to take more states in the basis to work in the same voltage window. To perform the calculations for the model 4 we had to decrease the voltage window and double the basis (see the table 4.1).

It's interesting to mention few other numerical challenges which we faced during the computations. One of them is the appearance of negative populations in the resulting RDM in some regimes. This problem is mentioned also by other authors [24] and seems to be a common issue in a ME theory. In some cases the  $(\mathcal{L}^r + \mathcal{N})$  matrix may appear to be noninvertible. It's possible to check how "good" the matrix is calculating its singular values (using, for example, LAPACK subroutines). If the

matrix has zero singular values, problems during the inversion should be expected. Physically it may mean that the ME has more than one stationary solution. It is not surprising for highly symmetrical motor models with many degenerate states at the bridge. Since this issues don't appear for models considered in this work, we don't discuss them here. However, they may be discussed in future works.

#### 4.2.4 Analytical solution for the elastic model

The results which are derived in this section are well known. They are included for completeness, general discussion and as the important special case of more complicated models. We start from the general equation (4.30) and clarify the action of Liouvillian parts  $\mathcal{L}_0$  and  $\mathcal{L}_1$  on  $\rho$ . The derivation procedure has a lot of similarities with the one described in the section 4.2.1. Model 1 Hamiltonian parts are given by formulas (3.7) with coupling coefficients (3.6). In the elastic transport regime RDM is just 2x2 matrix and blocks  $\rho_{ij}$  in the decomposition (3.14) are numbers. Using this decomposition and commutation relations for  $d$ -operators (3.8) it's easy to show that

$$\mathcal{L}_0\rho = -i\varepsilon_0(\rho_{10}d^\dagger - \rho_{01}d). \quad (4.88)$$

To derive an action of  $\mathcal{L}_1$  it's useful to start from the formula (4.46). Since  $h_0 = 0$  and  $h_1 = \varepsilon_0$  in model 1, time evolution of operators  $d$ ,  $d^\dagger$  and  $V_{dk}$  is trivial. This operators should be substituted to (4.46) to get

$$\begin{aligned} \mathcal{L}_1\rho = & -\int_0^\infty d\tau \sum_k \{ \\ & e^{-i(\varepsilon_k - \varepsilon_0)\tau} (1 - f_k) V_{dk}^2 (d^\dagger d \rho) + e^{+i(\varepsilon_k - \varepsilon_0)\tau} f_k V_{dk}^2 (d d^\dagger \rho) \\ & - e^{-i(\varepsilon_k - \varepsilon_0)\tau} f_k V_{dk}^2 (d^\dagger \rho d) - e^{+i(\varepsilon_k - \varepsilon_0)\tau} (1 - f_k) V_{dk}^2 (d \rho d^\dagger) \\ & + e^{+i(\varepsilon_k - \varepsilon_0)\tau} (1 - f_k) V_{dk}^2 (\rho d^\dagger d) + e^{-i(\varepsilon_k - \varepsilon_0)\tau} f_k V_{dk}^2 (\rho d d^\dagger) \\ & - e^{+i(\varepsilon_k - \varepsilon_0)\tau} f_k V_{dk}^2 (d^\dagger \rho d) - e^{-i(\varepsilon_k - \varepsilon_0)\tau} (1 - f_k) V_{dk}^2 (d \rho d^\dagger) \}. \end{aligned} \quad (4.89)$$

Using the  $\xi$ -functions definition (4.53) and decomposition (3.14) we may write

$$\begin{aligned} \mathcal{L}_1\rho = & -i\{d^\dagger d[\rho_{11}\xi_2^*(\varepsilon_0) + \rho_{00}\xi_1(\varepsilon_0) - \rho_{11}\xi_2(\varepsilon_0) - \rho_{00}\xi_1^*(\varepsilon_0)] \\ & + d d^\dagger[\rho_{00}\xi_1^*(\varepsilon_0) + \rho_{11}\xi_2(\varepsilon_0) - \rho_{00}\xi_1(\varepsilon_0) - \rho_{11}\xi_2^*(\varepsilon_0)] \\ & + d^\dagger[\rho_{10}\xi_2^*(\varepsilon_0) - \rho_{10}\xi_1(\varepsilon_0)] + d[\rho_{01}\xi_1^*(\varepsilon_0) - \rho_{01}\xi_2(\varepsilon_0)]\}. \end{aligned} \quad (4.90)$$

When  $\mathcal{L}_0\rho$  and  $\mathcal{L}_1\rho$  are calculated, they can be substituted to the full equation (4.30) which we write as

$$\frac{\partial}{\partial t}[\rho_{00}dd^\dagger + \rho_{11}d^\dagger d + \rho_{01}d + \rho_{10}d^\dagger] = \mathcal{L}_0\rho + \mathcal{L}_{1l}\rho + \mathcal{L}_{1r}\rho, \quad (4.91)$$

where superoperator  $\mathcal{L}_1$  must be specified for left and right leads separately. As in the section 4.2.1, the equation can be split to four, and two of them, which describe behavior of  $\rho_{00}$  and  $\rho_{11}$ , will be independent from other two for  $\rho_{01}$  and  $\rho_{10}$ . Moreover, since the equations (4.90) contain differences of complex conjugated terms we may get rid of  $\xi$ -functions real parts (4.59). After all the transformations, equations for two relevant blocks of RDM read

$$\begin{aligned} \frac{\partial}{\partial t}\rho_{00} &= -\Gamma_l(\varepsilon_0)f_l(\varepsilon_0)\rho_{00} + \Gamma_l(\varepsilon_0)[1 - f_l(\varepsilon_0)]\rho_{11} \\ &\quad -\Gamma_r(\varepsilon_0)f_r(\varepsilon_0)\rho_{00} + \Gamma_r(\varepsilon_0)[1 - f_r(\varepsilon_0)]\rho_{11}, \\ \frac{\partial}{\partial t}\rho_{11} &= +\Gamma_l(\varepsilon_0)f_l(\varepsilon_0)\rho_{00} - \Gamma_l(\varepsilon_0)[1 - f_l(\varepsilon_0)]\rho_{11} \\ &\quad +\Gamma_r(\varepsilon_0)f_r(\varepsilon_0)\rho_{00} - \Gamma_r(\varepsilon_0)[1 - f_r(\varepsilon_0)]\rho_{11}. \end{aligned} \quad (4.92)$$

To find the stationary solution we assume left hand sides to be equal to zero and add additional equation  $\rho_{00} + \rho_{11} = 1$ , which guarantee the correct normalization of the RDM. Solutions are

$$\begin{aligned} \rho_{00} &= \frac{\Gamma_l(\varepsilon_0)[1-f_l(\varepsilon_0)]+\Gamma_r(\varepsilon_0)[1-f_r(\varepsilon_0)]}{\Gamma_l(\varepsilon_0)+\Gamma_r(\varepsilon_0)}, \\ \rho_{11} &= \frac{\Gamma_l(\varepsilon_0)f_l(\varepsilon_0)+\Gamma_r(\varepsilon_0)f_r(\varepsilon_0)}{\Gamma_l(\varepsilon_0)+\Gamma_r(\varepsilon_0)}. \end{aligned} \quad (4.93)$$

To derive the formula for current we use (4.65) with the correct time evolution of operators which correspond to the model 1.  $\xi$ -functions definition (4.53) and decomposition (3.14) are applied to get

$$\begin{aligned} I &= i\text{Tr}_s\{d^\dagger d\xi_1^*(\varepsilon_0)\rho_{00} - dd^\dagger\xi_2^*(\varepsilon_0)\rho_{11} + d^\dagger d\xi_2(\varepsilon_0)\rho_{11} \\ &\quad + d\xi_2(\varepsilon_0)\rho_{01} - dd^\dagger\xi_1(\varepsilon_0)\rho_{00} - d^\dagger\xi_1(\varepsilon_0)\rho_{10}\}. \end{aligned} \quad (4.94)$$

Taking the trace, excluding the real parts of  $\xi$ -functions, and substituting formulas (4.59) for the imaginary parts, current can be expressed as

$$I = \rho_{00}\Gamma_l(\varepsilon_0)f_l(\varepsilon_0) - \rho_{11}\Gamma_l(\varepsilon_0)[1 - f_l(\varepsilon_0)] \quad (4.95)$$

(widths  $\Gamma$  and Fermi functions  $f$  in the formula for current are taken for the left lead). The stationary solution (4.93) should be substituted to (4.95) to get the final

formula

$$I = \frac{\Gamma_l(\varepsilon_0)\Gamma_r(\varepsilon_0)[f_l(\varepsilon_0) - f_r(\varepsilon_0)]}{\Gamma_l(\varepsilon_0) + \Gamma_r(\varepsilon_0)}. \quad (4.96)$$

# Chapter 5

## Results and Discussion

This chapter is divided to two parts. In the first part we compare scattering approach with the master equation approach. During the comparison, which is performed using models 1 and 2, interrelation between two approaches is discussed. The good correspondence between results in a weak coupling regime is demonstrated for the elastic transport model 1. The differences between two approaches are traced to the treatment of the vibrational states population in the model 2. Boltzmann factors, which are used in the generalized Landauer formula as an unoccupied bridge populations, are showed to be a poor approximation in the inelastic transport regime. An alternative way to calculate populations in a scattering approach is proposed as a possible way of improvement.

Molecular motor models 3 and 4 are discussed in the second part. The discussion starts from the charge transport properties of the model 3, where the different angular dependence of the molecule-lead coupling and its influence on the current is studied. The detailed analysis of CVC and vibrational excitation curves is performed. Molecular motor effect for the model 3 is demonstrated in the section 5.2.2, where the voltage dependence of the angular momentum mean value is studied. Attention is paid to the conditions which are necessary to observe the effect, particularly to the symmetry in the junction. In the last section the realistic model 4 and its promising rotational properties are discussed.

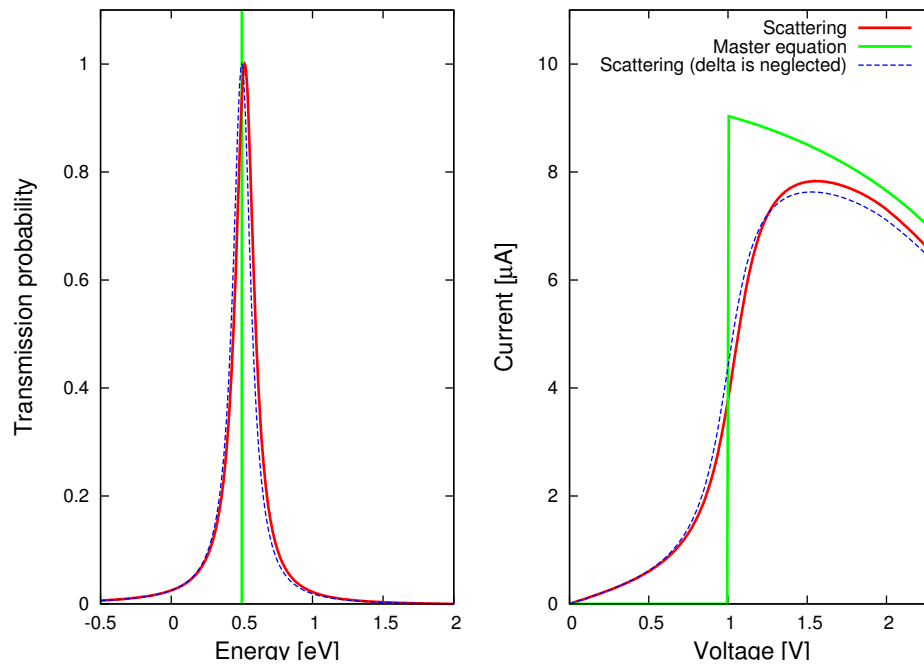


Figure 5.1: Transmission function and CVC for the model 1

## 5.1 Comparison of scattering and ME approaches

### 5.1.1 Weak coupling limit

To understand better the more complicated inelastic case we start with the trivial case of elastic model 1, where the scattering approach gives the exact results. Let's compare analytical formulas (4.21) and (4.96) for current, derived for the model 1 using scattering and ME approaches

$$I_1^{\text{scat}} = \frac{1}{2\pi} \int dE \frac{\Gamma_l(E)\Gamma_r(E)}{[E - \varepsilon_0 - \Delta_l(E) - \Delta_r(E)]^2 + \frac{1}{4}[\Gamma_l(E) + \Gamma_r(E)]^2} [f_l(E) - f_r(E)], \quad (5.1)$$

$$I_1^{\text{me}} = \frac{\Gamma_l(\varepsilon_0)\Gamma_r(\varepsilon_0)[f_l(\varepsilon_0) - f_r(\varepsilon_0)]}{\Gamma_l(\varepsilon_0) + \Gamma_r(\varepsilon_0)}. \quad (5.2)$$

CVC calculated using this formulas are showed at the fig. 5.1 (right). Different approaches give curves which may look different at first glance, but, in general, their behavior is similar. The decrease of the current after approximately 1.5 V is connected with the fact that left and right leads have finite conduction band widths. While we increase the voltage left lead band goes higher in energy and right lead goes lower, decreasing the overlap between bands. As a result current decreases and, at

certain voltage (which is not on the graph), disappears at all. Both current curves at the fig. 5.1 have the step at the same voltage, which appears when the Fermi sea level in the left lead  $\mu_l = U/2$  reaches the energy of the bridge state  $\varepsilon_0$ . The obvious difference between two curves is that the step in the scattering approach result is much wider. Scattering calculations in this case are more precise, since the information about the width of the bridge's transmission function peak is lost in the second order WBR ME (see the fig. 5.1). In ME approach the width of the step at CVC is defined by the width of the Fermi-Dirac distribution, which is of the order of  $kT$ .

It's also interesting to stress here that the real parts of self energies  $\Delta_\alpha$  don't enter the master equation version of the formula. In the scattering formula they represent a small energy shifts (renormalization). In fig. 5.1, where scattering calculation results with and without  $\Delta_\alpha$  are plotted, we can see that their influence to the final curves is small. Both energy levels renormalization and transmission peaks widening should be expected at higher orders of ME theory.

ME approach is designed for the weak coupling regime. It may be demonstrated, that the width of the transmission function peak is connected with the coupling strength. In a case of weak coupling the width of the peak is also small and results, obtained using different methods, are close to each other. Formulas (5.1) and (5.2) coincide when the coupling goes to zero. To find this limit we neglect the self energies real parts in (5.1) and rewrite the formula in the form

$$I_{\text{scat}} = \int dE \frac{\Gamma_l(E)\Gamma_r(E)[f_l(E) - f_r(E)]}{\Gamma_l(E) + \Gamma_r(E)} \delta_\eta(E - \varepsilon_0), \quad (5.3)$$

where

$$\delta_\eta(E - \varepsilon_0) = \frac{1}{\pi} \frac{\eta}{(E - \varepsilon_0)^2 + \eta^2} \quad (5.4)$$

is the Cauchy-Lorentz distribution with the half-width

$$\eta = \frac{\Gamma_l(E) + \Gamma_r(E)}{2}. \quad (5.5)$$

It is known that

$$\lim_{\eta \rightarrow 0} \delta_\eta(x) = \delta(x), \quad (5.6)$$

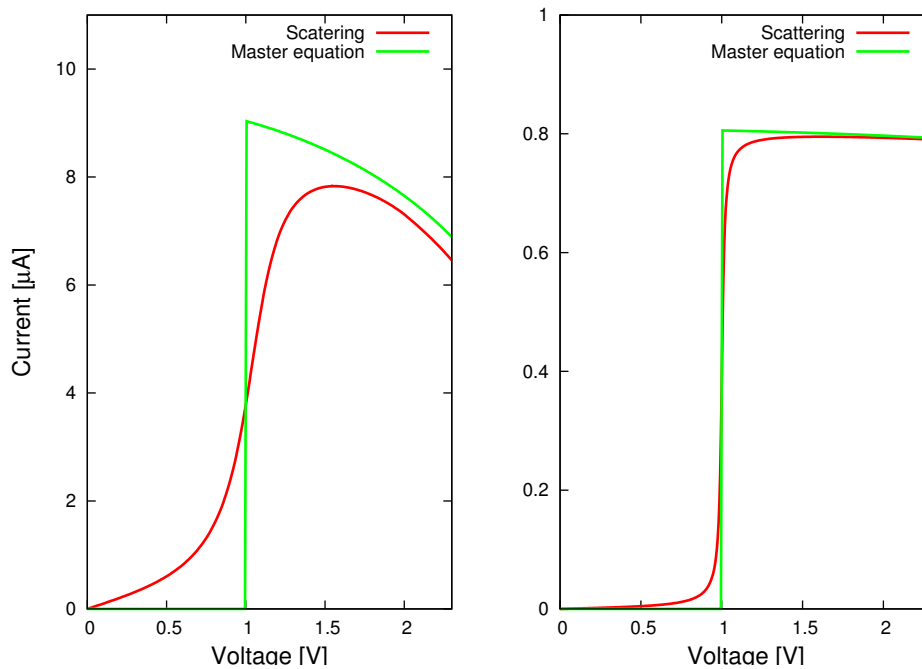


Figure 5.2: Influence of the band width and coupling strength to the current. At the left graph  $\beta_1 = 1.0$  and  $\beta_2 = 0.2$ . At the right graph  $\beta_1 = 3.0$  and  $\beta_2 = 0.1$ .

where  $\delta(x)$  is the Dirac delta function. Thus, if the coupling is small enough, we may assume that  $\delta_\eta(E - \varepsilon_0)$  behaves almost like a delta function. It removes the integral and the formula (5.3) coincide with (5.2).

Half-width  $\eta$  depends on energy  $E$  through the functions  $\Gamma_\alpha$  which are, thus, responsible for the width of the transmission function peak. Its maximum value is

$$\eta_{\max} = \frac{2\beta_2^2}{\beta_1}. \quad (5.7)$$

Both methods give almost identical results in the regimes where the coupling strength  $\beta_2$  is small and the conduction band width  $\beta_1$  is large (see the fig. 5.2).

### 5.1.2 Importance of vibrational populations

The Model 2 is well suited to discuss principle differences between the ME and scattering approaches. In the inelastic transport regime single electron approximation, which is assumed in the scattering approach, can be among the factors that distinguish calculations results significantly. Despite the fact, that there is just one electronic state at the molecular bridge and electrons can't interact directly, they

still can interact indirectly through the molecular vibrations. This is taken into account in the ME approach.

We are going to compare the scattering theory formula for current (4.29) with its ME version (4.69). Since both of them are a bit bulky, they should be modified first to make the comparison easier. To present the formula (4.29) in a more tractable way, we introduce the transmission rates for electron tunneling from the left lead to the right and vice versa which read

$$\begin{aligned} W_{mm'}^{r\leftarrow l} &= \frac{1}{2\pi} \int dE [1 - f_r(E - E_{m'})] \Gamma_r(E - E_{m'}) |\langle m' | G_s | m \rangle|^2 \\ &\quad \times \Gamma_l(E - E_m) f_l(E - E_m), \\ W_{mm'}^{l\leftarrow r} &= \frac{1}{2\pi} \int dE [1 - f_l(E - E_{m'})] \Gamma_l(E - E_{m'}) |\langle m' | G_s | m \rangle|^2 \\ &\quad \times \Gamma_r(E - E_m) f_r(E - E_m). \end{aligned} \quad (5.8)$$

Indexes  $m_i$  and  $m_f$  from (4.29) are renamed here to  $m$  and  $m'$  respectively. Using this notations, scattering theory approach formula reads

$$I_2^{\text{scat}} = \sum_m P_m \sum_{m'} W_{mm'}^{r\leftarrow l} - \sum_m P_m \sum_{m'} W_{mm'}^{l\leftarrow r}, \quad (5.9)$$

To make the ME version of the formula (4.69) more transparent we neglect the real parts of  $\xi$ -functions. This approximation was already discussed in the previous section as well as in the chapter 4. For the model 2 we also substitute  $V_d(m, v) = \langle m | v \rangle$  (see the chapter 3) to the formulas. Another thing which can be done is to neglect the off-diagonal elements of RDM (coherences). Although in all the calculations presented in this work coherences are taken into account, we found them to play a little role in the formulas for current and vibrational excitation energy. We, thus, neglect them just in this section to simplify the analytical form of (4.69). The modified version of the formula we express through the rates

$$\begin{aligned} \mathcal{W}_{mv}^{s\leftarrow l} &= f_l(E_v - E_m) \Gamma_l(E_v - E_m) |\langle m | v \rangle|^2, \\ \mathcal{W}_{vm}^{l\leftarrow s} &= [1 - f_l(E_v - E_m)] \Gamma_l(E_v - E_m) |\langle m | v \rangle|^2, \end{aligned} \quad (5.10)$$

which give the transmission probability for electron hopping from the left lead to the molecule and back inducing vibrational transitions between occupied bridge states  $m$  and unoccupied bridge states  $v$ . As usual in this work we use index "s" to denote the molecular bridge. The formula for current reads

$$I_2^{\text{me}} = \sum_m \rho_m \sum_v \mathcal{W}_{mv}^{s\leftarrow l} - \sum_v \rho_v \sum_m \mathcal{W}_{vm}^{l\leftarrow s}, \quad (5.11)$$

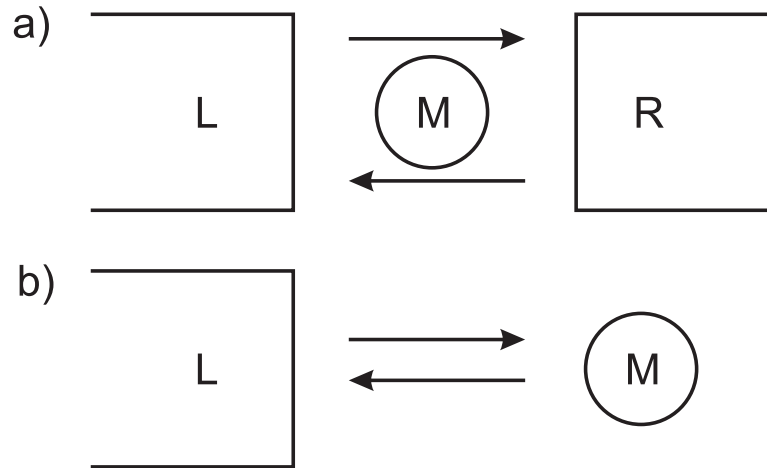


Figure 5.3: Schematic representation of formulas for current in scattering (a) and ME (b) approaches.

where  $\rho_m \equiv \rho_{00}(m, m)$  and  $\rho_v \equiv \rho_{11}(v, v)$ .

Before the comparison of the CVC calculated using both formulas it's interesting to say few words about mechanisms of tunneling which are incarnated in formulas (5.9) and (5.11). Both of them consist of two terms which correspond to two current fluxes which pass the junction in opposite directions. As it is clear from the structure of the formulas, in the ME approach this fluxes move between the left lead and the molecule (equivalently, it can be the right lead and the molecule). The stationary state of the molecule, which is given here by populations  $\rho_m$  and  $\rho_v$  of unoccupied and occupied bridge, is known exactly. We get it solving the ME. In the scattering approach fluxes are composed in a way, that they describe the tunneling from the left lead to the right lead through the molecule (see the fig. 5.3). According to the specific of the scattering theory there is no much attention payed to the internal state of the molecule. Populations  $P_m$  are assumed to be in thermal equilibrium. They are given by the Boltzmann distribution. For this reason, for example, a tunneling electron doesn't "feel" changes, which were made in the bridge vibrational state by a previous electron. All the internal dynamics of the molecular bridge in scattering approach is hidden in the Green's operator  $G_s$  (see the formula (5.8)).

Now let's compare CVC obtained using different approaches which are showed in the fig. 5.4. Since the bridge has internal degree of freedom in this model and the tunneling probability depends on the state of the bridge, the concept of the

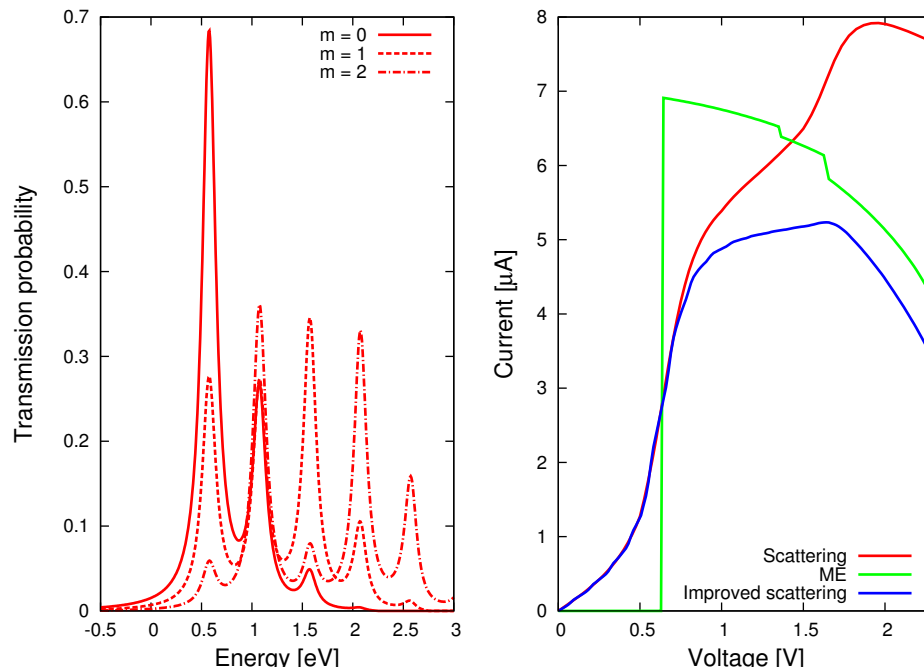


Figure 5.4: Transmission functions and current voltage characteristics of the bridge in model 2. Blue line is explained in the section 5.1.3

transmission function should be clarified. Left graph at the fig. 5.4 illustrates the probability, that the electron at certain energy will pass through the bridge and change its vibrational state from the initial state  $m$  ( $m = 0$  correspond to the ground state) to any other state, i.e. it's summed through all final states. As we can see from the picture, existence of vibrational degrees of freedom on the bridge, leads to the situation, when the transmission function has multiple peaks, which correspond to different vibrational transitions. It leads also to the multiple "vibrational steps" at the current-voltage characteristics. Such steps may appear at the voltage  $U$  if the chemical potential  $\mu_l = U/2$  (or  $\mu_r = -U/2$ ) reaches a certain resonant energy, which correspond to a certain vibrational transition at the bridge, and a new tunneling channel opens up.

The scattering and ME approaches results, which are plotted with solid red and green lines at the fig. 5.4, have significant differences. The curves exhibit resonant steps at voltages  $U_1 = 2(E_v^0 - E_m^0) = 0.64$  V,  $U_2 = 2(E_m^2 - E_v^0) = 1.36$  V and  $U_3 = 2(E_v^1 - E_m^0) = 1.64$  V. Both curves behave very similar at  $U_1$ . The main difference is that the step is much wider in the scattering approach. This happens

for the same reasons which were discussed in the previous section. ME curve drops at  $U_2$  and  $U_3$ , while scattering curve has no feature at  $U_2$  and at  $U_3$  there is a step-like increase of the current. There are obviously no similarities at higher voltages.

One of the possible sources of disagreement can easily be found. Usage of the Boltzmann distribution of populations  $P_m$  in the formula (5.9) leads to the situation when the molecule is almost in its ground vibrational state<sup>1</sup>. Populations of higher states are negligibly small. Moreover, the distribution is the same for all voltages. If only ground state is populated, among all transmission functions (3 of them are plotted at the fig. 5.4) we take into account only one (solid line), which describe tunnelings through the bridge in ground state. It contains three peaks, first two of them belong to the interval of voltages of interest and, being integrated in the Landauer formula, forms two wide steps at  $U_1$  and  $U_3$  which we can see at the current graph (fig. 5.4).

In contrast to the scattering theory description, in ME approach the molecular bridge reaches some stationary state after a large amount of tunneling events. The populations distribution in this state strongly depends on voltage and, in general, is very different from the temperature distribution  $P_m$  at the nonzero voltages. See the fig. 5.5, where stationary populations distributions, obtained from the ME calculations, are showed for two different voltages. It demonstrates that the Boltzmann distribution  $P_m$  is, actually, a very poor approximation of the vibrational states populations, especially at high voltages.

### 5.1.3 Balance equation

To get the realistic populations distribution within the framework of the scattering theory, it's possible to write the dynamical equation for the time evolution of  $P_m$ . To do it, first, we use the definition (5.8) to introduce the quantity

$$W_{mm'} = W_{mm'}^{r\leftarrow l} + W_{mm'}^{l\leftarrow r} + W_{mm'}^{l\leftarrow l} + W_{mm'}^{r\leftarrow r}, \quad (5.12)$$

---

<sup>1</sup>At least up to the room temperature which is a highest temperature considered in this work

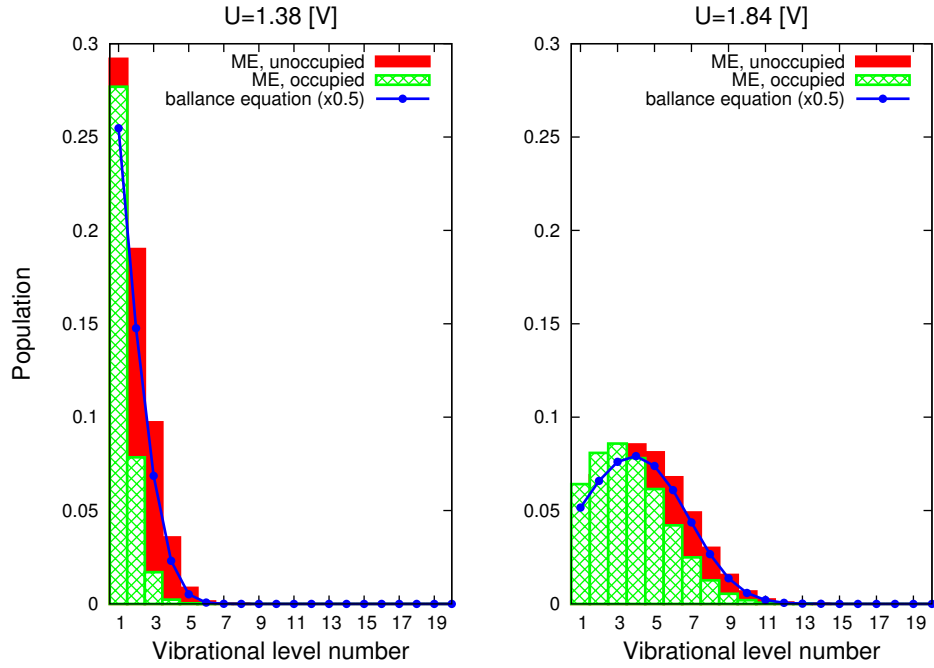


Figure 5.5: Stationary vibrational states populations of the bridge (model 2) calculated using the ME and balance equation techniques for two different voltages.

which gives the rate to change the bridge's vibrational state from  $m$  to  $m'$  as a result of all possible events connected with the dynamics of electrons. Two new terms

$$\begin{aligned} W_{mm'}^{l\leftarrow l} &= \frac{1}{2\pi} \int dE \omega_{mm'}^{l\leftarrow l}(E) f_l(E - E_m) [1 - f_l(E - E_{m'})], \\ W_{mm'}^{r\leftarrow r} &= \frac{1}{2\pi} \int dE \omega_{mm'}^{r\leftarrow r}(E) f_r(E - E_m) [1 - f_r(E - E_{m'})] \end{aligned} \quad (5.13)$$

describe the excitation (or deexcitation) induced by electrons reflected from the bridge. Equivalently,  $W_{mm'}$  can be written as

$$\begin{aligned} W_{mm'} &= \frac{1}{2\pi} \int dE |\langle m' | G_s | m \rangle|^2 \\ &\times \{ \Gamma_l(E - E_m) f_l(E - E_m) + \Gamma_r(E - E_m) f_r(E - E_m) \} \\ &\times \{ \Gamma_l(E - E_{m'}) [1 - f_l(E - E_{m'})] + \Gamma_r(E - E_{m'}) [1 - f_r(E - E_{m'})] \}. \end{aligned} \quad (5.14)$$

The rate equation for  $P_m$  reads

$$\frac{dP_m}{dt} = \sum_{m'} W_{m'm} P_{m'} - \sum_{m''} W_{mm''} P_m. \quad (5.15)$$

It has the following interpretation: the population  $P_m$  changes itself in time as a result of two probability fluxes. One goes from the state  $m$  to all other states  $m''$  and the other one comes from all states  $m'$  to  $m$ . To get the stationary population

distribution the time derivative in (5.15) is set to zero, must be solved. We call it a "balance equation". It may be written in the form

$$\sum_{m'} [W_{m'm} - \delta_{m'm} \sum_{m''} W_{m'm''}] P_{m'} = 0 \quad (5.16)$$

Solution of (5.16) gives the distributions which are very similar to those obtained from the ME (see the fig. 5.5). The principal difference is that in scattering approach we don't have occupied bridge populations  $p_v$  and the normalization condition  $\sum P_m = 1$  is different from the normalization in ME approach  $\sum \rho_m + \sum \rho_v = 1$ . To present populations in the fig. 5.5 at the same scale we multiply  $P_m$  with 0.5.

Using population distributions obtained from the balance equation instead of Boltzmann factors in the formula (5.9) we get the CVC which is plotted with blue at the fig. 5.4. This result is based on the non-equilibrium population distributions and, also, poses the information about the transmission peaks width. In this sense it unites the advantages of both methods. From computational point of view the necessity to solve the balance equation for each voltage makes scattering calculations much slower. Despite the fact that the balance equation is "twice smaller", than the ME (there is no occupied bridge data there), we still have to integrate matrices in the scattering approach. Together with the balance equation, it can be even slower than the ME approach.

#### 5.1.4 Fluxes analysis

Having in mind the experience obtained analyzing the model 1, the reasonable question appears, if it's possible to make coupling smaller and improve the convergence between green and blue curves in the fig. 5.4? To check it we decrease  $\beta_2$  from 0.2 eV to 0.05 eV. Resulting curves are plotted at the fig. 5.6. Scattering calculations here are enhanced using populations obtained from the balance equation.

Together with the CVC we present also the vibrational excitation voltage dependence. To calculate it in the ME approach the formula (4.73) is used. Similar formula for scattering approach doesn't take into account occupied bridge populations  $\rho_v$ , it reads

$$\langle H_s \rangle_{scat} = \sum_m E_m P_m. \quad (5.17)$$

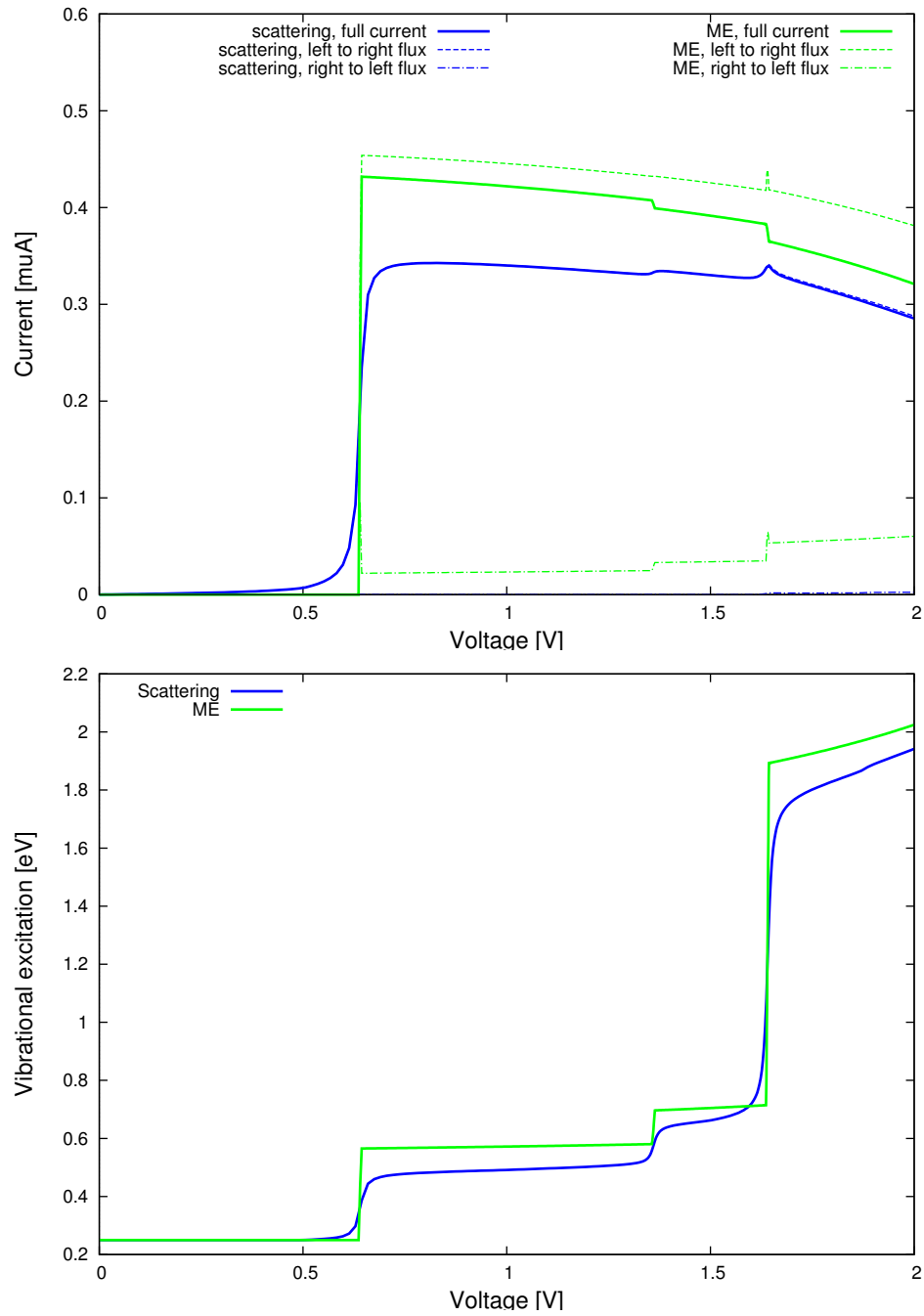


Figure 5.6: Current and vibrational excitation voltage dependences for the model 2, calculated using the ME and scattering approaches. Current fluxes from the left to the right and from the right to the left are plotted by dashed and dash-dotted lines respectively.

When populations  $P_m$  are approximated by the Boltzmann factors, which doesn't depend on voltage,  $\langle H_s \rangle_{scat}$  is constant. Using the balance equation to calculate  $P_m$ , we get the vibrational excitation voltage dependence which is in good correspondence with the ME result (see the fig. 5.6). It can be considered as another demonstration of the validity of the balance equation.

Current curves are closer in the fig. 5.6 than in the fig. 5.4 but they are still qualitatively different. In a small coupling regime all steps at  $U_1$ ,  $U_2$  and  $U_3$ , which were discussed in the previous section, are now clearly seen at both curves (they are also accompanied by the steps at vibrational excitation curves at the same voltages). The principle difference is connected with steps at  $U_2$  and  $U_3$ . Current curves behave very different at this voltages.

Since the formulas for current (5.9) and (5.11) both can be divided to two fluxes, it may be interesting to analyze them separately to get the additional data about differences in two approaches. "Left to right" and "right to left" fluxes are plotted with dashed and dash-dotted lines in the fig. 5.6. Subtracting the second one from the first one we get the full current (solid line). In the scattering approach flux which goes from the right lead to the left is negligibly small and the the full current is composed mainly from the left to right flux. In the ME approach right to left flux is significant, and it contains those steps which produce overall current drops at  $U_2$  and  $U_3$  in the full current. Comparing just left to right flux in ME with overall current in scattering approach, we find them to be very similar.

## 5.2 Molecular motor models

### 5.2.1 Current and excitation function

We start the discussion of the motor models from the charge transport properties of the junction in the model 3. The CVC and the vibrational excitation energy of the molecular bridge for models 3a-c at temperature  $T = 50\text{K}$  are shown in fig. 5.7. Let us first focus on the current-voltage curve. The red curve for the model 3a exhibits the behavior expected for the model with small coupling between vibrations and the electronic motion. We observe a resonance step at the voltage of

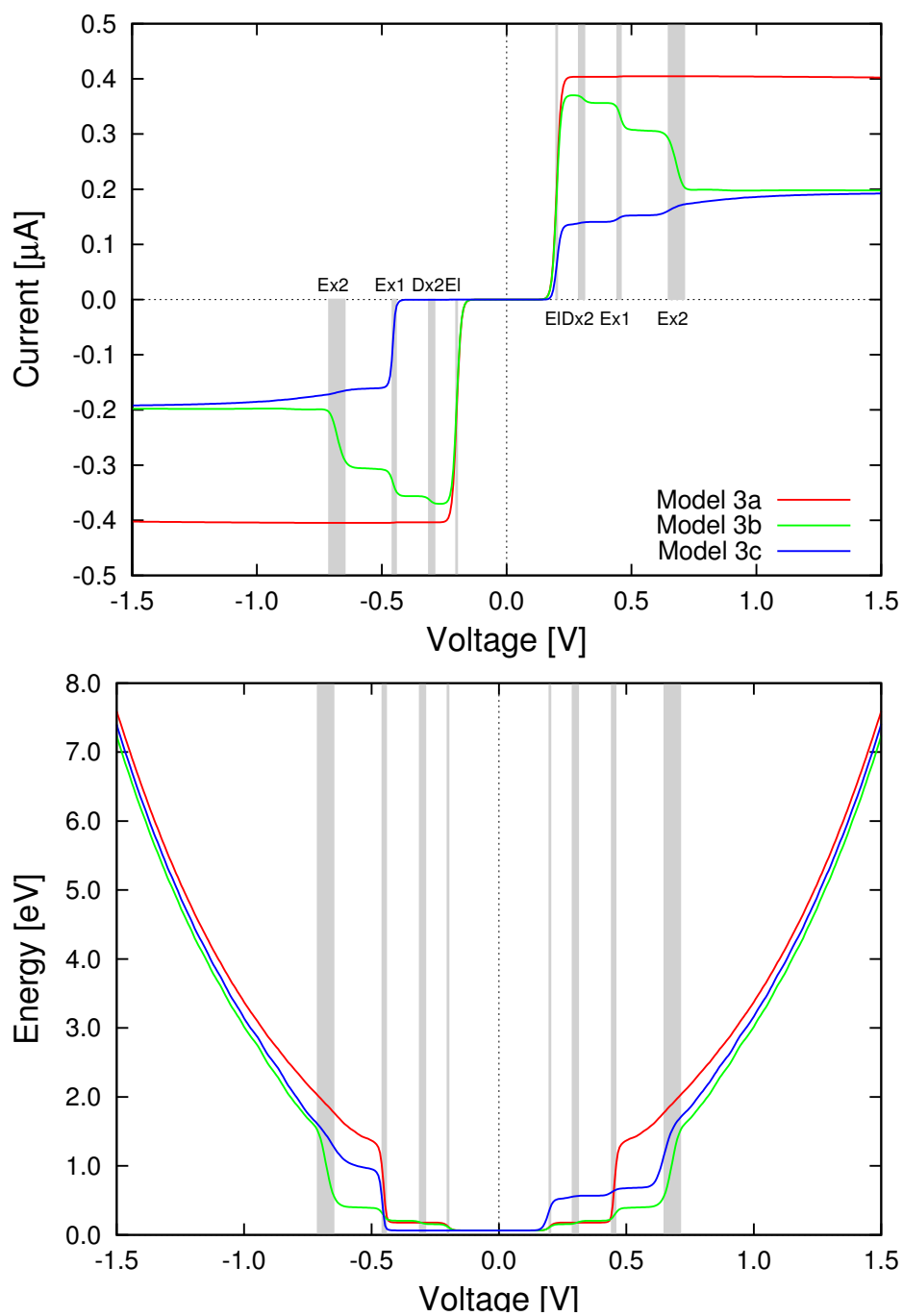


Figure 5.7: Current (top) and mean value of excitation energy  $\langle H_s \rangle$  (bottom) as a function of voltage, applied to the junction, for models 3a-c at temperature  $T = 50$  K. The shaded bars show the positions of the steps derived from the energies of the molecular levels (see the text).

Series	Process	$\omega_{mv} = E_v - E_m$	$ \langle m V_{dl} v\rangle ^2$	$ \langle m V_{dr} v\rangle ^2$
El	$e_k + M_m^0 \leftrightarrow M_{v=m}^1$	0.1	0.2 – 1	$\sim 10^{-4}$
Ex1	$e_k + M_m^0 \leftrightarrow M_{v=m+1}^1$	0.21-0.23	0.005 – 0.015	0.05 – 0.3
Ex2	$e_k + M_m^0 \leftrightarrow M_{v=m+2}^1$	0.31-0.36	0.001 – 0.06	0.001 – 0.01
Ex3	$e_k + M_m^0 \leftrightarrow M_{v=m+3}^1$	0.42-0.48	< 0.005	< 0.005
Dx1	$e_k + M_m^0 \leftrightarrow M_{v=m-1}^1$	-(0.01-0.03)	0.005 – 0.015	0.05 – 0.3
Dx2	$e_k + M_m^0 \leftrightarrow M_{v=m-2}^1$	-(0.16-0.12)	0.001 – 0.05	0.001 – 0.01
Dx3	$e_k + M_m^0 \leftrightarrow M_{v=m-3}^1$	-(0.23-0.28)	< 0.005	< 0.005

Table 5.1: Inelastic one-electron attachment and detachment processes. Table gives the threshold electron energies of the inelastic processes and approximate size of the matrix elements responsible for the transitions due to electrons from left and right leads. All values are in units of eV.

0.2 V corresponding to twice the charging energy of the molecule 0.1 eV. The models 3b (green line) and 3c (blue line) differ by more complicated step structure and the different stationary value of current finally reached. The second difference is easily understood. While the coupling to the leads has the same overall strength for all of the models ( $\beta_2 = 0.07$  eV), the coupling in the model 3b depends on the angular variable which makes it effectively smaller when the system starts to vibrate. The angular dependence is also a source of the negative differential conductance since the coupling in the model 3b reaches the maximum for the angles near the equilibrium position of the vibrational coordinate  $\varphi$ , which is where the system stays for low voltages. In model 3c the coupling to the right lead  $V_{dr}(\varphi)$  has maximum strength in the different position, which makes the effect of negative differential conductance to disappear. Both models 3b and 3c have the same average value of couplings  $V_{d\alpha}(\phi)$  ( $\alpha = l, r$ ) and the asymptotic value of current for large voltages is therefore identical for both models.

To explain the details of the step-like behavior of the curves we start from the mechanism of sequential tunneling through the bridge. Electron conduction is thus

understood as a sequence of charging

$$e_k + M_m^0 \rightarrow M_v^1 \quad (5.18)$$

and discharging

$$M_v^1 \rightarrow M_m^0 + e_k \quad (5.19)$$

events on the bridge. In the first event (charging) the electron starts in one of the leads in state  $k$  and jumps into the unoccupied bridge in the vibrational state  $m$  turning it into occupied bridge in the vibrational state  $v$ . In the second event the electron starts in the occupied bridge in the state  $v$  and leaves the bridge in the state  $m$  jumping into the leads to the state  $k$ . The energy is conserved in both of the events

$$\varepsilon_k + E_m = E_v, \quad (5.20)$$

where  $\varepsilon_k$  is the energy of an electron in a state  $k$ . In equation (3.26) we defined  $E_m$  and  $E_v$  as the vibrational energies of the unoccupied and occupied bridge respectively. Each  $\omega_{mv} \equiv E_v - E_m$  defines a threshold energy for one possible in/out channel, which becomes available for tunneling at voltage  $U = \pm 2\omega_{mv}$  (when chemical potentials of the leads are equal  $\mu_\alpha = \pm \frac{U}{2} = \pm \omega_{mv}$ ) and can (but not necessary will) show itself as a step in the picture 5.7. Since the structure of energy levels is the same for all models 3a-c, we can expect the steps at the same voltages for all models. For the detailed analysis of the steps we show the values of the threshold energies  $\omega_{mv} \equiv E_v - E_m$  in table 5.1. The transitions are divided in several groups. In the first group (denoted El) the vibrational state of the molecule is unchanged and  $v = m$ . The corresponding threshold energy is  $\omega_{mv} = 0.1eV$  independent of the value of  $m$ . This is a consequence of the shape of the two potentials in Hamiltonians (3.43) for the model 3, which is identical except of vertical and horizontal shift (see the fig. 3.5). There are also excitation groups Ex1-Ex3 corresponding to  $v = m + 1$ ,  $v = m + 2$  and  $v = m + 3$ . In the harmonic approximation the threshold energies would also be independent of  $m$ . The table 5.1 shows the range of values of  $\omega_{mv}$  for low states  $m = 0, 1, \dots, 10$  (the choice of this maximum value of  $m$  is guided by the attained excitation energy show in the lower part of the figure). The last, "deexcitation" groups Dx1-Dx3 are characterized by  $v = m - 1$ ,  $v = m - 2$  and  $v = m - 3$ .

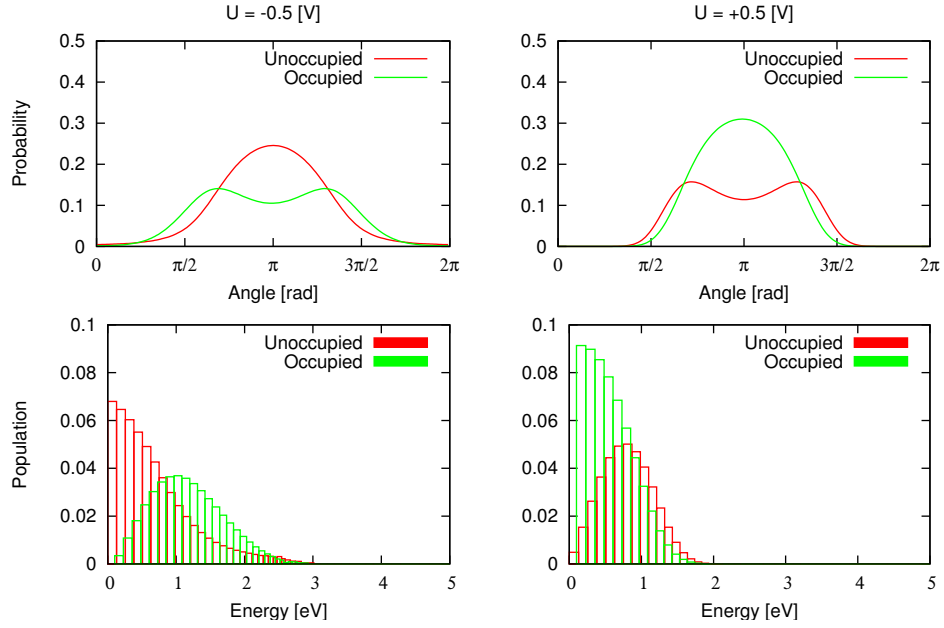


Figure 5.8: Angle distributions and populations calculated independently for unoccupied and occupied bridge in model 3c.

If we compare the predicted positions of the steps  $U = \pm 2\omega_{mv}$  given by the values from the table 5.1 with the positions of the steps in the fig. 5.7, we see that the steps correspond to voltages approximately 0.2, 0.3, 0.45 and 0.7, i. e. to series El, Dx2, Ex1 and Ex2. Remarkable is that for the voltage  $|U| > 0.8V$  vibrational energy of the bridge doesn't show any steps and grows parabolically for all models. The current-voltage characteristics also become smooth in this voltage region. The level of excitation of the molecule is too high for the harmonic approximation to apply and many different vibrational states are involved. We expect that quasi-classical theory could be applied in this regime.

In the equilibrium ( $U = 0$ ) only one lowest vibrational level  $E_m^0 = 0.065 \text{ eV}$  is populated (it correspond to the minimum at the vibrational excitation curve in fig. 5.7). Bridge remains "closed" for current until the first step occurs at the voltage 0.2 V, when the whole El set of channels opens. If we consider bridge originally in its ground state with energy  $E_m^0$  the first tunneling event

$$\varepsilon_k + E_{m=0} \xrightarrow{\text{El}} E_{v=0} \begin{cases} \xrightarrow{\text{El}} E_{m=0} + \varepsilon_k \\ \xrightarrow{\text{Dx1}} E_{m=1} + \varepsilon_{k'} \end{cases} \quad (5.21)$$

can leave the bridge in the excited state  $E_{m=1}$  through the channel Dx1. When the next electron comes and the bridge is already in the excited state, tunneling can excite it even higher, but only by one quantum per tunneling event. Excitation to the high levels is limited by competing process of deexcitation. This picture is the same for all three models. To appreciate the differences among them we must look at Franck-Condon factors  $|\langle m|V_{dl}|v\rangle|^2$  and  $|\langle m|V_{dr}|v\rangle|^2$  responsible for the strength of each  $e_k + M_m^0 \leftrightarrow M_v^1$  transition. For the model 3a it is  $V_{dl} = V_{dr} = \text{constant}$ . Since the potentials differ only slightly, it is  $\langle m|v\rangle \simeq \delta_{mv}$  (states are almost orthogonal) and the El channels are dominant with only small contribution of Ex1, Dx1 and virtually no contribution for higher channels. This explains why the red curves in current-voltage and excitation graphs show steps only at voltages corresponding to these channels. To understand behavior for the models 3b and 3c the values  $|\langle m|V_{d\alpha}|v\rangle|^2$  are shown in the table 5.1. We have to keep in mind that  $V_{dl}=V_{dr}$  for the model 3b. The values of  $|\langle m|V_{dr}|v\rangle|^2$  shown in the last column are the ones for the model 3c. There is pronounced difference in the first step at  $U = 0.2\text{V}$  between models 3b and 3c. Now we can understand that. While the both charging and discharging of the bridge proceeds dominantly through El channel for the model 3b (giving the step similar to model 3a) the discharging to right electrode through channel El is strongly suppressed for model 3c. The current conduction is thus possible dominantly thanks to discharging through the channel Dx1 to right lead for the model 3c. This gives smaller value of current, but higher value of vibrational excitation for this model. Also for higher voltages the sizes of steps in excitation curves follow the sizes of the Franck-Condon factors.

One striking feature apparent from the figure 5.7 is the asymmetry of the curves for the model 3c. This is a consequence of the asymmetry  $|\langle m|V_{dl}|v\rangle|^2 \neq |\langle m|V_{dr}|v\rangle|^2$ . For the negative voltages the channel El is not available in model 3c even for  $U < -0.2$ , because the charging has to proceed from the right electrode and Franck-Condon factor  $|\langle m|V_{dr}|v\rangle|^2$  is suppressed by 4 orders of magnitude. Charging of the bridge becomes possible only with availability of the process Ex1. Both current flow and vibrational excitation thus take place only for negative voltages  $U \lesssim -0.45$ .

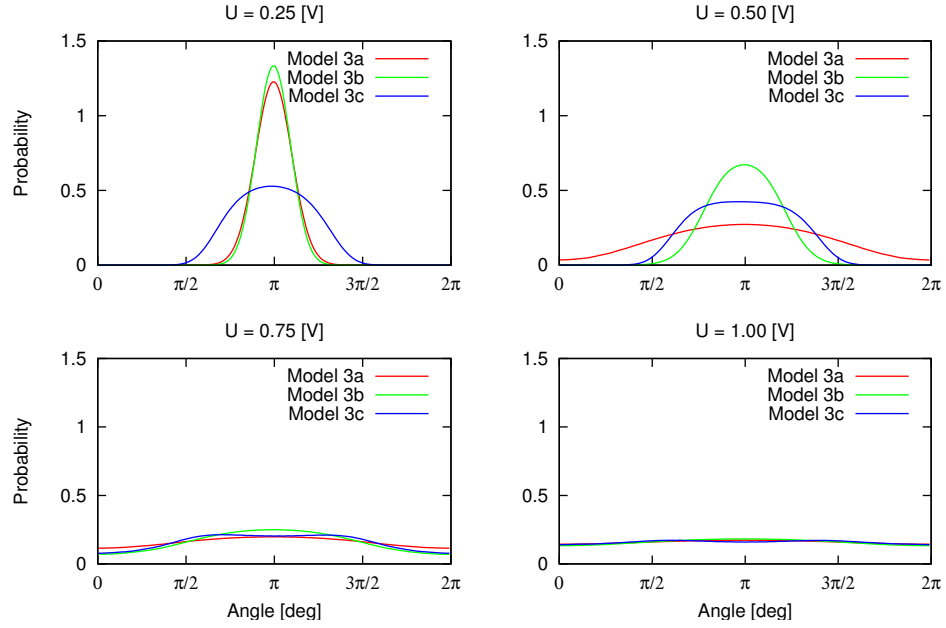


Figure 5.9: Angular probability distribution of the bridge  $p(\varphi)$  at different voltages.

Another way to look at this asymmetry is to inspect the angle distributions

$$p_0(\varphi) \equiv \text{Tr}\{d d^\dagger \rho |\varphi\rangle \langle \varphi|\} \quad (5.22)$$

$$p_1(\varphi) \equiv \text{Tr}\{d^\dagger d \rho |\varphi\rangle \langle \varphi|\} \quad (5.23)$$

and populations  $\rho_v$  of vibrational levels on the occupied and  $\rho_m$  on the unoccupied bridge respectively. They are shown in the fig. 5.8 for voltages  $U = \pm 0.5$  V. We can make an observation, that at negative voltages, when electrons tunnel from the right to the left and the right lead is the donor of electrons, occupied bridge angle distribution "tunes" itself to have maximums closer to the maximums of the coupling. At positive voltages unoccupied bridge angle distribution takes profile of the right coupling, which acts as an acceptor of the electrons this time. It can be concluded that the angle dependent part of the coupling can influence the angle distribution in the leads in a way, that the coupling which couples the donor lead influence the occupied bridge space and the acceptor lead coupling influence the unoccupied space. Resulting asymmetry can be found also in population distributions in the lower part of the fig. 5.8. Similar distributions for models 3a and 3b (not shown here) exhibit no asymmetry for change  $U \rightarrow -U$  and the distributions  $\rho_m$  and  $\rho_v$  for unoccupied

and occupied states are almost identical.

In the figure 5.9 we compare the angular distributions  $p(\varphi) = \text{Tr}\{\rho|\varphi\rangle\langle\varphi|\} = p_0(\varphi) + p_1(\varphi)$  for all models 3a-c at the voltages  $U = 0.25, 0.5, 0.75$  and  $1.0$ . There is a common trend for the angle to become more and more delocalized while the voltage grows. The degree of delocalization follows from the excitation curve in the figure 5.7 (bottom). At  $U = 0.25$  the distribution for the model 3c is the broadest one, but already at  $U = 0.50$  the model 3a distribution width becomes larger. Above the last step in the excitation and current curves the angle is completely delocalized.

Current for models 3b and 3c is asymptotically factor of two smaller than the same value for the model 3a. At large voltages angle distribution at the bridge is more or less homogeneous. For this reason angle-dependent part of the coupling for models 3b and 3c, which is equal to  $(\cos(\varphi - \varphi_\alpha))^2$ , reaches its mean value 0.5. For the model 3a angle-dependent part of the coupling is constant and equal to 1, which is two times larger.

### 5.2.2 Angular momentum and motor effect

We plot the mean value of the angular momentum  $\langle L_z \rangle$  against the voltage applied across the junction in fig. 5.10. According to our calculations for models 3a-3c the mean value of the angular momentum  $\langle L_z \rangle$  is in general non-zero and can reach values of the order of the reduced Planck constant  $\hbar$ . The value strongly depends on the voltage, applied to the junction. This is an interesting fact since we deal with an example of the molecular scale device which can perform rotations controlled by voltage applied to the device. For example,  $\langle L_z \rangle$  can grow with the voltage and change its sign (which means changing of the direction of rotation) when the polarity is inverted. Note that this inversion of the rotation sign with the sign of the voltage is observed only in the model 3c. There is no way to distinguish the sign of voltage in the symmetric models 3a and 3b and  $\langle L_z \rangle$  there is an even function of  $U$ . The voltage dependence of angular momentum is not straightforward for these models, containing local minima and maxima that may be difficult to understand in detail.

In all models 3a-c the molecule does not rotate when the absolute value of the voltage is smaller than 0.4 V. The onset of each curve follows the degree of vibra-

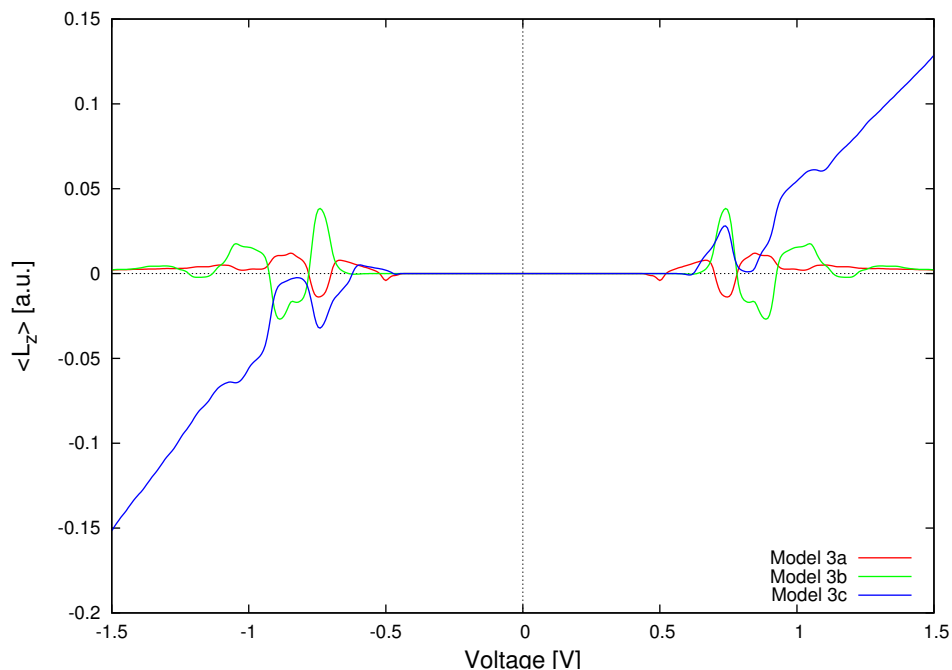


Figure 5.10: Mean value of the angular momentum of the molecule  $\langle L_z \rangle$  as a function of voltage for models 3a, 3b and 3c at the temperature  $T = 50$  K

tional excitation of the molecule (confront bottom part of figure 5.7). This behavior reflects the fact, that the molecule should be excited enough and overcome the rotational barrier at 2.5-2.6 eV in order to perform rotational movement. Significant population of the states above the barrier can be expected only when the mean value of the vibrational energy of the bridge molecule (bottom part of the figure 5.7) is order of magnitude of 1eV. The potentials (i. e. also vibrational levels) are the same for all three models a-c, but different couplings lead to different population and therefore also to different rotational curves. Another way to restate this discussion is to look again at the angle distribution functions at the fig. 5.9. Molecule, which can perform rotational movement has the angle distribution which is delocalized through the whole interval  $[0, 2\pi]$ . We see, that at 0.5 V only model 1a has this property. But at 0.75 V all three models can rotate. This observations are in correspondence with the fig. 5.10, where only model 1a exhibits significant nonzero  $\langle L_z \rangle$  at 0.5 V (at positive voltages).

Curves at the fig. 5.10 show in general two different types of behavior: fluctuations around zero for lower voltages and the regular growth after approximately

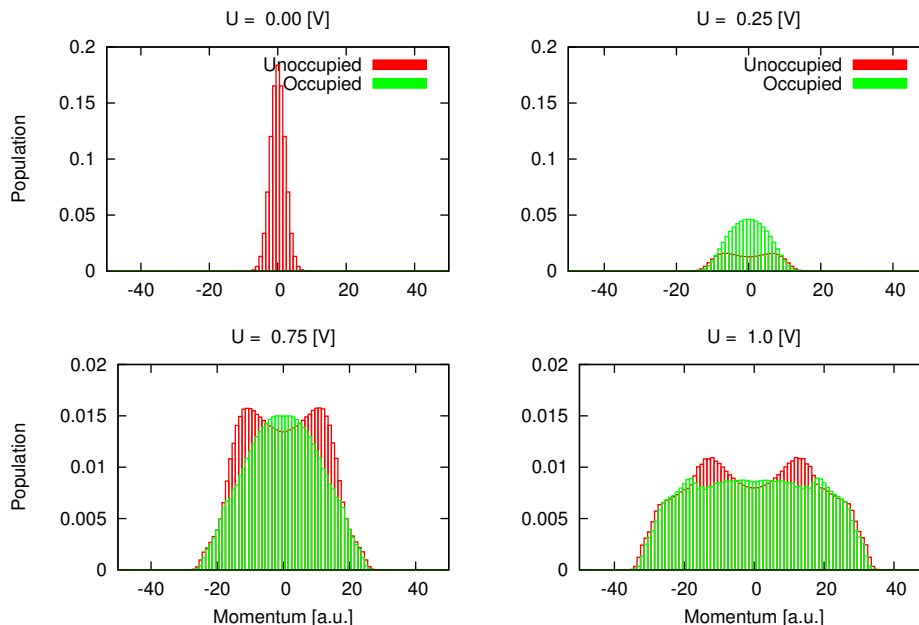


Figure 5.11: Populations  $\rho_{00}(l, l)$  and  $\rho_{11}(l, l)$  in the angular momentum basis for Model 3c at different voltages.

$\pm 0.8$  V which appears only for model 3c. To understand it better let's look at the energies of vibrational states in molecular potentials shown in figure 3.5 in more details. It was already mentioned before, that the states well above the rotational barrier are almost free rotor states. They are represented by delocalized wavefunctions. On the contrary, the states which are close to the ground state are well localized and almost coincide with the states of the harmonic oscillator. We can check the importance of specific states for the rotational asymmetry numerically, by excluding certain groups of states from the consideration during calculations. It turns out that the lowest states almost don't participate in the rotations. Large values of angular momentum are reached only if the states above rotational barriers are excited and the coupling to the left and right lead is different like in the model 3c.

In the ME approach the off-diagonal elements of RDM are often neglected resulting in the equation only for populations  $\rho_m$  and  $\rho_v$  of the states. We used this line of thinking in the section 5.1.2 to compare the formulas for current. If we want to capture the motor effect we have to consider the off-diagonal elements at least for

the near degenerate states close to or above the rotational barrier. To understand this let us consider the states high above the barrier. They almost coincide with free rotor states which are proportional to  $\cos \varphi$  and  $\sin \varphi$  (see the table 3.1) and can be expressed in terms of eigenstates of angular momentum  $|l\rangle$  (defined from the equation (4.79)) as linear combinations  $|\pm\rangle = |l\rangle \pm |-l\rangle$ . But mean value of  $L_z$  in both  $|+\rangle$  and  $|-\rangle$  is zero. Considering only diagonal elements of RDM for these two states would also give vanishing  $\langle L_z \rangle$  in the formula (4.80). Only keeping the off-diagonal elements of RDM we can recover nonzero angular momentum. For the same reason populations  $\rho_m$  and  $\rho_v$  can't be used to understand the details of  $\langle L_z \rangle$  behavior, since they simply contain no information about it. The situation is different in  $l$ -representation since populations  $\rho_{00}(l, l)$  and  $\rho_{11}(l, l)$  enter the formula (4.80) and, thus, can be used for analysis. These populations are shown in fig. 5.11 for four voltages. According to the formula (4.80), the nonzero mean value of angular momentum is a consequence of asymmetry of these pictures with respect to  $l = 0$ . For example, last two pictures at the voltages  $U = 0.75$  and  $U = 1.00$  have small asymmetry (about 1 per cent, not possible to see at the figure). This asymmetry will be much more pronounced in the model 4.

Nonzero angular momentum which, after all, means, that the molecule has a preferable direction of rotation should be the result of the asymmetry in the physical system itself. In our models we deal with two types of them: asymmetry in potential energies of charged and uncharged bridges and coupling asymmetry in the model 3c for left and right electrode. Both are important to observe the motor effect. In fig. 5.12 we present the values of  $\langle L_z \rangle$  for the model 3c with the voltage fixed at  $U = 1.5$  V. It is plotted as a function of charged bridge potential shift  $\varphi_1$  and right coupling shift parameter  $\varphi_r$ . Red line on the figure mark the values actually used in model 3c. The angular momentum first grows with  $\varphi_1$  but higher shifts suppress the effect again. This effect is similar to the Frank-Condon blockade for the current observed in [23]. Selecting optimum value of this parameter can enhance the angular momentum by factor of 3. Coupling becomes symmetrical when  $\varphi_r = \pi$  or  $\varphi_r = 2\pi$  as in model 3b. According to the fig. 5.12 it is possible to maximize the "motor effect" by optimizing  $\varphi_r$  by the factor of 2.

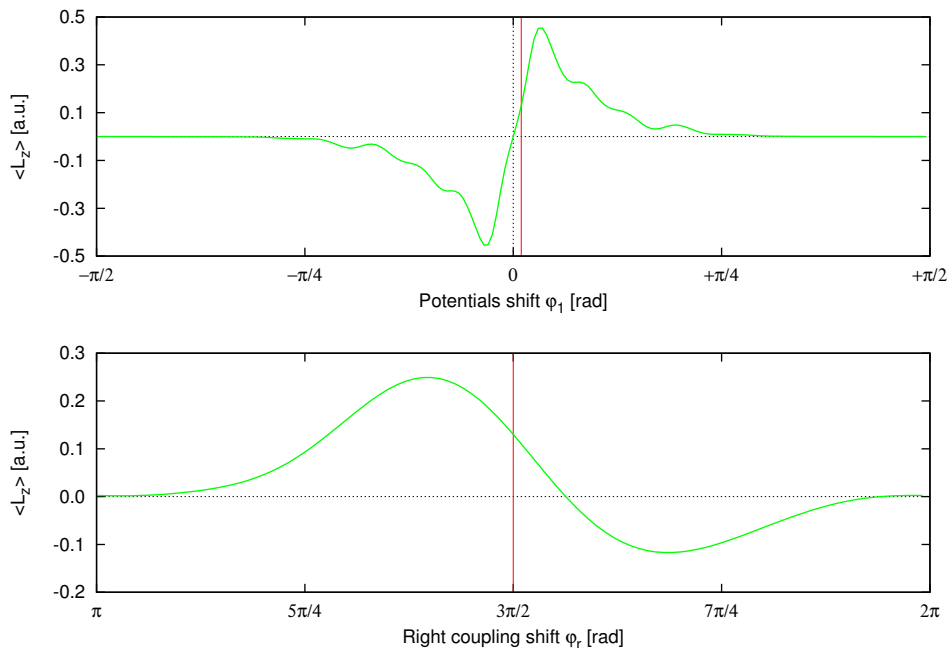


Figure 5.12: Dependence of the mean value of angular momentum  $\langle L_z \rangle$  at voltage  $U = 1.5V$  on the model parameters of potential shift  $\varphi_1$  (top) and coupling asymmetry  $\varphi_r$  (bottom) in model 3c.

### 5.2.3 Towards realistic models

In this section we discuss the "physical" model 4. Current and excitation function of the molecule for three different temperatures are plotted at the fig. 5.13 as a function of the voltage. Density of possible tunneling channels in the model 4 is much higher than in model 3, which is the consequence of the large moment of inertia of the rotor. Moreover, ground states energies of the unoccupied and occupied bridge almost coincide. It means, that the bridge is opened for electrons with zero energy and tunneling events can happen at zero voltage (current will still be zero, since both tunneling directions are equiprobable). Despite the large amount of possible channels, we observe a zero current plateau in the fig. 5.13. This can be explained by the small values of Frank-Condon overlaps for the low-lying vibrational states in both potentials. This is the same effect as discussed in [23] for the model with harmonic vibrations. The current plateau disappears for the calculation at higher temperature, where higher states, not subjected to Frank-Condon blockade, are excited already for the zero voltage.

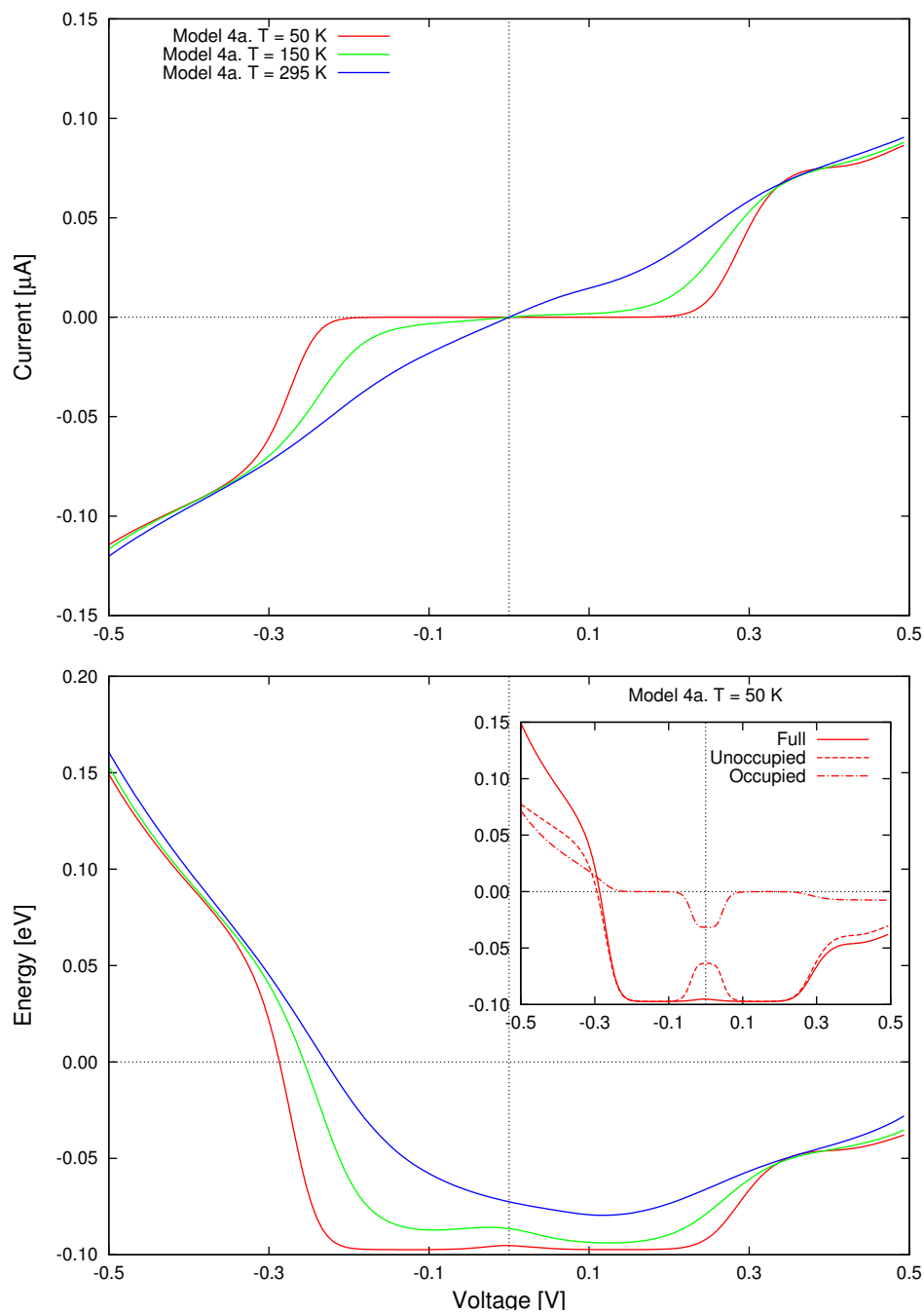


Figure 5.13: Current and the excitation function for the model 4a are plotted as a function of the bias voltage. The results for the three different temperatures (including the room temperature) are shown. The inset in the bottom part shows the contribution to vibrational energy from unoccupied and occupied bridge for the temperature 50 K.

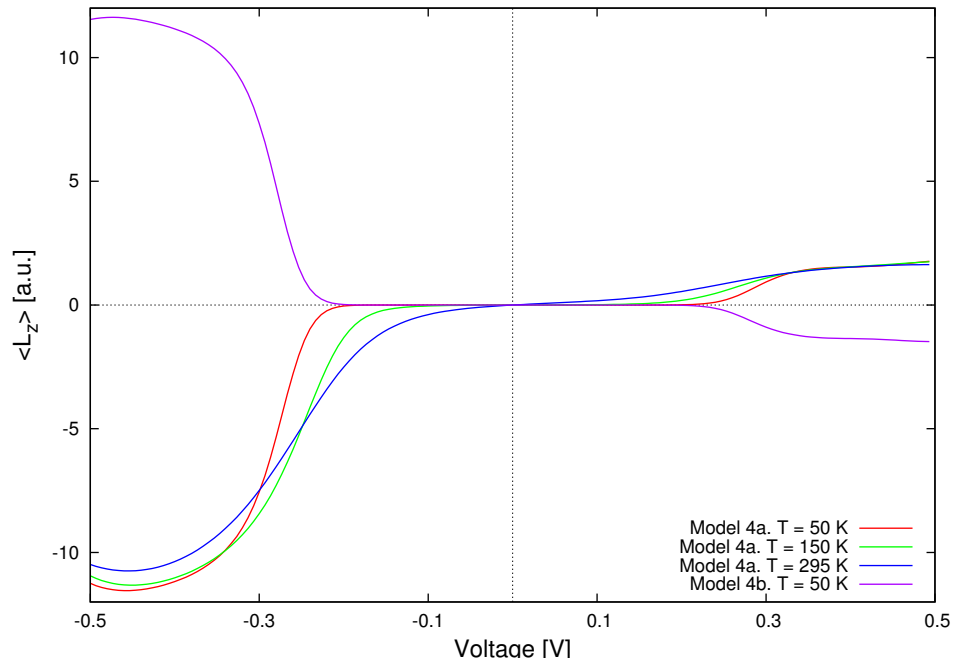


Figure 5.14: Mean value of the angular momentum of the molecule  $\langle L_z \rangle$  as a function of voltage for the models 4a and 4b. The temperature dependence is also shown for model 4a.

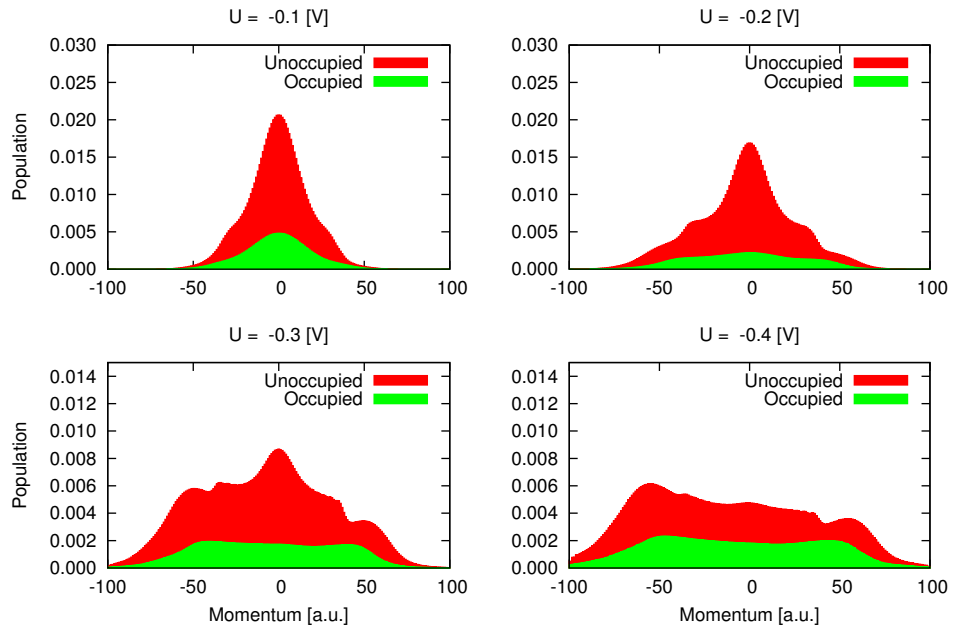


Figure 5.15: Populations distributions  $\rho_{00}(l, l)$  and  $\rho_{11}(l, l)$  of the RDM in momentum basis are plotted for different bias voltages.  $T = 295$  K.

Temperature effects become much more important for model 4 than it was for model 3. It is connected with the fact, that even at smallest temperatures considered here (50K),  $kT$  is comparable with a distance between energy levels of the molecule. It is also interesting to note, that the vibrational excitation curve in the bottom part of figure 5.13 does not have the minimum at zero voltage, but at approximately  $U = \pm 0.15$  V. This implies the cooling effect of the current, which was already observed experimentally [22] and also discussed theoretically [54, 13, 17].

Both the excitation function and the angular momentum voltage dependence are strongly asymmetrical, which is not surprising, because of strongly asymmetrical coupling. It is also obvious from the fig. 3.6, that the left lead coupling strength is minimal in the area where unoccupied bridge wave functions are localized, which makes the overall coupling of the left lead smaller as compared with the right lead.

Dependence of the angular momentum on voltage (fig. 5.14) is much smoother than it was for model 3c. It is another consequence of a large moment of inertia  $I$  of the rotor, which makes the system "more classical" and smooth the quantum features out of the graphs. The angular momentum also reaches much higher values up to  $12\hbar$  inside the considered voltage interval which could partially be attributed to high moment of inertia. Temperature has some influence on the shape of angular momentum curve but the maximum value of the angular momentum reached is rather insensitive to the temperature. From this we can conclude, that the motor effect can be observed at room temperature as well as at cryogenic temperatures.

As we discussed before, nonzero angular momentum mean values are connected with asymmetries in population distributions of the states with well defined angular momenta, as they are plotted at the fig. 5.15. Large values of  $\langle L_z \rangle$  are accompanied with a large asymmetries which are clearly seen for  $U = -0.3$  V and  $U = -0.4$  V.

At the end of the chapter we would like to focus once again on the  $\varphi$ -space symmetry question. As it was already stressed in the previous section, this factor is a very important observation condition for the motor effect. As an advanced version of the fig. 5.12 which was used in model 3 to analyze symmetry, for the model 4 we present the figure 5.16. It shows all possible values of  $\langle L_z \rangle$  as a function of  $\varphi_1$  and  $\varphi_r$ , while the voltage is fixed at  $U = -0.5$  V. This picture is computationally

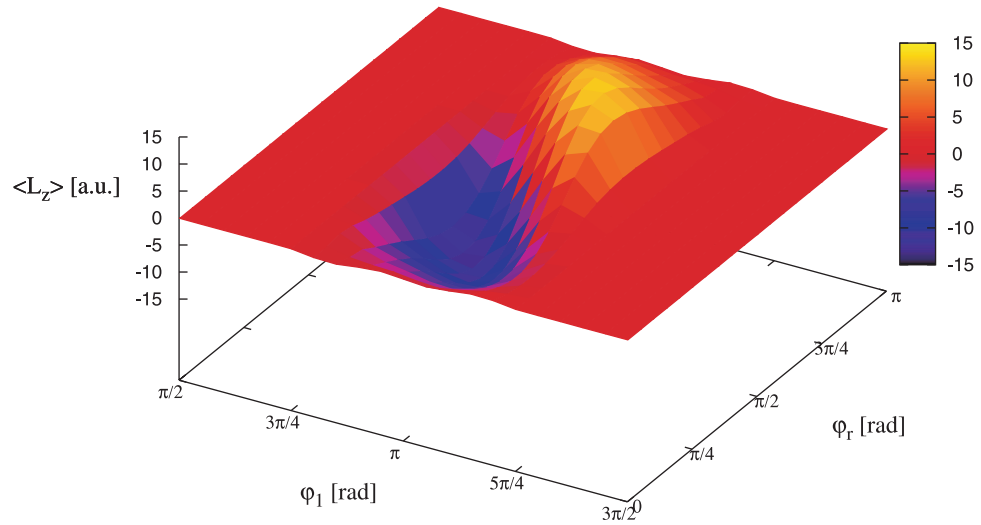


Figure 5.16: Influence of the parameters  $\varphi_1$  and  $\varphi_r$  on the angular momentum mean value for the voltage  $U = -0.5$  V.

heavy and required about 50 hours of ordinary PC time to calculate it. Varying the symmetry breaking parameters (potentials and coupling shifts), one can change  $\langle L_z \rangle$  between  $-15\hbar$  and  $+15\hbar$ . There are also a lot of possible regimes where the motor effect practically disappears (mainly it's caused by a large potential shift  $\varphi_1$ ). The question, what kind of symmetry a given junction should possess to maximize the motor effect, remains open. It goes behind the topic of the thesis.

# Chapter 6

## Conclusion

In this work we have demonstrated how the scattering approach and the ME approach can be applied to calculate a current through the molecular junctions. To discuss different aspects of the charge transport phenomena both approaches were applied to the models of the junction with and without internal vibrational degrees of freedom.

First we briefly discuss both approaches in the elastic transport regime (model 1) where the scattering approach is exact. ME calculations coincide well with the scattering results when the coupling between the leads and the molecular bridge is small, which is a consequence of the perturbative nature of WBR ME. This also implies that the second order ME approach can not take into account a bridge's transmission function width, as well as a small energy renormalization. It is clearly seen in comparison of CVC. The steps in CVC in the ME approach are broadened only by the Fermi-Dirac distribution in leads.

Next we discuss the vibrationally inelastic transport regime (model 2) which can not be treated analytically and may reveal the qualitative differences between CVC, calculated using scattering and ME approaches. This regime suits well to discuss the molecule's vibrational states populations and their influence to the charge transport calculation. It's demonstrated, that the Boltzmann factors, used in the generalized Landauer formula, provide a bad approximation of bridge's stationary populations, especially at high voltages. We have fixed this issue suggesting the balance equation in the framework of the scattering theory to calculate the realistic bridge's popula-

tions and, thus, improve the method. However, since the molecular bridge can be found with certain probability in occupied or unoccupied state, and the scattering theory (even with the balance equation improvement) allows to work explicitly only with unoccupied states populations, the description is still not as detailed as in the ME approach. The last one explicitly takes into account populations of occupied and unoccupied states. If the ME is solved and RDM is calculated we, for example, can answer the question, what is the overall probability to find the bridge occupied or unoccupied. Such a detailed description of the molecular bridge makes the ME approach more accurate in the nonelastic regime than the scattering approach.

As a next step we investigate the inelastic charge transport beyond the harmonic approximation. For this purpose original set of models of the molecular bridge, produced from the chain of benzene rings, is formulated. There are both purely theoretical models among them, designed to catch different interesting parametric regimes in anharmonic junction (models 3a, 3b and 3c), and also realistic models (4a and 4b) which are parametrized using the available data about molecular rotations.

Influence of anharmonic vibrations to the charge transport properties of the junction is discussed in details. It is shown how the steps in the current-voltage characteristics can be analyzed in this case. Additional data about the vibrational excitation voltage dependence, states populations and angle distribution was also used in the analysis. Vibrational states which are located above the potential energy barrier against the full rotation are mainly populated at high voltages. In this case the character of processes in the junction may switch from the purely quantum regime, with step-like CVC, to the regime where all the dependences are smooth. We expect that some other, less detailed level of description (probably semi-classical) can be successfully applied to treat the system in this case. It is also shown how the symmetry in the junction, which enters through the angle dependent coupling to the left and right leads, may significantly change CVC. Negative differential resistance, for example, may appear as a result of certain coupling regime.

As an example of phenomena which can't be discovered in the harmonic approximation we have studied the motor effect, i.e. the response of the angular momentum of the molecule to the voltage applied across the junction. Rotational moment of

the bridge is investigated in different regimes, i.e. for different asymmetry in the junction. We have demonstrated that the mean value of the angular momentum, indeed, strongly depends on the voltage. In the realistic molecular motor model the absolute value of angular momentum, depending on the symmetry, may reach significant values (up to  $15\hbar$ ) in the selected voltage window. For the asymmetrically coupled bridge the direction of the angular momentum of the molecule can be controlled with the polarity of the voltage. The nonzero angular momentum is reached when levels above the rotational barrier are populated. From the computational point of view we have to stress that although the current thorough the junction can accurately be described from the master equation calculation with the diagonal part of the reduced density matrix only (i.e. the populations of the molecular states) the off-diagonal elements (coherencies) are essential for the calculation of the angular momentum.

This work indicates that the rotational motion of a molecular group should in fact be a very common phenomenon. There are only two conditions required: 1) presence of some part of the molecule capable of the rotation with moderately small potential barrier against this rotation and 2) breaking of the mirror symmetry in the junction (chirality of the junction).

# Bibliography

- [1] Neil W. Ashcroft and N. David Mermin. *Solid State Physics*. Brooks Cole, 1976.
- [2] Arieh Aviram and Mark A. Ratner. Molecular rectifiers. *Chemical Physics Letters*, 29(2):277–283, Nov 1974.
- [3] K. Blum. *Density matrix theory and applications*. New York, 1981.
- [4] P. S. Cornaglia, D. R. Grempel, and H. Ness. Quantum transport through a deformable molecular transistor. *Phys. Rev. B*, 71(7):075320, Feb 2005.
- [5] S. Datta. *Electronic transport in mesoscopic systems*. Cambridge Univ Pr, 1997.
- [6] W. Domcke. Theory of resonance and threshold effects in electron-molecule collisions: the projection-operator approach. *Physics Reports*, 208(2):97–188, 1991.
- [7] Andrea Donarini. *Dynamics of Shuttle Devices*. PhD thesis, Technical University of Denmark, 2004.
- [8] Andrea Donarini, Milena Grifoni, and Klaus Richter. Dynamical symmetry breaking in transport through molecules. *Phys. Rev. Lett.*, 97(16):166801, Oct 2006.
- [9] D. Egorova, M. Thoss, W. Domcke, and H. Wang. Modeling of ultrafast electron-transfer processes: Validity of multilevel redfield theory. *The Journal of Chemical Physics*, 119:2761, 2003.

- [10] T. Eirola and O. Nevanlinna. Numerical linear algebra; iterative methods. *Lecture notes, Helsinki University of Technology*, 2003.
- [11] Remy Fortrie and Henry Chermette. Vibronic quasi-free rotation effects in biphenyl-like molecules. td-dft study of bifuorene. *JCTC*, 3(3):852–859, 2007.
- [12] M. Galperin, M.A. Ratner, and A. Nitzan. Molecular transport junctions: vibrational effects. *Journal of Physics: Condensed Matter*, 19(10):103201, 2007.
- [13] Michael Galperin, Keiji Saito, Alexander V. Balatsky, and Abraham Nitzan. Cooling mechanisms in molecular conduction junctions. *Phys. Rev. B*, 80(11):115427, Sep 2009.
- [14] J. Gaudioso, L. J. Lauhon, and W. Ho. Vibrationally mediated negative differential resistance in a single molecule. *Phys. Rev. Lett.*, 85(9):1918–1921, Aug 2000.
- [15] G.H. Golub and C.F. Van Loan. *Matrix computations*. Johns Hopkins Univ Pr, 1996.
- [16] L. Y. Gorelik, A. Isacsson, M. V. Voinova, B. Kasemo, R. I. Shekhter, and M. Jonson. Shuttle mechanism for charge transfer in coulomb blockade nanostructures. *Phys. Rev. Lett.*, 80(20):4526–4529, May 1998.
- [17] R. Hartle, C. Benesch, and M. Thoss. Vibrational nonequilibrium effects in the conductance of single molecules with multiple electronic states. *Phys.Rev.Lett.*, 102(14):146801, 2009.
- [18] H. Haug and A.-P. Jauho. *Quantum Kinetics in Transport and Optics of Semiconductors*. Springer, 1996.
- [19] W. Ho. Single-molecule chemistry. *J.Chem.Phys.*, 117(24):11033–11061, Dec 2002.
- [20] RD Horansky, TF Magnera, JC Price, and J. Michl. Artificial dipolar molecular rotors. *Lect. Notes Phys.*, 711:303–330, 2007.

- [21] Noel S. Hush. An overview of the first half-century of molecular electronics. *Annals of the New York Academy of Sciences*, 1006:1–20, 2003.
- [22] Z. Ioffe, T. Shamai, A. Ophir, G. Noy, I. Yutsis, K. Kfir, O. Cheshnovsky, and Y. Selzer. Detection of heating in current-carrying molecular junctions by raman scattering. *Nature Nanotechnology*, 3(12):727–732, 2008.
- [23] Jens Koch and Felix von Oppen. Franck-condon blockade and giant fano factors in transport through single molecules. *Phys. Rev. Lett.*, 94(20):206804, May 2005.
- [24] D. Kohen, CC Marston, and DJ Tannor. Phase space approach to theories of quantum dissipation. *The Journal of Chemical Physics*, 107(13):5236, 1997.
- [25] P. E. Kornilovitch, A. M. Bratkovsky, and R. Stanley Williams. Bistable molecular conductors with a field-switchable dipole group. *Phys. Rev. B*, 66(24):245413, Dec 2002.
- [26] Kwan S. Kwok and James C. Ellenbogen. Moletronics: future electronics. *Materials Today*, 5(2):28–37, 2002.
- [27] Jorg Lehmann, Sigmund Kohler, Volkhard May, and Peter Hanggi. Vibrational effects in laser-driven molecular wires. *The Journal of Chemical Physics*, 121(5):2278–2288, 2004.
- [28] M. Leijnse and M. R. Wegewijs. Kinetic equations for transport through single-molecule transistors. *Phys. Rev. B*, 78(23):235424, Dec 2008.
- [29] C. B. Madsen, L. B. Madsen, S. S. Viftrup, M. P. Johansson, T. B. Poulsen, L. Holmegaard, V. Kumarappan, K. A. Jorgensen, and H. Stapelfeldt. A combined experimental and theoretical study on realizing and using laser controlled torsion of molecules. *The Journal of Chemical Physics*, 130(23):234310, 2009.
- [30] Gerald D. Mahan. *Many-Particle Physics*. Plenum Press, 1993.
- [31] A. Mitra, I. Aleiner, and A. J. Millis. Phonon effects in molecular transistors: Quantal and classical treatment. *Phys. Rev. B*, 69(24):245302, Jun 2004.

- [32] C. J. Muller, J. M. van Ruitenbeek, and L. J. de Jongh. Conductance and supercurrent discontinuities in atomic-scale metallic constrictions of variable width. *Phys. Rev. Lett.*, 69(1):140–143, Jul 1992.
- [33] T. Novotný, A. Donarini, and A. Jauho. Quantum shuttle in phase space. *Phys. Rev. Lett.*, 90(25):256801, Jun 2003.
- [34] E.A. Osorio, K. O’Neill, N. Stuhr-Hansen, O.F. Nielsen, T. Bjørnholm, and H.S.J. van der Zant. Addition energies and vibrational fine structure measured in electromigrated single-molecule junctions based on an oligophenylenevinylene derivative. *Advanced Materials*, 19(2):281–285, 2007.
- [35] Hongkun Park, Andrew K. L. Lim, A. Paul Alivisatos, Jiwoong Park, and Paul L. McEuen. Fabrication of metallic electrodes with nanometer separation by electromigration. *Applied Physics Letters*, 75(2):301–303, 1999.
- [36] Hongkun Park, Jiwoong Park, Andrew K. L. Lim, Erik H. Anderson, A. Paul Alivisatos, and Paul L. McEuen. Nanomechanical oscillations in a single-c60 transistor. *Nature*, 407:57–60, 2000.
- [37] Irina Petreska, Ljup čo Pejov, and Ljup čo Kocarev. Controlling the torsional stochastic switching in phenylene ethynylene oligomer molecules by external electrostatic fields. *Phys. Rev. B*, 78(4):045209, Jul 2008.
- [38] Jan Prachar. Model tesne vazby a jeho aplikace na molekularni elektroniku a transport v mezoskopickych systemech. Master’s thesis, Univerzita Karlova v Praze, 2006.
- [39] J. Rammer and H. Smith. Quantum field-theoretical methods in transport theory of metals. *Rev. Mod. Phys.*, 58(2):323–359, Apr 1986.
- [40] M. Ratner and D. Ratner. *Nanotechnology: A gentle introduction to the next big idea*. Prentice Hall Press Upper Saddle River, NJ, USA, 2002.
- [41] M.A. Reed, C. Zhou, C.J. Muller, T.P. Burgin, and J.M. Tour. Conductance of a molecular junction. *Science*, 278(5336):252–254, Oct 1997.

- [42] Dvira Segal and Abraham Nitzan. Heating in current carrying molecular junctions. *J. Chem. Phys.*, 117(8):3915, 2002.
- [43] Y. Selzer and D.L. Allara. Single-molecule electrical junctions. *Annual Review of Physical Chemistry*, 57:593–623, May 2006.
- [44] R. H. M. Smit, Y. Noat, C. Untiedt, N. D. Lang, M. C. van Hemert, and J. M. van Ruitenbeek. Measurement of the conductance of a hydrogen molecule. *Nature*, 419:906–909, Oct 2002.
- [45] BC Stipe, MA Rezaei, and W. Ho. Single-molecule vibrational spectroscopy and microscopy. *Science*, 280(5370):1732, 1998.
- [46] J.R. Taylor. *Scattering theory: the quantum theory on nonrelativistic collisions*. Wiley New York, 1972.
- [47] Carsten Timm. Tunneling through molecules and quantum dots: Master-equation approaches. *Phys.Rev.B*, 77(19):195416, 2008.
- [48] A. Troisi, M.A. Ratner, and A. Nitzan. Vibronic effects in off-resonant molecular wire conduction. *The Journal of Chemical Physics*, 118(13):6072, 2003.
- [49] Seiji Tsuzuki, Tadafumi Uchimarui, Kazunari Matsumura, Masuhiro Mikami, and Kazutoshi Tanabe. Torsional potential of biphenyl: Ab initio calculations with the dunning correlation consisted basis sets. *J.Chem.Phys*, 110(6):2858, 1999.
- [50] Martin Čížek, Michael Thoss, and Wolfgang Domcke. Theory of vibrationally inelastic electron transport through molecular bridges. *Phys.Rev.B*, 70:125406, 2004.
- [51] Martin Čížek, Michael Thoss, and Wolfgang Domcke. Charge transport through a flexible molecular junction. *Czech J. Phys*, 2005.
- [52] Boyang Wang, Lela Vuković, and Petr Král. Nanoscale rotary motors driven by electron tunneling. *Phys. Rev. Lett.*, 101(18):186808, Oct 2008.

- 
- [53] M.R. Wegewijs and K.C. Nowack. Nuclear wavefunction interference in single-molecule electron transport. *New Journal of Physics*, 7:239, 2005.
- [54] Stefano Zippilli, Giovanna Morigi, and Adrian Bachtold. Cooling carbon nanotubes to the phononic ground state with a constant electron current. *Phys. Rev. Lett.*, 102(9):096804, Mar 2009.